Master Thesis, c961052

Principles of Electroosmotic Pumps

Anders Brask

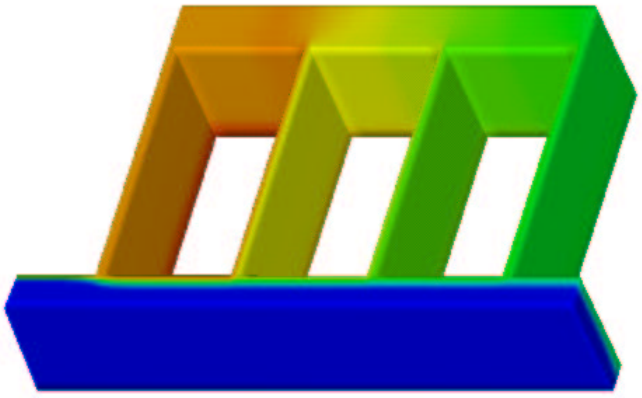

Supervisors: Henrik Bruus and Goran Goranović

Technical University of Denmark

Mikroelektronik Centret - MIC

February 26, 2003

Abstract

Microfluidics is about the manipulation of liquids in small channels. It is expected to revolutionize chemical and biological analysis systems. Devices such as pumps, valves, mixers and sensors are essential for making a so-called Lab-on-a-Chip.

One of the promising type of micropumps is driven by electroosmosis (EO). EO pumps are purely driven by electric fields and have no moving parts. Various types of physical and chemical phenomena involved in EO pumps are described in the thesis. An analytical approach to characterization (Q-p) of EO pumps is proposed. This method is compared with numerical computational fluid dynamics. The principles are applied to two existing EO pumps, and agreement within a few percent between model and simulation is achieved.

Two novel designs are presented: (1) The Two-Liquid Viscous Pump that can pump all types of liquids. A simplified model and simulation are presented capturing the essence of the pumping principles. (2) The Shallow Reservoir pump is a modification of an existing pump, allowing simple integration into a chip. Design guidelines on the reservoir dimensions are given.

Resumé

Mikrofluidik handler om styring/kontrol af væsker i mikrokanaler. Teknikken forventes at revolutionere kemiske og biologiske analysesystemer. Komponenter så som pumper, ventiler, mixere og sensorer er essentielle for realiseringen af det såkaldte Lab-on-a-Chip.

En type af de lovende mikropumper er drevet af elektroosmose (EO). Elektroosmotiske pumper er alene drevet af elektriske felter og har ingen bevægelige dele. Den bagvedliggende fysik og kemi er beskrevet i rapporten. En analytisk metode til karakterisering (Q-p) af EO pumper er foreslået. Metoden er sammenlignet med numeriske beregninger med computational fluid dynamics. De to metoder er anvendt på to eksisterende pumper, og overensstemmelse indenfor et par procent er opnået.

To nye pumpedesigns er præsenteret: (1) Den viskose to-væske pumpe kan pumpe alle typer væsker ved hjælp af elektroosmose. En simplificeret model og simuleringer er præsenteret. Sammen beskriver de principperne i den nye pumpeteknik. (2) Den flade reservoir pumpe er en modificeret udgave af en eksisterende pumpe. Den nye pumpe kan integreres i et kanalsystem på en chip. Dette muliggøres ved hjælp af de omtalte reservoirs. Dimensioneringen af disse reservoirs er beskrevet.

Preface

The present master thesis is submitted in candidacy to the cand. polyt. title at Technical University of Denmark. The project is made within the μTAS group at Mikroelektronik Centret - MIC.

The group was founded in 1999. The first simulation effort was made by Goran Goranović. On his initiative the Microfluidic simulation group within the μTAS project was started in 2001. The group initially consisted of Ph.D. student Goran Goranović and four master students with various backgrounds in computational fluid dynamics, applied mathematics, physics and chemistry. Midway in the project associate professor Henrik Bruus was assigned as the project leader of the microfluidic theory and simulation group. The total duration of the project was 8th months. The work at hand is to a large extent pioneering in the microfluidic simulation area.

I would like to thank Goran Goranović and Henrik Bruus for a dedicated effort as supervisors. The COVENTOR support in Europe, especially dr. ir. Joost van Kuijk, has been very helpful. I would also like to thank Lennart Bitsh, Mads Jakob Jensen and Flemming Rytter Hansen for their intellectual contributions and their good spirits.

Anders Brask
Lyngby, May 2002.

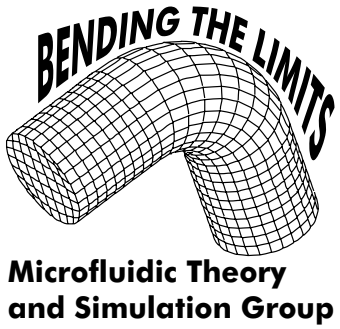

Figure 1: The logo that was made during the project to hang on the door of our office, so that everyone on MIC passing our door could see what was going on.

Contents

List of Figures

List of Symbols

Symbol	Description	Unit
a	Characteristic length	m
c	Molar concentration	mol m^{-3}
D_{heat}	Heat diffusion coefficient	m^2 s^{-1}
D_{layer}	Pumping layer thickness	m
D_{mass}	Mass diffusion coefficient	m^2 s^{-1}
e	Elementary charge	1.602×10^{-19} C
E	Electric field	V m^{-1}
F	Faradays constant	9.649×10^4 C mol^{-1}
g	Gravity	9.82 m s^{-2}
H	Specific enthalpy	J kg^{-1}
I	Electric current	C s^{-1}
$\mathbf{I}$	Electric current flux vector	C s^{-1} m^{-2}
$\mathbf{J}$	Molar flux vector	mol s^{-1} m^{-2}
k	Boltzmans constant	1.381×10^{-23} J K^{-1}
M	Molar mass	g mol^{-1}
n	Relative concentration	
N_A	Avogadros number	6.022×10^{23} mol^{-1}
p	Pressure	N m^{-2}
P	Ohmic heating	W m^{-3}
Pe_{mass}	Peclet number, mass diffusion	
q	Energy density	J m^{-3}
Q	Flow rate	m^3 s^{-1}
$\mathbf{r}$	Position vector	m
R	Gas constant	8.315 J mol^{-1} K^{-1}
R_{hyd}	Hydraulic resistance	kg m^{-4} s^{-1}
R_{elec}	Electrical resistance	Ω
Re	Reynolds number	
T	Temperature	K
u	Velocity	m s^{-1}
$\mathbf{u}$	Velocity vector	m s^{-1}
u_{eo}	Helmholtz velocity	m s^{-1}
U	Velocity	m s^{-1}
U_{int}	Specific internal energy	J kg^{-1}
v	Reaction velocity	mol s^{-1}
z	Number of charges	

Symbol	Description	Unit
α_{eo}	Electroosmotic mobility	$\mathrm{m}^2\ (\mathrm{V\ s})^{-1}$
α_{ep}	Electrophoretic mobility	$\mathrm{m}^2\ (\mathrm{V\ s})^{-1}$
δ	Stern layer thickness	m
ΔG	Gibbs free energy	$\mathrm{J\ mol}^{-1}$
Δp_{eo}	Electroosmotic pressure	$\mathrm{N\ m}^{-2}$
ϵ	Dielectric constant	$\mathrm{C\ (V\ m)}^{-1}$
ϵ_0	Vacuum permittivity	$8.854 \times 10^{-12}\ \mathrm{C\ (V\ m)}^{-1}$
ϵ_r	Relative permittivity	
ζ	Zeta potential	V
η	Efficiency	
θ	Angle	
κ	Aspect ratio	
λ_D	Debye length	m
λ_{elec}	Electrical conductivity	$(\Omega\ \mathrm{m})^{-1}$
λ_{heat}	Thermal conductivity	$\mathrm{W\ (m\ K)}^{-1}$
μ	Dynamic viscosity	$\mathrm{kg\ (m\ s)}^{-1}$
μ_{chem}	Chemical potential	J
$\overline{\mu}_{\mathrm{chem}}$	Electrochemical potential	J
ν	Kinematic viscosity	$\mathrm{m}^2\ \mathrm{s}^{-1}$
ϕ	Electric potential	V
ϕ_a	Applied potential	V
ϕ_i	Intrinsic potential	V
ψ	Electric potential	V
π	Pi	3.14159...
ρ	Mass density	$\mathrm{kg\ m}^{-3}$
ρ_E	Charge density	$\mathrm{C\ m}^{-3}$
σ_0	Surface charge density	$\mathrm{C\ m}^{-2}$
τ_{ij}	Shear stress	$\mathrm{N\ m}^{-2}$
τ'	Stress tensor	$\mathrm{N\ m}^{-2}$

Chapter 1

Introduction

Microfluidics, the manipulation of liquids in small channels, is a new and promising technology expected to revolutionize chemical and biological analysis systems.

Miniaturization of traditional analysis systems has many advantages. The aim is to integrate a complete micro total analysis system (μTAS) on a device. Such devices can be made very compact and portable. Medical diagnostics, environmental monitoring and on-line process control are some of the promising areas. These new devices are expected to exceed the existing systems in speed and accuracy. An important feature of the microsystems is that they will be cheap once they are mass-produced, making the technology widely available at a low cost.

The field of μTAS is truly cross-disciplinary, including chemistry, condensed matter physics, optics, material science, and hydraulic engineering. A microfluidic analysis system could comprise several microfluidic components such as pumps, valves, mixers, filters and separators. They are the building blocks for the fluidic part of a Lab-on-a-Chip. The thesis at hand is exclusively dealing with the pump devices used for such a chip, Fig 1.1.

Figure 1.1: A schematic of a mixing channel. The devices consist of two layers: the substrate, in which the channels have been etched (blue), and the lid (transparent). The lid is attached to the substrate using a process called bonding. Holes have been drilled in the lid for access to the channels.

The flow in microfluidics is laminar, whereas macroscopic flow is usually turbulent. Within the last 20 years, computational fluid dynamics (CFD) have been widely used in the industry for designs of airfoils, cars, pumps, etc. These CFD programs can also be applied to microfluidics, with certain limitations, however. The existing programs can only describe the electro kinetic phenomena such as electroosmosis from a macroscopic level. However, the microfluidic handling CFD programs are however becoming increasingly sophisticated in order to meet the demands from customers. The use of simulations in microfluidics reduces the development time and increases the understanding, but does

not replace experiments. Only modelled phenomena are included in simulations, whereas experiments include everything.

Development of novel microfluidic devices requires a thorough understanding of microflows and the properties of the liquids. The continuum approximation does apply to flows in microchannels. The governing equations are the Navier-Stokes and the continuity equation. A definitive characteristic of microfluidics is the laminar (not turbulent) nature of the flow. The Reynolds number[1] in a typical macroscopic flow, say a running water faucet, is $Re \approx 10^4$. In microfluidics a typical Reynolds number would be $Re \approx 10^{-1}$. One may imagine honey coming out of the water faucet instead of water yielding an equivalent low Reynolds number.

Pumping in a microfluidic system is accomplished using either pressure or electroosmosis (EO). The pressure source can be either external or integrated into the device. This thesis will concentrate on pumps that can be integrated into a chip - in particular electroosmotic pumps.

Electroosmosis is an electro chemical surface phenomena. At a solid-liquid interface charged ions may be chemically bound to the interface. The excess of surface charges attracts ions of opposite charge (counterions). These mobile counterions can be manipulated by an external electric field to generate an electroosmotic flow (EOF), Fig. 1.2.

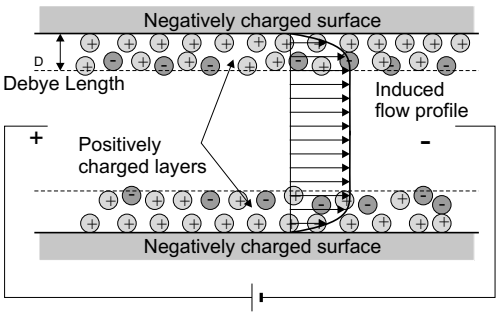

Figure 1.2: Schematic illustration of electroosmotic flow (EOF). The two electrodes generate an electric field that exerts a force on the charged Debye layer. A balance between electrical and viscous forces arises in the charged Debye layer.

In the following list an introduction to the chapters and their contents will be given.

- **Physics of Liquids**
  The starting point will be the physics of liquids with emphasis on microfluidics and electroosmosis. Then the microfluidic flow characteristics and physical properties of liquids are discussed. This discussion is followed by an introduction to the theory of electroosmotic flow. The microscopic theory will be held on a thorough, but introductory level. The theory of colloid science is very comprehensive and a topic of intensive research at the moment. The important conclusions from the microscopic theory are extracted and transferred to the elementary flow analysis.

[1] Nondimensional number expressing the ratio between inertial forces and viscous forces. In turbulent and laminar flows the corresponding Reynolds numbers are high and low, respectively.

- **Elementary Flow Analysis**
  The elementary flow analysis covers both a detailed flow analysis and a more macroscopic approach. Much of the theory is well established, but in this context it is applied to a new area. An EO pump may be analyzed in a macroscopic manner, setting up an equivalent electrical circuit. This approach will be seen to be a very valuable model for various EO pumps. Especially the effect of combining analytical modelling with computational fluid dynamics is seen to be beneficial.

- **Computational Fluid Dynamics**
  A brief introduction to Computational Fluid Dynamics (CFD) is given. Application of CFD to microfluidics is a very new area. The microfluidic oriented CFD-package COVENTOR is used to simulate four different EO pumps. Some of the special boundary conditions and limitations of the program are discussed.

- **Overview of Micropumps**
  All research must start with a literature survey. Different types of modern micropump designs are presented and commented. A good physical understanding of various physical effects is essential in making new designs. An overview provides the opportunity to investigate the findings of others and apply them to new ideas.

- **Models and simulations**
  Based on the overview chapter two cascade pumps are selected. The parallel cascade pump developed by Morf *et al.*, 2001, and the Low-voltage cascade pump developed by Takamura *et al.*, 2001. A thorough analysis is assisted by analytical models and CFD. On the authors request, Takamura conceded to giving the information that made the analysis possible. The results reveal many interesting things. Some of the knowledge gathered in this chapter is projected into new designs.

- **Novel Designs**
  In this chapter the introduced principles are used for making new pump designs. EO pumps can only operate with conducting liquids. Nonpolar liquids are usually nonconducting and cannot be pumped using traditional EO pumps. The idea is to position a sheet of polar liquid between the nonpolar liquid and the interface. A two-liquid EO pump is developed effectively expanding the range of pumping liquids to all liquids. The pump is given the name: "The Two-liquid Viscous Pump".

  With inspiration in the shallow/planar pump developed by Chen, 2000, a new integrated design is achieved using reservoirs the so-called: "Shallow Reservoir Pump". The pump design is very promising with respect to flow rate and backpressure. The introduced concepts may also be useful in other microfluidic applications.

Chapter 2

Physics of Liquids

2.1 Momentum and Continuity

In this section we shall investigate the governing equations and the types of flows a microfluidic system may comprise. In this thesis we are exclusively dealing with liquids - however, the governing equations are valid for both gases and liquids, commonly denoted fluids.

The governing equations in fluid dynamics are the continuity and the Navier-Stokes equation. They are based on the assumption that a fluid is a continuum. This is generally a good approximation because the molecular spacing λ_{mol} is very small compared to the length scales considered, Lautrup.

$$\lambda_{\text{mol}} = \left(\frac{M}{\rho N_A}\right)^{\frac{1}{3}} \tag{2.1}$$

Example: *The Molecular Spacing*
For water the average molecular spacing is $\lambda_{\text{mol,water}} = 0.31$ nm which is roughly equivalent to the size of a molecule. In the case of air the average molecular spacing is much larger. $\lambda_{\text{mol,air}} = 3.6$ nm. These length scales are tiny. However, the continuum approximation must be kept in mind when dealing with microfluidics.

The continuity equation states

$$\frac{\partial \rho}{\partial t} + \boldsymbol{\nabla} \cdot (\rho \mathbf{u}) = 0. \tag{2.2}$$

If the fluid is incompressible, the divergence of the velocity is zero, $\boldsymbol{\nabla} \cdot \mathbf{u} = 0$. If the density ρ is constant, the fluid is incompressible. It is, however, not possible to deduct that an incompressible fluid has a constant density.

The forces acting on a fluid element can be divided into surface forces and body forces. The surface forces may be described by a stress tensor τ'. τ_{ij} is the component of stress, i.e., force per unit area, acting in the i-direction on a surface element in the j-direction. The the sum of body forces is labelled g_i. The diagonal components of the stress tensor are called pressures. The Navier-Stokes

equation,

$$\rho\frac{Du_i}{Dt} = \frac{\partial\tau_{ij}}{\partial x_j} + g_i, \tag{2.3a}$$

$$\rho\frac{Du_i}{Dt} = -\boldsymbol{\nabla}p + \mu\boldsymbol{\nabla}^2 u_i + g_i. \tag{2.3b}$$

The latter form of the Navier-Stokes equation is generally valid for incompressible Newtonian fluids[1]. The substantial derivative of the velocity,

$$\frac{D\boldsymbol{u}}{Dt} = \frac{\partial\boldsymbol{u}}{\partial t} + \mathbf{u}\cdot\boldsymbol{\nabla}\mathbf{u}, \tag{2.4}$$

contains nonlinear convective terms, also called inertia terms. As long as these terms are small compared to the viscous term, the flow is said to be laminar. A measure for the ratio between inertial and viscous forces is the Reynolds number defined as

$$Re = \frac{L\ u}{\nu}, \tag{2.5}$$

where L and u is a characteristic length and velocity, respectively. The Reynolds number at the transition between laminar and turbulent flow is of the order 10^3, depending on the geometry and type of flow[2]. For a Poiseuille flow in a tube the critical Reynolds number is $Re_{\text{crit}} \approx 580$. In microfluidics the flow is almost always laminar due to the micro length scales $L \approx 100$ μm, small velocities $u \approx 1$ mm/s and kinematic viscosity 1.00×10^{-6} m^2/s yielding a Reynolds number of $Re = 0.1$.

At very low Reynolds numbers the flow is also said to be creeping which means that the inertial effects are negligible. This happens at Reynolds numbers $Re < 5$, Yang, 2001. The mathematical implication of this is that nonlinear terms in the Navier-Stokes equation disappear.

If the flow is free of vorticity, the governing equations simplify considerably. This type of flow is called potential flow. Viscous flow is generally not potential flow, but in some special cases it may be described as such. Given the appropriate boundary conditions electroosmotic flow can be described as potential flow independent of the Reynolds number, Appendix F, Cummings *et al.*, 2000.

2.2 The Energy Equation

In viscous flows there will be dissipation of energy through irreversible processes. In practice this means that mechanical and electrical energy are dissipated to heat. The temperature of the system will increase until an equilibrium between heat generation and heat transport is obtained. The energy equation is applied, Landau and Lifshitz,

$$\frac{\partial}{\partial t}\left(\frac{1}{2}\rho u^2 + \rho U_{\text{int}}\right) = -\boldsymbol{\nabla}\cdot\left(\rho\mathbf{u}(\frac{1}{2}u^2 + H) - \mathbf{u}\cdot\tau' - \rho c_p D_{\text{heat}}\boldsymbol{\nabla}T\right). \tag{2.6}$$

[1] In Newtonian fluids the shear stress and the rate of strain are proportional. For example, water is Newtonian whereas, e.g., blood is non-Newtonian.

[2] For example, the wave boundary layer in an ocean wave may not be fully turbulent before $Re = 10^6$

The left hand side of Eq. (2.6) is the rate of change in mechanical and thermal energy respectively, $\frac{1}{2}\rho u^2$ and ρU_{int}. The right hand side is the divergence of the energy flux, i.e., source terms. The unit is power per volume. The first term is the kinetic energy $\rho u^2/2$ and enthalpy ρH. The second term is the internal friction due to the viscosity. The last term is the heat transport. A more detailed discussion of the terms will be done in the following.

Rewriting Eq. (2.6), assuming steady state, and adding the term for ohmic heating $P = \lambda_{\text{elec}} E^2$, we obtain

$$0 = \boldsymbol{\nabla} \cdot \left(\rho \mathbf{u} (\frac{1}{2} u^2 + H) - \mathbf{u} \cdot \tau' - \rho \; c_p \; D_{\text{heat}} \boldsymbol{\nabla} T \right) + \lambda_{\text{elec}} E^2. \tag{2.7}$$

In the following we shall apply Eq. (2.7) to a uniform steady flow between two infinitely large plates with the y-axis parallel to their normal vectors. The flow is partially driven by EO and pressure in the x-direction.

- **Mass transport**
  The divergence of the mass transport is zero because the flow is uniform.

- **Internal friction**
  In order to determine the internal friction we must know the velocity field $\mathbf{u}$ and the stress tensor τ'. The flow can be written as $\mathbf{u} = (u, 0, 0)$ having only one component in the x-direction. The stress tensor is a 3×3 matrix. The diagonal elements are the pressures. The only other nonzero elements are $\tau_{xy} = \tau_{yx} = \mu \frac{du}{dy}$, according to the viscosity law valid for Newtonian fluids. The stress tensor is symmetric $\tau_{ij} = \tau_{ji}$, Lautrup.

$$\tau' = \begin{bmatrix} \tau_{xx} & \tau_{xy} & \tau_{xz} \\ \tau_{yx} & \tau_{yy} & \tau_{yz} \\ \tau_{zx} & \tau_{zy} & \tau_{zz} \end{bmatrix} = \begin{bmatrix} -p & \mu \frac{du}{dy} & 0 \\ \mu \frac{du}{dy} & -p & 0 \\ 0 & 0 & -p \end{bmatrix} \tag{2.8}$$

  Calculating the divergence of the product $\mathbf{u} \cdot \tau'$ yields

$$\boldsymbol{\nabla} \cdot (\mathbf{u} \cdot \tau') = \boldsymbol{\nabla} \cdot \left(-up, \; u\mu \frac{du}{dy}, \; 0 \right) \tag{2.9}$$

$$= -u \frac{dp}{dx} + \mu \left[\left(\frac{du}{dy} \right)^2 + u \frac{d^2 u}{dy^2} \right] \tag{2.10}$$

  Eq. (2.10) may be simplified using by the Navier-Stokes equation for the same problem. The last term on the right hand side is the power that the electrical force adds to the fluid with charge density ρ_E.

$$0 = -\frac{dp}{dx} + \frac{d\tau_{xy}}{dy} + \rho_E E \tag{2.11}$$

$$-\rho_E E = -\frac{dp}{dx} + \mu \frac{d^2 u}{dy^2} \tag{2.12}$$

  By multiplying Eq. (2.12) with u and inserting in Eq. (2.10) we obtain

$$\boldsymbol{\nabla} \cdot (\mathbf{u} \cdot \tau') = \mu \left(\frac{du}{dy} \right)^2 - u \rho_E E \tag{2.13}$$

- **Heat transport**
  The heat transport is only calculated for the liquid, but in order to be of practical relevance, the problem should be expanded to include the walls (planes). The present analysis is done for the fluid only.

$$\rho c_p \boldsymbol{\nabla} \cdot (D_{\text{heat}} \boldsymbol{\nabla} T) = \rho c_p D_{\text{heat}} \frac{d^2 T}{dy^2} \tag{2.14}$$

- **Ohmic heating**
  The ohmic heating P is given as

$$P = \lambda_{\text{elec}} E^2 \tag{2.15}$$

  For a Debye layer of finite thickness, some corrections should be made to the conductivity, Rice and Whitehead, 1965.

The final energy equation is

$$0 = \mu \left(\frac{du}{dy} \right)^2 - u \rho_E E + \rho c_p D_{\text{heat}} \frac{d^2 T}{dy^2} + \lambda_{\text{elec}} E^2 \tag{2.16}$$

The first term is always positive and may be interpreted as the viscous dissipation. The second term is always negative. It is equivalent to the mechanical power that the EOF generates. The third term is the heat transport which must balance the other terms in thermal equilibrium. The last term is the ohmic heating. In case of an applied pressure gradient, this will enter the equation by the first term, i.e., viscous dissipation.

2.3 The Electric Double Layer

The basis of electroosmotic (EO) pumps is the formation and manipulation of electric double layers (EDL). It is very important to understand the underlaying physics in order to make good approximations. As a starting point, we consider the charge transport in a liquid.

The flux of a charged species $\mathbf{J}$ is governed by different effects. The general description of these phenomena is governed by a general potential as a function of pressure, temperature, electric state, concentrations, composition of phases, etc. An analytical description, however, is not feasible due to the nonlinear characteristics of the potential. If the electrolyte is dilute this is not a problem, because then the transport effects may be linearly superposed.

The involved transport processes are electromigration, diffusion, and convection. If a charged species is subjected to an electric field it will migrate, i.e., electromigration. If we neglect the effects of external and induced magnetic fields, we obtain the following form of the Nernst-Planck equation, Probstein

$$\mathbf{J}_i = -\alpha_i z_i c_i \boldsymbol{\nabla} \phi - D_{\text{mass,i}} \boldsymbol{\nabla} c_i + c_i \mathbf{u}, \tag{2.17}$$

where $\mathbf{J}_i$ is the molar flux of the i-th species due to electromigration, mass diffusion and convection in that order. The mobility is related to the mass diffusivity $D_{\text{mass,i}}$ and the thermal energy kT as $\alpha_i = eD_{\text{mass,i}}/(kT)$. Eq. (2.17)

is only valid for dilute concentrations. Hence, in the following analysis the electrolytes are assumed to be dilute.

If we consider a charged surface in contact with a dilute, fully dissociated salt, the charged surface will attract the ions of the opposite charge, the so-called counterions. Hence, an area will exist where the concentration of counterions is larger than that of the coions [3]. This phenomena leads to the formation of an electric double layer, or Debye layer. In Fig. 2.1 the wall charge is negative. The double term refers to the fact that there are two layers. The inner layer, which is immobile due to strong electrical forces, and the outer layer, the diffusive layer, which may be affected by an external electric field. The surface charge arises from chemical reactions as discussed in Sec. 2.7.

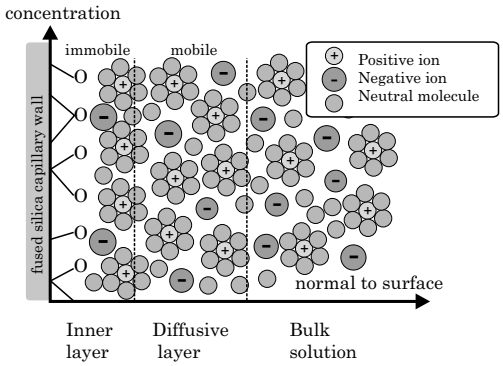

Figure 2.1: Structure of electric double layer with an inner immobile layer. The system consisting of wall and liquid is electrical neutral. The diffuse layer is mobile and can therefore be manipulated by an external electric field. The positive ions are hydrated. Some of the negative ions are specifically adsorbed at the surface, Keith *et al.*

2.4 Thickness λ_D of the Double Layer

The thickness of the electrical double layer is governed by a balance between diffusion and electrical forces. The length is also known in the literature as the Debye length. It is a characteristic length scale for the electrical screening. First we introduce the electrochemical potential $\overline{\mu}_{\mathrm{chem},i}$, which is the free energy of the last arrived particle. It consists of an electric and chemical potential. The gradient of the electrochemical potential must be zero in equilibrium, i.e., steady state. If this was not the case, a flow would be induced. The chemical potential is given as

$$\mu_{\mathrm{chem},i} = \mu^0_{\mathrm{chem},i} + kT \ln n_i, \tag{2.18}$$

where $n_i = c_i/c_i^0$ is the concentration of ions relative to a reference concentration. $\mu^0_{\mathrm{chem},i}$ is the standard chemical potential which is equal to the chemical potential when $n_i = 1$. The Debye length is found by balancing repulsive diffusive forces with attractive electrical forces, which is the same as requiring $\boldsymbol{\nabla}\overline{\mu}_i = 0$.

$$\boldsymbol{\nabla}\overline{\mu}_i = \boldsymbol{\nabla}\mu_{\mathrm{chem,i}} + z_i e \boldsymbol{\nabla}\phi, \tag{2.19}$$

$$\boldsymbol{\nabla}\mu_{\mathrm{chem,i}} = -z_i e \boldsymbol{\nabla}\phi, \tag{2.20}$$

In one dimension we get

$$\frac{d\mu_{\mathrm{chem}},i}{dx} = -z_i e \frac{d\phi}{dx}. \tag{2.21}$$

[3] The charges of the coions have the same sign as the charges of the surface.

Inserting Eq. (2.18) into Eq. (2.21) yields

$$\frac{1}{n_i}\frac{dn_i}{dx} = -\frac{z_i e}{kT}\frac{d\phi}{dx}. \tag{2.22}$$

Integrating Eq. (2.22), the Boltzmann distribution (2.24) is obtained by requiring that $\phi = 0$ when $n_i = 1$. This is equal to setting $c_i = c_i^0$, where the latter is the salt concentration of the bulk fluid.

$$n_i = \exp(-\frac{z_i e}{kT}\phi), \tag{2.23}$$

$$c_i = c_i^0 \exp(-\frac{z_i e}{kT}\phi). \tag{2.24}$$

The Debye layer is not electrically neutral. Hence, the Poisson equation, which states the relation between the electric field and the charge density, is invoked. For simplicity the dielectric constant is assumed spatially invariant, and hence reduces Eq. (2.25a) to Eq. (2.25b). This approximation is not very good because of the strong polarization effects in the Debye layer. The problem is discussed in Sec. 2.6.

$$\boldsymbol{\nabla}\cdot(\epsilon\boldsymbol{\nabla}\phi) = -\rho_E, \tag{2.25a}$$

$$\boldsymbol{\nabla}^2\phi = -\frac{\rho_E}{\epsilon} \tag{2.25b}$$

The charge density is inserted in the Poisson equation Eq. (2.25b) along with the Boltzmann distribution, Eq. (2.24).

$$\frac{d^2\phi}{dx^2} = -\frac{1}{\epsilon}\sum c_i z_i e \tag{2.26}$$

This is a nonlinear differential equation, due to the exponential terms on the right-hand side. The solutions will be discussed in Sec. 2.5. For now we will use the Debye-Hückel approximation $\frac{z_i\phi}{kT} \ll 1$, in which case $\exp(\frac{z_i\phi}{kT}) \approx 1 - \frac{z_i\phi}{kT}$.

$$\frac{d^2\phi}{dx^2} = -\frac{1}{\epsilon}\sum c_i^0(1 - \frac{z_i e\phi}{kT}) \tag{2.27a}$$

$$= -\frac{1}{\epsilon}\Big(\sum e c_i^0 z_i - \sum c_i^0 z_i^2 e^2 \frac{\phi}{kT}\Big) z_i e \tag{2.27b}$$

$$= \frac{e^2}{\epsilon kT}(\sum z_i^2 c_i^0)\phi \tag{2.27c}$$

$$= \kappa^2\phi. \tag{2.27d}$$

In the Eq. (2.27b), the first sum is zero because the bulk liquid is electrically neutral. In the last equation, the term in front of ϕ contains a characteristic length scale, $1/\kappa = \lambda_D$, which is the Debye length. The Debye length is also a measure for the thickness of the double layer.

$$\lambda_D = \frac{1}{\kappa} = \sqrt{\frac{\epsilon kT}{e^2\sum z_i^2 c_i^0}} \tag{2.28a}$$

$$= \sqrt{\frac{\epsilon kT}{2e^2 z^2 c}} \tag{2.28b}$$

In Eq. (2.28b), the salt is assumed symmetric for simplicity. The error by making this approximation is quite small, since the concentration of the counterions is much larger than that of the coions.

The thickness of the double layer depends on the temperature T, concentration c and valence number z of the ions. At a distance of approximately $3\lambda_D$, the potential will be reduced to 2% of its near surface value.

At high temperatures the ions move quickly which leads to a decrease in the shielding since they are dispersed more. For high concentrations the shielding is more effective because the charge density is larger.

The double layer thickness is dependent on the concentration of the buffer, $\lambda_D = 1.09 \times 10^{-9}\epsilon(z\sqrt{c})^{-1}$ at room temperature. Hence, if the buffer concentration or the ionic strength[4] is increased, the double layer is compressed. This affects the potential distribution, and the zeta potential is reduced.

The zeta potential is expected to become larger (in magnitude) for small electrolyte concentrations.

Example: *Thickness of Double Layer*
At a temperature of 25^oC, the above expression computes to $\lambda_D = 9.61 \times 10^{-9}(z\sqrt{c})^{-1}$, where the dielectric constant for water has been used: $\epsilon = 78.3\epsilon_0$. For a concentration of 10^2 mol/m^3 (0.1M), $\lambda_D = 0.961$ nm. So in this case, the EDL is no more than approximately 10 atoms wide.

2.5 The Electric Potential

Consider a circular capillary filled with an aqueous solution. At the solid-liquid interface an EDL is formed. The ion concentrations c_i are connected with the electric potential ϕ through the Poisson equation, Eq. (2.25b). The capillary length is assumed to be much larger than the radius. Adopting cylindrical coordinates with x as the longitudinal coordinate, the $\frac{\partial^2}{\partial x^2}$-terms may be neglected because variation is very small compared to the radial variation. Furthermore, the solution is assumed symmetric, so the angular variation is also disregarded.

$$\frac{1}{r}\frac{\partial}{\partial r}\left(r\frac{\partial \phi}{\partial r}\right) = -\frac{\rho_E}{\epsilon} \tag{2.29a}$$

$$= -\frac{Fz}{\epsilon}(c_+ - c_-). \tag{2.29b}$$

It is convenient to split up the potential in two parts. A radial component $\psi(x, r)$ and a longitudinal component $\Phi(x)$.

$$\phi(x, r) = \Phi(x) + \psi(x, r) \tag{2.30}$$

In order to find the concentrations, the ion flux is considered. In equilibrium the radial flux of ions must be zero. This requirement is inserted into the Nernst-Planck equation, Eq. (2.17). By integrating the radial component of the Nernst-Planck equation and using that the diffusivity is $D_{\text{mass}} = RT\alpha$, the Boltzmann

[4] Ionic strength is a quantity representing interactions of ions with water molecules and other ions in a solution $I = \frac{1}{2}\sum z_i^2 n_i$.

distribution is obtained

$$0 = -\frac{z}{RT} D_{\text{mass}} F c \frac{\partial \psi}{\partial r} - D_{\text{mass}} \frac{\partial c}{\partial r}, \tag{2.31}$$

$$\frac{z}{RT} F \frac{\partial \psi}{\partial r} = -\frac{1}{c} \frac{\partial c}{\partial r}, \tag{2.32}$$

$$-\frac{z}{RT} F \psi = \ln(c) + \text{const}, \tag{2.33}$$

$$c_{\pm} = c_0 \exp\left(\mp \frac{zF\psi}{RT} \right), \tag{2.34}$$

where α is the mobility of the ions. By inserting the Boltzmann distribution Eq. (2.34) in Eq. (2.29b), the following nonlinear second order ordinary differential equation (ODE) arises. For simplicity, the variables have been made dimensionless, $r^* = r/a, \lambda^* = \lambda_D/a$ and $\psi^* = zF\psi/(RT)$.

$$\lambda^{*\,2} \frac{1}{r^*} \frac{\partial}{\partial r^*} \left(r^* \frac{\partial \psi^*}{\partial r^*} \right) = \sinh(\psi^*). \tag{2.35}$$

In combination with the boundary conditions this forms a nonlinear boundary value problem (BVP).

$$\frac{\partial \psi^*}{\partial r^*} = 0, \quad \text{at} \quad r^* = 0, \tag{2.36}$$

$$\psi^* = \zeta^*, \quad \text{at} \quad r^* = 1. \tag{2.37}$$

The zeta potential will be explained in Sec. 2.7 for now it is simply the potential at the wall interface.

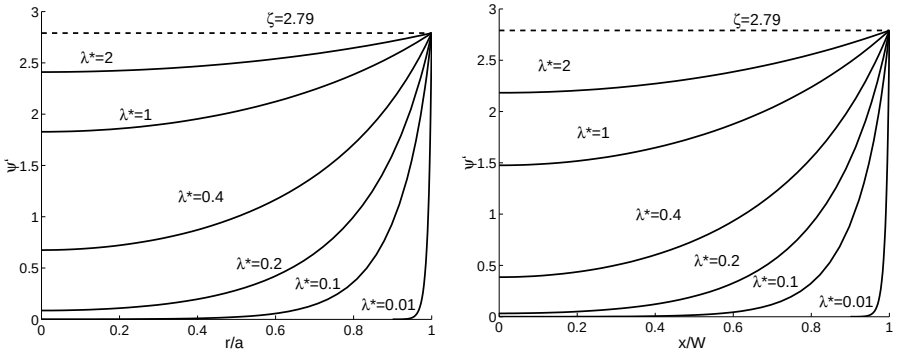

Figure 2.2: Nondimensional screening potential ψ^* in two different geometries: (a) In a radial channel where the length scale is the radius of the channel. (b) Potentials between two planes where the length scale is half the spacing of the planes.

In Fig. 2.2 the potentials have been calculated for different values of λ^* using the program in Appendix D, Potential solver. Two geometries are considered. A circular capillary in Fig. 2.2(a), and a one dimensional parallel plate geometry in Fig. 2.2(b). In the large cases of λ, the potential equals the zeta potential across the entire channel width. For small values of λ the potential is zero everywhere

except near the boundaries. This illustrates the different shielding effects. For small ratios the bulk flow is completely shielded, refer to Sec. 2.4. This will often be the case, since the Debye length is very small compared to most capillaries.

An analytical solution for the potential may be obtained by linearizing the right-hand side of Eq. (2.35), and the double layer thickness $\lambda_D \ll a$ must be small compared to the radius of the capillary. Hence curvature effects can be neglected. This is termed the Debye-Hückel approximation. The result is a simple exponential function. This result also emerges from the linearized parallel planes case, as this is the exact same case when the curvature effects are neglected.

$$\psi = \zeta \exp\big(-\frac{a-r}{\lambda_D}\big). \tag{2.38}$$

2.6 The Helmholtz-Smoluchowski velocity

The purpose of this section is to find the velocity as a function of an external electric field. The concepts introduced here are essential for a description of electroosmotic flow.

"Electroosmosis is the movement of liquid relative to a stationary charged surface (e.g., a capillary or porous plug) by an electric field. The pressure necessary to counterbalance electroosmotic flow is termed the electroosmotic pressure", Shaw. The equation governing the flow is the well known Navier-Stokes Eq. (2.3b).

Since the length scale of the Debye layer is very small $\lambda_D \approx 1-10$ nm the corresponding Reynolds number is of the order $Re \approx 10^{-6}$. Hence the inertial forces may be neglected in the boundary layer (diffusive layer). A discussion of inertia forces and Reynolds numbers can be found in Sec. 3.1. So the problem is reduced to a balance between electric forces and viscous forces. The maximum velocity in the boundary layer is then used as a boundary condition for the bulk flow. Introducing Poisons equation to eliminate the charge density ρ_E

$$\begin{aligned} \mu\boldsymbol{\nabla}^2\mathbf{u} &= \rho_E \boldsymbol{\nabla}\phi_a & (2.39)\\ &= -\epsilon\big(\boldsymbol{\nabla}^2\phi\big)\boldsymbol{\nabla}\phi_a & (2.40) \end{aligned}$$

To identify nonessential terms the x and y coordinates are scaled by the radius a and the Debye length λ_D respectively,

$$\begin{aligned} x &= a\,\tau, & (2.41)\\ y &= \lambda_D\,\eta. & (2.42) \end{aligned}$$

The Laplace operator of the intrinsic potential and the gradient of the applied potential in Eq. (2.40) are computed separately in Eqs. 2.43b and 2.43c. Note that the tangential term in the gradient of the intrinsic potential is expressed by means of the applied potential. Its magnitude is proportional to the applied field by the factor χ. This is a correction factor due to the polarization of the dielectric liquid within the Debye layer. The electric field in the Debye layer $E \approx 10^7$ V/m is much larger than the applied field $E \approx 10^4$ V/m. The terms

computes to

$$\boldsymbol{\nabla}\phi_i = \left(\frac{\chi}{a}\frac{\partial\phi_a}{\partial\tau}, \frac{1}{\lambda}\frac{\partial\phi_i}{\partial\eta}\right), \tag{2.43a}$$

$$\boldsymbol{\nabla}^2\phi_i = \frac{\chi}{a^2}\frac{\partial^2\phi_a}{\partial\tau^2} + \frac{1}{\lambda^2}\frac{\partial^2\phi_i}{\partial\eta^2}, \tag{2.43b}$$

$$\boldsymbol{\nabla}^2\mathbf{u} = \left(\frac{1}{a^2}\frac{\partial^2 u}{\partial\tau^2} + \frac{1}{\lambda^2}\frac{\partial^2 u}{\partial\eta^2}, \frac{1}{a^2}\frac{\partial^2 v}{\partial\tau^2} + \frac{1}{\lambda^2}\frac{\partial^2 v}{\partial\eta^2}\right). \tag{2.43c}$$

A value of the χ-factor is difficult to obtain. A more detailed physical description of the Debye layer is required. This is beyond the scope of the this analysis, but the χ-factor can be incorporated in an suitable choice of the dielectric constant for the Debye layer, in the following just denoted ϵ.

Collecting terms in the tangential direction, and neglecting terms of order λ/a or higher Eq. (2.40) becomes

$$\mu\frac{\partial^2 u}{\partial\eta^2} = -\epsilon\frac{d\phi_a}{dx}\frac{\partial^2\phi_i}{\partial\eta^2}. \tag{2.44}$$

Note that the gradient of the applied field is given in the x-y coordinates. By double integration with respect to η and use of the conditions $\frac{\partial u}{\partial\eta} = \frac{\partial\phi_i}{\partial\eta} = 0$ as $y \to \infty$ and that $\phi_i = \zeta$ at $u = 0$, the integrated equation yields the very important relation,

$$u_{\text{eo}} = \frac{\epsilon\zeta}{\mu}\frac{d\phi_a}{dx} = \alpha_{\text{eo}}E_x, \tag{2.45}$$

$$\alpha_{\text{eo}} = -\frac{\epsilon\zeta}{\mu}, \tag{2.46}$$

which is the Helmholtz-Smoluchowski relation, refer Fig. 2.3. Eq. (2.45) is also known as the electroosmotic velocity, where α_{eo} is the EO mobility and E_x the electric field. Recent research has shown that the zeta potential is ambiguous in that sense that for one mobility there may be two corresponding zeta potentials, Hunter 2001. It is therefore important to emphasize that it is the EO mobility α_{eo} that is important with respect to EO pumps.

The electric field is given by the potential and the electrode separation. If a dielectric is present the field is unchanged, but the charges at the electrodes are increased in magnitude. One should be careful not to confuse this setup with an isolated capacitor, with fixed charges, in which the field is reduced because of the dielectric.

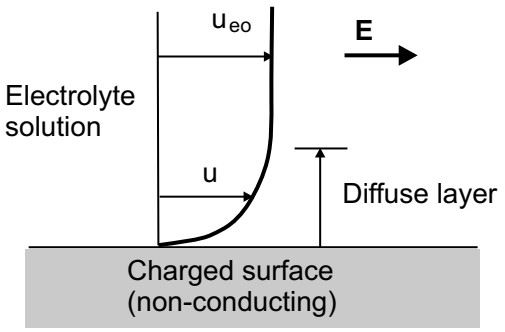

Figure 2.3: Flow produced by an electric field acting on a charged diffuse double layer. The electroosmotic velocity is denoted $u_{\rm eo} = \alpha_{\rm eo}\, E$. There is overall charge neutrality.

Example: *EO velocity*
From an experiment conducted by Cummings *et al.*, 2000. The applied electric field is 50 V over 20 mm. $E_x = 2.5{\times}10^3$ V/m. The zeta potential, $\zeta = -100$ mV so $u_{\rm eo} = 200$ μm/s. The dielectric constant is $\epsilon = 78.3\ \epsilon_0$ and the dynamic viscosity $\mu = 1.0 \times 10^{-3}$ kg (m s)$^{-1}$ are those of water at room temperature.

2.7 The Zeta Potential

The thickness of the double layer is given by the Debye length λ_D. The derivation of the Debye length was based on the assumption that the ions are points. In real life the ions are not that small compared with the Debye length. So when considering the boundary condition for the potential, we must have a more accurate description. The center of the inner most ions are in a finite distance from the surface. This inner layer is called the Stern layer, Fig. 2.4. This layer is bounded by strong electrostatic forces $E \approx 10^7 - 10^8$ V/m and hence is immobile. The counterions are attracted to the surface and in this way screening the surface charge.

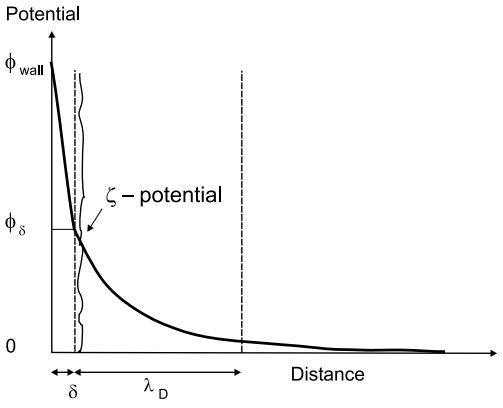

Figure 2.4: Structure of electric potential in the double layer with inner Stern layer. The thickness of the Stern layer is approximately the width of an atom $\delta \approx 0.1$ nm. The zeta potential is defined at the surface of shear. In other words where the ions start to move, Probstein.

The zeta potential is defined as the potential difference across the Debye layer from the shear surface between the charged surface and the electrolyte to the far field (zero), Probstein. The zeta potential is typically of the order

$\zeta \approx 1 - 200$ mV. The system, liquid and surface, is electrically neutral. So the wall charge must equal that of the fluid charge with opposite sign. Far away from the wall, the fluid is electrically neutral, Adamson and Gast.

We are considering glass as the main material that the capillaries are made of. Other materials such as polymers (e.g., PMMA) can also be used. Such materials are interesting with respect to mass production and fast prototyping, but glass/siliconoxide offers the highest level of refinement available, i.e., the most accurate structures.

If siliconoxide (silica or quartz) is immersed in water, the potential is generated by a chemical reaction at the surface. The silanol groups SiOH are changed to either $SiOH_2^+$ or SiO^- depending on the buffers pH value, Fig. 2.5.

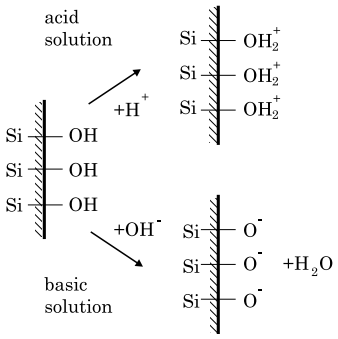

Figure 2.5: Chemical reactions for Silicon in aqueous mediums with different pH. Silanol groups react with the ions in the aqueous solution, creating an excess of charge at the surface.

In this way the zeta potential may be varied by the pH of the buffer solution. At the some pH-level, point of zero charge (PZC), the wall potential is zero. For high pH levels the change in EO mobility is marginal. A suitable choice of the buffers pH-value must be considered in order to have effective electroosmotic pumping.

$$\mathrm{SiOH} + \mathrm{H}^+ \rightarrow \mathrm{SiOH}_2^+ \tag{2.47}$$

$$\mathrm{SiOH} + \mathrm{OH}^- \rightarrow \mathrm{SiO}^- + \mathrm{H_2O} \tag{2.48}$$

$$\mathrm{pK_a}(-\mathrm{SiOH}) \approx 6 \tag{2.49}$$

2.8 Diffusion of Mass and Momentum

Mass Diffusion

If two mixable liquids are placed together, they will mix without any stirring. The process is called mass diffusion. Later in the report a pump that utilizes two liquids will be presented. Hence, it will be useful to introduce some of the basic knowledge about diffusion.

The diffusion of mass is related to the mobility of molecules within the liquid. A large diffusion coefficient D_{mass} means that molecules are relatively free to move. The movement can be described as a series of short jumps - random walk, Atkins [6]. The root means square average d of the position is given as

$$d = \sqrt{2D_{\mathrm{mass}}\, t}. \tag{2.50}$$

Example: *Travelling Molecules*
The Diffusion coefficient for water is $2.26 \times 10^{-9}\mathrm{m}^2/\mathrm{s}$ at room temperature. Then the average molecule travels 2 cm away from its origin in a day. This may seem surprisingly low and in practice there will nearly always be some convective motion.

Returning to the concept of the random walker the diffusion coefficient may be expressed as

$$D_{\mathrm{mass}} \approx \frac{\ell^2}{\tau_{\mathrm{col}}} = \ell \; u_{\mathrm{molecule}} \tag{2.51}$$

Where ℓ is the mean free path between collisions, τ_{col} is the time between the collisions, and u_{molecule} is the average velocity. The diffusivity increases with temperature, since the average velocity is $u_{\mathrm{molecule}} \propto \sqrt{T}$. The molecular diffusion increases with temperature, because the molecules can then more easily escape from the attractive forces exerted by their neighbors. In general, the molecules in a fluid have kinetic energies comparable with the intermolecular potential energy. A pair distribution function g may be defined as the probability of finding a molecule in the range δr. For a crystal lattice the g-function has sharp peaks, indicating neighboring molecules. For a fluid the g-function is smeared out increasingly with temperature. The probability for a molecule to jump to a vacant lattice site[5] is thought to follow an Arrhenius temperature dependence, Eq. (2.52), Atkins, [6]. The diffusion D_{mass} is increasing with temperature T,

$$D_{\mathrm{mass}} = D^o_{\mathrm{mass}} \exp\left(-\frac{\Delta G}{RT}\right). \tag{2.52}$$

The problem with this theory is that the intermolecular potential ΔG is a purely an empirical constant and widely, debated as in the article by Alder and Hildebrand, (Activation Energy: Not Involved in Transport Processes in Liquids, 1973). However, the activation energy theory is quite common because of its good agreement with experiments, Atkins, [6]. The viscosity is related to the mass diffusion coefficient, as we shall see later.

Viscosity

A Newtonian fluid is defined as a fluid in which the relation between shear stress and rates of strain is linear. This is a constitutive relation because it gives a relation between applied force and deformation.

For convenience the two types of viscosity are defined in Eq. (2.53). ν is the kinematic viscosity, μ is the dynamic viscosity and ρ is the density of the fluid

$$\nu = \frac{\mu}{\rho}. \tag{2.53}$$

The kinematic viscosity may be considered as the diffusion coefficient for momentum. The diffusion constants have the same unit. The kinematic viscosity

[5] Molecules in liquids are not ordered as molecules in solids. However we will adopt this description as an best approximation.

is related to the mass diffusion coefficient D_{mass}. If the D_{mass} increases, the molecules will be more mobile, and hence transfer more momentum. Thus, the viscosity should show the same temperature dependence as the mass diffusivity, Table 2.1.

Species	Temperature °C	ν m^2/s	D_{mass} m^2/s
Water	5	1.51×10^{-6}	1.31×10^{-9} (self-diffusion)
Water	15	1.14×10^{-6}	1.78×10^{-9} (self-diffusion)
Water	25	0.890×10^{-6}	2.26×10^{-9} (self-diffusion)
Water	35	0.723×10^{-6}	2.92×10^{-9} (self-diffusion)
Water	45	0.602×10^{-6}	3.56×10^{-9} (self-diffusion)
Water	50	0.547×10^{-6}	-
Water	100	0.30×10^{-6}	-
Ethanol	25	1.07×10^{-6}	1.24×10^{-9} (in water)
Glycine	25	-	1.06×10^{-9} (in water)
Dextrose	25	-	0.673×10^{-9} (in water)
Sucrose	25	-	0.522×10^{-9} (in water)

Table 2.1: Diffusion and viscosity constants, Atkins [7], Mills.

Mass diffusion and Viscosity

We have now described both mass diffusion and momentum diffusion (viscosity). From this description it is clear that some relation must exist between the diffusion coefficient D_{mass} and the mobility of the molecules. This empirical relation is the Einstein relation.

$$\left.\begin{array}{rl} D_{\text{mass}} = & \frac{\alpha RT}{zF} \\ \alpha = & \frac{ez}{f} \end{array}\right\} D_{\text{mass}} = \frac{RT}{fN_A} = \frac{kT}{f} \tag{2.54}$$

If one assumes that the frictional drag for the molecule travelling through the liquid is proportional to the velocity, Stokes Law, $f = 6\pi\mu a$, may be applied. The dimension of f is force per velocity. Experiments using magnetic resonance have shown that results will at least be of the right order of magnitude, Atkins, [7]. From these assumptions the Stokes-Einstein equation emerges, Eq. 2.55. This is the missing link between diffusivity and viscosity under the given assumptions.

$$D_{\text{mass}} = \frac{kT}{6\pi\mu a}, \tag{2.55}$$

where a is the effective radius of the ion, μ the dynamic viscosity, k the Boltzmann constant and T the temperature of the liquid.

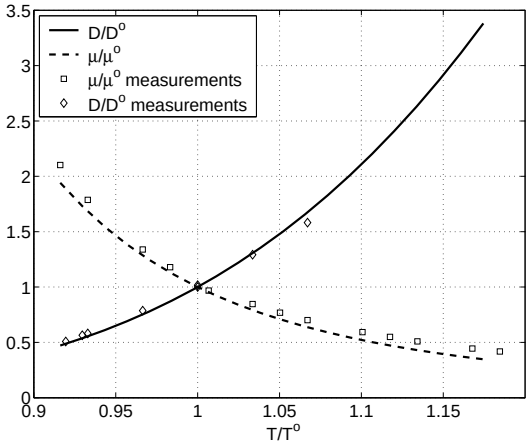

Figure 2.6: Diffusivity and dynamic viscosity calculated using the Arrhenius and Stokes-Einstein relations, Eqs. (2.52) and (2.55). The best fit was obtained with $\frac{G}{RT^o} = 8$ where $T^o = 298K$. Values are made nondimensional with values at $T^o = 298K$.

2.9 Thermal Diffusion

Thermal diffusion is different from mass diffusion. In thermal diffusion the interaction between molecules is considered. If a material is a good heat conductor, it will have a large thermal diffusion coefficient. In many liquids heat will be transported by means of convection. This phenomenon is not interesting in this context.

$$\lambda_{\text{heat}} = \frac{D_{\text{heat}}}{\rho c_p} \tag{2.56}$$

where λ_{heat} is the heat transfer coefficient, and c_p is the heat capacity for constant pressure. Generally, if a material is a good heat conductor, it will also be a good electrical conductor.

	T K	ρ kg/m^3	c_p kJ/(kgK)	λ_{heat} W/(mK)	D_{heat} m^2/s
Water	300	998	4.18	0.56	$1.3 \cdot 10^{-7}$
Ethanol	300	789	2.43	0.17	$8.9 \cdot 10^{-8}$
Glycerol	300	1261	2.43	0.29	$9.5 \cdot 10^{-8}$

Table 2.2: T is the temperature, ρ is the density, c_p is the heat capacity, λ_{heat} is the thermal conductivity, and D_{heat} is the thermal diffusivity, Andersen.

2.10 Mass Diffusion

Miscible Liquids

If two miscible liquids are placed adjacent to each other, diffusion will occur until there are no gradients in the concentration. The mathematical formulation of this phenomenon is the diffusion equation. A number expressing the importance of diffusion compared to convection is the Peclet number

$$Pe_{\text{mass}} = \frac{L\ u}{D_{\text{mass}}}. \tag{2.57}$$

For small Peclet numbers $Pe_{\text{mass}} < 1$, diffusion is the dominating effect. This can easily be the case in microfluidics.

Consider a channel with two miscible liquids A and B. Liquid A occupies the fraction a/W of the channel and liquid B occupies the rest. This is the initial condition (IC). The boundary value problem (BVP) requires an IC with continuous derivatives Eq. (2.58d) for mathematical reasons. The BCs are homogeneous Neumann conditions. A Neumann boundary condition sets a value for the derivative. The BVP, Eq. (2.58), may be solved analytically, Strauss,

$$\begin{aligned}
\text{PDE} \quad & \frac{\partial c}{\partial t} - D_{\text{mass}} \frac{\partial^2 c}{\partial x^2} = 0, && (2.58a)\\
\text{BC1} \quad & \frac{\partial}{\partial t} c(0,t) = 0, && (2.58b)\\
\text{BC2} \quad & \frac{\partial}{\partial t} c(W,t) = 0, && (2.58c)\\
\text{IC} \quad & c_{\text{IC}}(x) = 0.5 \left(1 + \tanh\left[\frac{\gamma}{W}(x-a)\right]\right), && (2.58d)
\end{aligned}$$

where γ determines the steepness of the initial condition. Using a Fourier expansion we get

$$c(x,t) = \frac{1}{2}A_0 + \sum_{n=1}^{\infty} A_n \exp\Big[- D_{\text{mass}} t \big(\frac{n\pi}{W}\big)^2 \Big] \cos\big(\frac{n\pi x}{W}\big), \qquad (2.59)$$

where the Fourier coefficients

$$A_n = \frac{2}{W} \int_0^W c_{\text{IC}}(x) \cos(\frac{n\pi x}{W}) dx, \qquad (2.60)$$

are found by numerical integration, Appendix D, Diffusion. An important feature in the solution is the characteristic time scale that emerge, $t^o = \frac{W^2}{D_{\text{mass}}}$. This time scale governs the problem entirely, and may be used to evaluate the importance of diffusion in laminar flow.

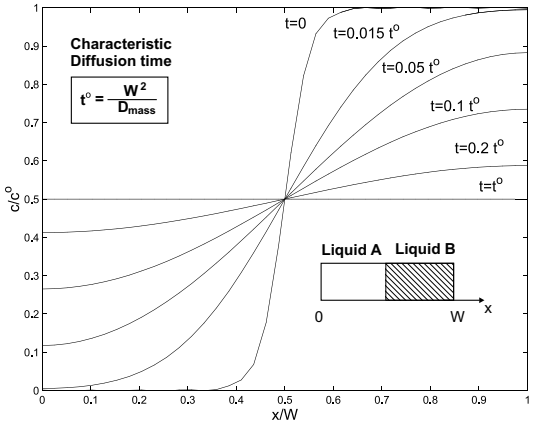

Figure 2.7: Time evolution of the concentration in a narrow channel. If the width $W = 10\ \mu$m and the self-diffusion constant for water, $D_{\text{mass}} = 2.26 \times 10^{-9}\text{m}^2/\text{s}$, was used, then $t^o = 0.044\ s$. The diffusion is very fast for this small length scale.

Immiscible Liquids

The other case is two immiscible liquids. Two liquids will not mix if one of them is polar and the other is nonpolar. If the solution is stirred, the phases will be

mixed on a macroscopic level, but after a period of time the original phases will be restored. The most well-known example of two such immiscible liquids are water (polar) and oil (nonpolar). The interface between the two phases is very thin, i.e., only a few layers of molecules. The properties of molecules and ions in this layer differ essentially from the properties in the bulk volume, Shaposhnikova, 1999. The properties at the interface are not relevant in the scope of this report, and may be disregarded.

2.11 Conductivity of Liquids

Calculating the electric current flux includes knowledge of the ion concentration distribution. Three terms are important: the electromigration, diffusion and convection. Electromigration will be the dominant term since no longitudinal charge gradients are expected.

$$\mathbf{I} = -F^2 \boldsymbol{\nabla}\phi \sum z_i^2 \alpha_i c_i - F \sum z_i D_i \boldsymbol{\nabla} c_i + F\mathbf{u} \sum z_i c_i. \tag{2.61}$$

The electroosmotic flow speed is proportional to the electric field under some conditions. An approximate velocity is given by the Helmholtz-Smoluchowski relation. Increasing the electroosmotic flow speed can therefore be done by increasing the field. The fluid will be heated by the electrical current due to the resistivity. The heating of the fluid may not be desirable, because it could damage some biological samples being transported.

The conductivity of an ion solution is governed by the electrolyte, the temperature and the concentration. The charged ions are affected by the electric field. Hence, they will obtain an ordered migration velocity. This velocity is governed by a balance between inelastic collisions and the electrical force acting on an ion, Probstein.

For dilute solutions the Kohlrausch's law of the independent migration of ions apply. This law states that the conductivities may be superposed linearly for a solution.

Cations	λ^o_{elec} cm^2 S/mol	Anions	λ^o_{elec} cm^2 S/mol
Ba^{2+}	127.2	Br^-	78.1
Ca^{2+}	119.0	SO_4^{2-}	160.0
Na^+	50.1	Cl^-	76.35
K^+	73.5	NO_3^-	71.46
H^+	349.6	OH^-	199.1

Table 2.3: Limiting ionic molar conductivities in water at $T = 298$ K, Atkins, [7]. The conductivity is obtained by multiplying the concentration with the molar conductivity.

From Table 2.3 and Eq. (2.62) the ionic mobilities may be calculated, in particular the electrophoretic mobility α_{ep},

$$\alpha_{\text{ep}} = \frac{\lambda_{\text{elec}}}{zF}. \tag{2.62}$$

Kohlrausch' law applies only for very dilute solutions. So for higher concentrations the conductivity must be corrected by the following equation,

$$\lambda_{\text{elec}} = \lambda^0_{\text{elec}} - B\sqrt{c}. \tag{2.63}$$

λ^0_{elec} is the limit value for the molar conductivity. B is some constant determining the sensitivity of the concentration. Table values for some salts can be seen in table (2.4). Note that by summing the molar conductivities, e.g., for Na^+ and Cl^- in Table (2.3) one obtains the limit value for NaCl in Table (2.4).

Salt $[\lambda_{\text{elec}}] = \text{cm}^2/(\Omega\text{mol})$	1.0 mol/L	0.1 mol/L	0.01 mol/L	0.001 mol/L	≈ 0 mol/L
$AgNO_3$	77.8	109.09	124.68	130,45	133.4
Na_2SO_3	-	179.88	224.76	248.18	260.2
NaCl	85.8	106.69	118.45	123.68	126.5

Table 2.4: Molar conductivity for different salts. The rightmost column is the λ^o_{elec} values. The conductivity is obtained by multiplying the concentration with the molar conductivity, Andersen *et al.*

Example: *Electric resistance of a capillary*
A 10 mM ($c = 10$ mol/m^3) solution of Borax ($Na_2B_4O_7$) is considered. The radius of the capillary is $r = 100$ μm, and the length is $L = 1$ cm. Conductivity of the Borax solution $\lambda_{\text{elec}} = 3.41 \times 10^{-1}$ S/m, so the resistance is $R = \frac{L}{\pi r^2}\frac{1}{\lambda_{\text{elec}}} = 0.93$ MΩ.

2.12 Electroosmotic Mobility

As we saw in the previous section, the capillaries are likely to be heated considerably due to Joule heating. As we shall see later, the electroosmotic mobility may be approximated by the following relation,

$$\left.\begin{array}{rl} \alpha_{\text{eo}} = & \frac{\epsilon\zeta}{\mu} \\ \epsilon\psi_0 = & \sigma_0\lambda_D \\ \psi_0 \propto & \zeta \\ \lambda_D \propto & \sqrt{\epsilon T} \end{array}\right\} \alpha_{\text{eo}} \propto \frac{\sqrt{\epsilon T}}{\mu}. \tag{2.64}$$

where σ_0 is the surface charge density, and ψ_0 the surface potential. It is assumed that the surface charge density is independent of temperature, and that the zeta potential and the surface potential ψ_0 have the same temperature dependence. Furthermore, the equation is only a good approximation for small surface potentials $\psi_0 < 25$ mV. Hence, there are large uncertainties associated with the model. Experiments have shown indirectly that the EO mobility increases with temperature. From table values of ϵ and μ we may find the temperature dependence of α_{eo}. The values have been made dimensionless by values at a reference temperature, Fig. 2.8.

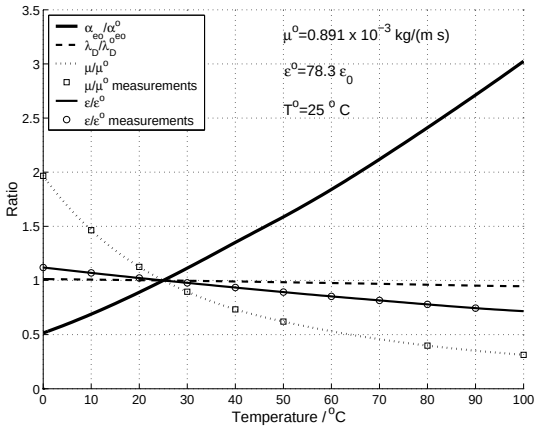

Figure 2.8: Various physical properties as functions of the temperature for water. Values have been made nondimensional by values at $T = 25^o$C. The curves are approximated by cubic splines. A typical value for $\alpha_{\text{eo}} = 0.06$ mm^2 (V s)$^{-1}$.

Example: *EO mobility Test Setup*
A simple experiment could be done in connection with the model. The heat problem can be solved analytically if the geometry is simple. Having EOF in a submerged circular capillary enables an analytical solution. With a fixed temperature on the outside of the capillary the stationary temperature within the capillary would be known. The analytical solution of the temperature is derived in Appendix H. The experiment could give measurements of the EO mobility as a function of the temperature.

Chapter 3

Elementary Flow Analysis

In this chapter we shall develop an understanding of flow analysis in microchannels, with emphasis on electroosmotic flow (EOF). The chapter is very important in relation to later analysis.

At first, a general analytical solution to a combined electroosmotic/pressure driven flow in circular capillary is obtained. The solution includes the effects of a finite Debye layer thickness. In the rest of the report the Debye layer is assumed infinitely thin unless otherwise is mentioned.

Secondly, analytical solutions to flow distributions in rectangular channels driven by electroosmosis and pressure are presented. The solutions for $u(x, y)$ are integrated, and relative flow rates Q^* are obtained. The relative flow rates are relevant in the subsequent flow analysis, mostly dealing with flow rates and pressures. A Q-p diagram for a pump is a plot of the flow rate versus pressure. The higher the counter pressure the lower the flow rate until the flow is stopped $Q = 0$ at the so-called backpressure.

Thirdly, we shall emphasize on some of the special characteristics of EOF.

Finally, the equivalent circuit theory is presented. The theory is conceptually identical to that of electric circuits. The introduced concepts are highly useful and are applicable to all of the considered designs.

3.1 Flow in a Circular Capillary

In this section we shall find the velocity distribution $u(x, y)$ without the infinitely thin Debye layer assumption. An analytical solution is possible due to the simple geometry. The electric potential and the corresponding charge distribution were found in Sec. 2.5.

The Navier-Stokes equation is applied to derive the velocity distribution in a circular capillary. The inertia terms have been neglected because of the creeping flow assumption. In creeping flow the Reynolds number is so small that inertia forces may be neglected. Simulations have shown that for Reynolds numbers below $Re < 5$, it virtually makes no difference whether or not inertia is included, Yang *et al.*, 2001.

Pressure needs to be included, because the entire capillary flow may not be

driven by electroosmosis.

$$0 = -\boldsymbol{\nabla} p + \mu \boldsymbol{\nabla}^2 \mathbf{u} - F(z_+ c_+ + z_- c_-)\boldsymbol{\nabla}\phi_a, \tag{3.1}$$

where the electric field has been replaced by minus the gradient of the applied potential ϕ_a. Using cylindrical coordinates for the axially symmetric capillary, we adopt (r, θ, x) with x in the direction of the flow. θ and r are in the angular and radial direction respectively. We are solving for the velocity in x-direction, $\mathbf{u} = (0, 0, u)$.

The mathematical form of Eq. (3.1) is a so-called inhomogeneous 2nd. order partial differential equation. The solution to the homogenous problem, $\boldsymbol{\nabla}^2 \mathbf{u} = 0$, is zero everywhere, so only the solution to the inhomogeneous problem is considered. The inhomogeneous terms, and hence the solution u, have no angular dependence.

The velocity profile is rotationally symmetric $\frac{\partial u}{\partial \theta} = 0$ and uniform $\frac{\partial u}{\partial x} = 0$, Eq. (3.1) becomes

$$\frac{\mu}{r}\frac{d}{dr}(r\frac{du}{dr}) = \frac{dp}{dx} + Fz(c_+ - c_-)\frac{d\phi_a}{dx}. \tag{3.2}$$

Using Eq. (2.29b) to eliminate the charge densities, one obtains the modified Navier-Stokes equation, which is then integrated with the appropriate boundary conditions.

$$\frac{\mu}{r}\frac{d}{dr}(r\frac{du}{dr}) = \frac{dp}{dx} - \frac{\epsilon}{r}\frac{d}{dr}(r\frac{d\psi}{dr})\frac{d\phi_a}{dx}, \tag{3.3a}$$

$$\left.\frac{du}{dr}\right|_{r=0} = 0, \quad \text{and} \quad \left.\frac{d\psi}{dr}\right|_{r=0} = 0, \tag{3.3b}$$

$$u(a) = 0, \quad \text{and} \quad \psi(a) = \zeta. \tag{3.3c}$$

The solution is

$$u(r) = -(\psi - \zeta)\frac{\epsilon}{\mu}\frac{d\phi_a}{dx} + \frac{r^2 - a^2}{4\mu}\frac{dp}{dx}. \tag{3.4}$$

Here the Debye-Hückel approximation Eq. (2.38) may be utilized for ψ, or more correctly the potentials given in Fig. 2.4. If the Debye-Hückel approximation is used, the equation becomes

$$u(r) = \frac{\epsilon\zeta}{\mu}\Big[1 - \exp\big(-\frac{a-r}{\lambda_D}\big)\Big]\frac{d\phi_a}{dx} + \frac{r^2 - a^2}{4\mu}\frac{dp}{dx}, \tag{3.5a}$$

$$Q = \frac{\epsilon\zeta}{\mu}\frac{d\phi_a}{dx}\pi a^2\Big(1 - 2\frac{\lambda_D}{a}\Big) - \frac{\pi a^4}{8\mu}\frac{dp}{dx}. \tag{3.5b}$$

Two important conclusions can be derived from Eq. (3.5b): (1) The flow rate, Q is reduced in the case of channel dimensions comparable with the Debye layer thickness. However Eq. (3.5b) is not valid for $a \approx \lambda_D$. (2) The flow rate induced by EO is proportional to $Q \propto a^2$, whereas the pressure driven flow is proportional to $Q \propto a^4$. Scaling of a capillary will therefore make EOF more effective in small capillaries. In the extreme case of uniform charge distribution (total Debye layer overlap), a parabolic flow profile will be induced, identical to that of pressure driven flow and $Q \propto a^4$.

3.2 Flow in a Rectangular Channel

In this section a wide range of flows in rectangular channels are investigated. In many microfluidic applications the cross sectional geometry is approximately rectangular[1]. The flow profiles are found using theory for partial differential equations (PDE). Separation of the variables and Fourier series is used for finding the flow profiles expressed as infinite series. The problem may be split up into the pressure driven flow and the EO driven flows. The Debye layer and the EO velocity is not resolved in this analysis, but merely considered as a moving wall BC. This is the infinitely thin Debye layer approximation.

The governing equation for the motion is the Navier-Stokes, Eq. (2.3b). For a steady and uniform flow this equation is simplified to

$$\nabla^2 u = \frac{1}{\mu}\frac{dp}{dz}, \tag{3.6}$$

$$= f(x,y). \tag{3.7}$$

This type of linear second order inhomogeneous PDE is often referred to as the Poisson equation. It is the governing equation for the type of flow called creeping flow or Stokes flow because of the lack of inertial effects. In the uniform case $f(x,y)$ is merely a constant. Fig. 3.1 illustrates the boundary value problem.

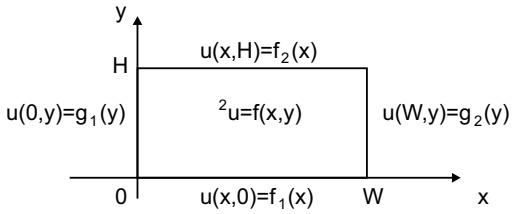

Figure 3.1: Poissons equation with inhomogeneous Dirichlet BCs. A Dirichlet BC specifies the absolute value of the dependent variable, in this case u. A Neumann BC specifies the derivative of the dependent variable.

An analytical approach is not straightforward because of the inhomogeneous PDE, which makes the separation of variables impossible. The remedy is to split up the problem in two, and then use the fact that the PDE is linear, Asmar. The individual solutions can then be superposed as $u = u_1 + u_2$, Fig. 3.2.

[1] Due to the fabrication techniques it is often difficult to etch vertically and the walls will tend to be slightly tilted or round.

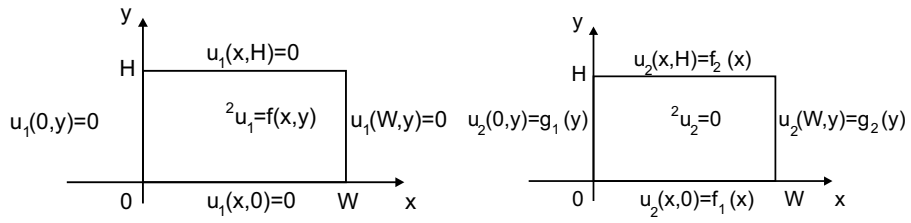

Figure 3.2: u_1 is governed by Poissons equation with homogeneous Dirichlet BCs whereas u_2 is governed by the Laplace equation with inhomogeneous Dirichlet BCs. Together they form the complete solution to the Poisson equation with inhomogeneous Dirichlet BCs, $u = u_1 + u_2$.

The relevant boundary conditions are wall $u = 0$ and velocity $u = U$. The latter is equivalent of electroosmotic flow where the Debye layer is assumed infinitely thin. The flow may also be pressure driven, which enters the equation through the inhomogeneous term. The procedure is to solve both the Laplace equation and the Poisson equation with the appropriate boundary conditions.

3.2.1 Solving the Laplace equation

Single moving wall

For simple geometries we can calculate the velocity field analytically. One of the most simple cases is the Couette flow, which is two infinity large plates in the xz-plane, separated by a distance H in the y-direction. The EO velocity is approximated with a moving wall. If the top plate is moving with the velocity U, we get the linear velocity profile,

$$u(y) = U\frac{y}{H}. \tag{3.8}$$

If then we consider a rectangular channel of finite width $2W$ and height $2H$, where only the lid is moving, things are much more complicated. This type of solution is useful if the flow is driven by electroosmosis on only one wall, or if one wall has another EO mobility than the others. In fabrication of microfluidic devices the lid is bonded on the device and may have a different EO mobilities. The detailed solution is given in Appendix A.

Two moving walls

Here we will look at the situation where two parallel planes are moving opposed by two fixed planes, Fig. 3.3. This corresponds to flow driven by electroosmosis on two walls. Boundary conditions and the simplified Navier-Stokes equation yields

$$u(W, y) = u(-W, y) = 0, \tag{3.9}$$

$$u(x, -H) = u(x, H) = U, \tag{3.10}$$

$$\text{Initial guess} \quad u(x, y) = U + f(x, y), \tag{3.11}$$

$$\text{Navier-Stokes} \quad \frac{1}{\mu}\frac{dp}{dz} = \frac{\partial^2 u}{\partial x^2} + \frac{\partial^2 u}{\partial y^2}. \tag{3.12}$$

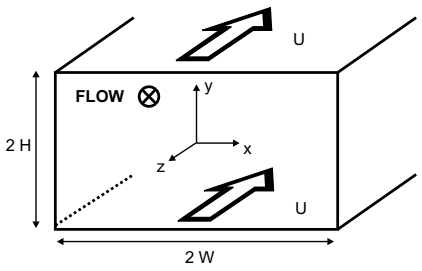

Figure 3.3: Rectangular channel flow driven by two moving walls. The velocity of the walls is U. The aspect ratio is defined as $\kappa = W/H$.

Inserting the initial guess into Navier-Stokes equation and solving for uniform pressure gives

$$\begin{aligned} 0 &= u_{xx} + u_{yy}, && (3.13a)\\ 0 &= f_{xx} + f_{yy}, && (3.13b)\\ f(W,y) &= f(-W,y) = -U, && (3.13c)\\ f(x,-H) &= f(x,H) = 0. && (3.13d) \end{aligned}$$

The governing equation is recognized as the Laplace equation with Dirichlet boundary conditions. Such a boundary value problem can be solved by the method of separation.

$$\begin{aligned} f_n(x,y) &= \sum g_n(x)\; h_n(y) && (3.14)\\ g_n(x) &= A_n \cosh(\lambda_n x) + B_n \sinh(\lambda_n x) && (3.15)\\ h_n(y) &= C_n \cos(\lambda_n y) + D_n \sin(\lambda_n y) && (3.16) \end{aligned}$$

The guess at $f_n(x,y)$ comes from the characteristic polynomial, refer to Appendix A for details. Due to symmetry we have $B_n = D_n = 0$. The boundary conditions give the eigenvalues $\lambda_n = (\frac{\pi}{2}+n\pi)/H$. From this set of eigenfunctions the solution may be found by determining the Fourier coefficients. Inserting the reduced guess in the boundary conditions gives

$$\begin{aligned} -U &= \sum_{n=0}^{\infty} A_n \cosh(\lambda_n W)\cos(\lambda_n y) && (3.17a)\\ -U &= \sum_{n=0}^{\infty} A_n^* \cos(\lambda_n y) && (3.17b)\\ A_n^* &= \frac{2}{H}\int_0^H -U\cos(\lambda_n y)dy && (3.17c)\\ &= \ldots = -\frac{2U}{\lambda_n}(-1)^n && (3.17d) \end{aligned}$$

Introducing the aspect ratio $\kappa = W/H$, the overall velocity field may be written as[2],

$$u(x,y)\frac{1}{U} = 1 - 2\sum_{n=0}^{\infty} \frac{(-1)^n}{\frac{\pi}{2}+n\pi} \frac{\cosh\left[(\frac{\pi}{2}+n\pi)\frac{x}{H}\right]}{\cosh\left[(\frac{\pi}{2}+n\pi)\kappa\right]} \cos\left[(\frac{\pi}{2}+n\pi)\frac{y}{H}\right]. \quad (3.18)$$

[2]Evaluating $u(x,y)$ on a pc requires that the expression is rewritten, see Appendix A

The flow rate is found by integrating $u(x, y)$ over the domain,

$$Q = 4WHU\Big[1 - \frac{2}{\kappa}\sum_{n=0}^{\infty}\frac{1}{\lambda_n^3}\tanh(\lambda_n\kappa)\Big], \tag{3.19}$$

$$= 4WHUQ^*. \tag{3.20}$$

This dimensionless flow rate, Fig. 3.4 is very useful in relation to pump designs. For a given aspect ratio and no counter pressure one may find the flow rate once the EOF velocity and geometry is known.

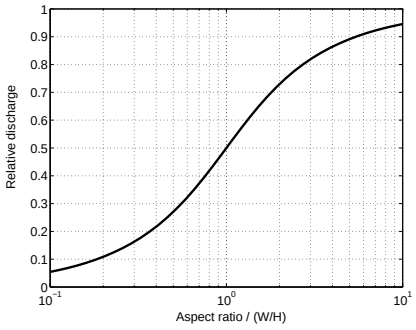

Figure 3.4: Relative flow rate Q^* of a two wall EO pump, as a function of the aspect ratio (W/H). Note that the graph is symmetric. $Q = 4WHUQ^*$ where W and H are half the width and height respectively. U is the velocity of the walls. The flow rate approaches 1 asymptotically $Q^* \to 1$, corresponding to full EOF.

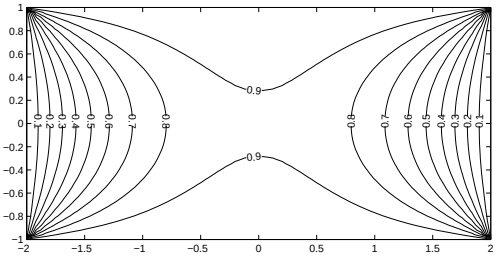

Figure 3.5: Contour plot of $u(x, y)$ made nondimensional by U and H. The aspect ratio is $W/H = 2$. The solution is two-fold symmetric. From Fig. 3.4 we see that the relative flow rate is 80%.

Fig. 3.4 and 3.5 are generated using a MATLAB program, Appendix D, Two Moving Walls.

Other Cases

Some other cases could be considered. Three moving walls opposed by one fixed wall, e.g., the lid. Four moving walls is trivial since the velocity field is uniform.

The walls could also move with different velocities. In most cases this can be solved by combining the above presented cases.

Example: *Effective EO mobility*
Consider a rectangular channel with two sets of opposing walls. The one set having the EO mobilities α_{eo}^A and α_{eo}^B respectively. The aspect ratio is 3, meaning that the channel is three times wider than it is deep. From Fig. 3.4 the nondimensional flow rate is read to be $Q^* = 0.82$. If $\alpha_{\text{eo}}^A > \alpha_{\text{eo}}^B$, the effective EO mobility is, $\alpha_{\text{eo,eff}} = \big(\alpha_{\text{eo}}^A - \alpha_{\text{eo}}^B\big)Q^* + \alpha_{\text{eo}}^B$.

3.2.2 Solving the Poisson Equation

Pressure driven flow

Pressure driven flow is very important, and it is almost always present in some part of the microfluidic network. Just a small section without EOF, or a change in EO mobility, will induce pressure driven flows.

In the previous section we solved the Laplace equation with inhomogeneous Dirichlet boundary conditions. If there is a pressure gradient, the governing equation alters to the Poisson equation, see Fig. 3.2(a). Remembering that the flow was steady state, and that $f(x,y) = f$ was a constant, the theory is that the solution may be expanded in a set of orthogonal eigenfunctions. Since we are dealing with homogeneous BCs it is appropriate to use sine functions.

$$u(x,y) = \sum_{n=1}^{\infty}\sum_{m=1}^{\infty} E_{mn} \sin\left(\frac{m\pi x}{W}\right) \sin\left(\frac{n\pi y}{H}\right). \tag{3.21}$$

Inserting this solution into the Poisson equation, and recalling that $f = \frac{1}{\mu}\frac{dp}{dz}$, yields

$$f = \sum_{n=1}^{\infty}\sum_{m=1}^{\infty} -E_{mn}\left[\left(\frac{m\pi}{W}\right)^2 + \left(\frac{n\pi}{H}\right)^2\right] \sin\left(\frac{m\pi x}{W}\right) \sin\left(\frac{n\pi y}{H}\right), \tag{3.22}$$

$$E_{mn} = \frac{-4}{WH\lambda_{mn}} \int_0^H \int_0^W f(x,y) \sin\left(\frac{m\pi x}{W}\right) \sin\left(\frac{n\pi y}{H}\right) dxdy, \tag{3.23}$$

where

$$\lambda_{mn} = \left(\frac{m\pi}{W}\right)^2 + \left(\frac{n\pi}{H}\right)^2. \tag{3.24}$$

The aspect ratio is defined as $\kappa = W/H$. The value of E_{mn} inserted into the equation for $u(x,y)$ gives

$$u(x,y) = \frac{-16W^2 f}{\pi^4} \sum_{k=0}^{\infty}\sum_{l=0}^{\infty} \frac{\sin\left[(2k+1)\pi\frac{x}{W}\right] \sin\left[(2l+1)\pi\frac{y}{H}\right]}{(2k+1)(2l+1)\left[(2k+1)^2 + (2l+1)^2\kappa^2\right]} \tag{3.25}$$

$$Q = \frac{-64W^3 Hf}{\pi^6} \sum_{k=0}^{\infty}\sum_{l=0}^{\infty} \frac{1}{(2k+1)^2(2l+1)^2\left[(2k+1)^2 + (2l+1)^2\kappa^2\right]} \tag{3.26}$$

From Eqs. 3.25 and 3.26 the relative flow rate Q^* and velocity profile $u(x,y)$ can be found for various aspect ratios, Fig. 3.6 and 3.7. From Eq. (3.26), we can see that $Q \propto f$. Recalling that $f = \frac{1}{\mu}\frac{dp}{dz}$ we see that an expression of the following form must apply

$$Q = \frac{\Delta p}{R_{\text{hyd}}}, \tag{3.27}$$

where R_{hyd} is the hydraulic resistance defined from Eqs. 3.26 and 3.27. This equation is very important, and forms the basis of the equivalent circuit theory.

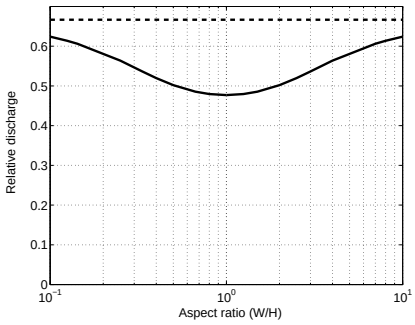

Figure 3.6: Relative flow rate Q^* of a pressure driven flow as a function of aspect ratio (W/H). Note that the graph is symmetric. $Q = 4WHUQ^*$ where W and H are half the width and height respectively. U is the maximum velocity. The nondimensional flow rate Q^* approaches $Q^* \to 2/3$ asymptotically for high and low aspect ratios.

A derivation of the asymptotic constant from Fig. 3.6 is straightforward. For large aspect ratios the flow is one dimensional. The dimensionless velocity profile is, $u(y) = 4y(1-y)$ so that $u(\frac{1}{2}) = 1$. $Q^* = \int_0^1 u(y)dy = \frac{2}{3}$.

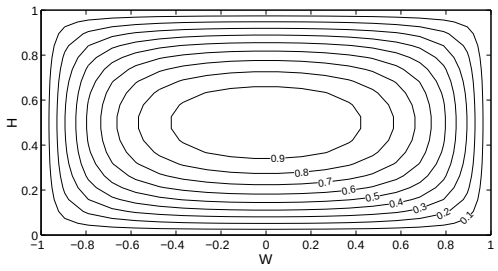

Figure 3.7: Contour lines of the pressure driven flow $u_{\mathrm{hyd}}(x, y)$. Made nondimensional with the maximum velocity. The aspect ratio $W/H = 2$. The flow is twofold symmetric with maximum in the center and zero velocity at the boundary.

3.2.3 Superposition

The solutions for different types of EO and pressure driven flows have been obtained. The total flow can be found by simply adding the two solutions due to the linear nature of the Poisson equation. However, one should mention that this includes the assumption that the EOF, i.e., the EO velocity, is independent of the pressure.

$$\mathbf{u} = \mathbf{u}_{\mathrm{eo}} + \mathbf{u}_{\mathrm{hyd}} \tag{3.28}$$

The flow rates can also be added. This linearity enables a macroscopic approach. The solutions are expressed in terms of infinite series. In order to estimate the error made when truncating the series, a graphical representation of the error can be seen on Fig. 3.8.

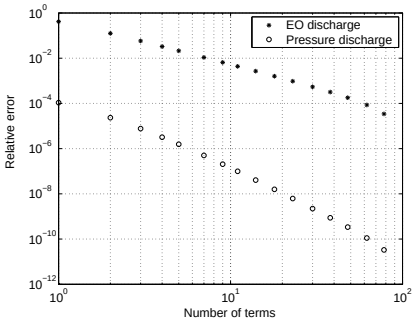

Figure 3.8: Log-log plot of the relative error estimate $|\frac{f(n)}{f(N)} - 1|$ versus number of terms, n. The values have been made nondimensional by the expression with most terms, N.

3.3 Electroosmotic Flow

In this section we shall describe some important features with EOF.

3.3.1 Constant Flow Rate

Consider EOF without counter pressure, with an infinitely thin Debye layer, with isotropic electrical conductivity, and constant EO mobility α_{eo}. The flow rate is then solely governed by the electric field E, EO mobility, and the area of the cross section A. The flux of the electric field in the channel is conserved because the walls are nonconducting. Combining these statements we obtain

$$\left.\begin{aligned} Q &= \alpha_{\text{eo}}\, E\, A \\ E\, A &= \text{const} \end{aligned}\right\} Q = \text{const} \tag{3.29}$$

The conclusion is that the flow rate is independent of the area of the cross section under the given assumptions. Hence, reducing the cross section does not reduce the flow. In Fig. 3.9 the well-known back step is depicted. In the case of laminar pressure driven flow we are creeping regime $Re = 0.11$, so no vortices are formed behind the step. The flow expands without losses.

With same conditions as previously mentioned the flow is a potential flow, refer Appendix F. It makes no difference to the streaklines whether the flow is coming from the right or the left. This is only the case with creeping and potential flow.

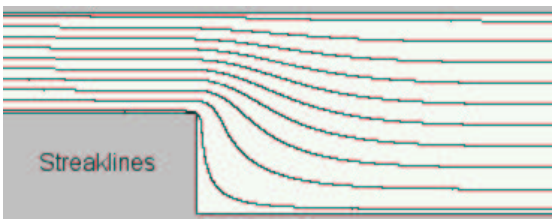

Figure 3.9: Streaklines in the back step geometry. The channel is 50 μm and 100 μm in the two sections respectively. The velocity in the narrow section is 2200 μm/s. The corresponding Reynolds number is $Re = 0.11 < 5$, so it can be described as a creeping flow without vorticity.

In case of a tapering, the larger electric field and consequently larger ohmic heating can affect the EO mobility which depends on temperature, refer to Fig. 2.8. Hence, a tapering may result in an increased flow rate. This effect could potentially be used as a passive flow control. Spatial differences in EO mobilities give rise to pressure gradients. Recent experiments with this effect have been made by Ross *et al.*, 2001.

If the channel dimensions becomes so small that they are comparable with the Debye length $a \approx \lambda_D$ the flow is reduced depending on the temperature effects, as previously mentioned.

Thermal effects in EOF are largely unexplored, but are nonetheless very important. Many experiments reported in the literature deviate from the linear theory because of temperature effects.

3.3.2 Transient Time

In applications it may be useful to estimate the time that it takes for a flow profile to develop. Assuming that the Debye layer responds instantaneously when the external field is applied, the time development of the velocity profile in the bulk fluid may be calculated using laminar theory with the appropriate boundary conditions. Here we consider a wall in the xz-plane, which is immersed in fluid and set in motion instantaneously with velocity U, parallel to the plane. The equation of motion for the velocity $u(y,t)$

$$\frac{\partial u}{\partial t} = \nu \frac{\partial^2 u}{\partial y^2}, \tag{3.30}$$

where y is the coordinate perpendicular to the wall. Applying the boundary conditions

$$u(0,t) = U \quad \text{and} \quad u(\infty,t) = 0, \tag{3.31}$$

we obtain the solution

$$u(y,t)\frac{1}{U} = 1 - \operatorname{erf}\Big(\frac{y}{\sqrt{4\nu t}}\Big). \tag{3.32}$$

The dynamic response time is very dependent of the distance, but also of the kinematic viscosity. If $\frac{y}{\sqrt{4\nu t}} = \text{const}$ the response time is, $t \propto \frac{a^2}{\nu}$ where a is a characteristic length. In a capillary this length would be the radius. In a rectangular geometry it would be the half-length of the smallest edge. The error function can be found in most mathematical programs such as MATLAB.

Example: *Time Scale*
Consider a wall immersed in water. At a distance of $y = 40$ μm the velocity will be 80 % of the terminal velocity U at $\frac{u}{U} = 0.8$ at 0.01 s after the wall is set in motion.

3.4 Equivalent Circuit Model

In a system featuring both electroosmotic flow and hydrodynamic flow, the average velocity in a channel may be calculated by adding the two contributions, as we saw in the previous section. The focus is shifted from flow profiles $u(x, y)$, to flow rates Q. It is readily seen from Eq. (3.28) that the following must apply

$$Q_{\text{total}} = Q_{\text{eo}} + Q_{\text{hyd}}. \tag{3.33}$$

As previously shown, the hydraulic flow rate may be written as

$$Q_{\text{hyd}} = \frac{\Delta p}{R_{\text{hyd}}}, \tag{3.34}$$

where Δp is the pressure drop across a device, and R_{hyd} is the hydraulic resistance of the device, see Table 3.1. Electroosmotic flow without counter pressure has a completely flat velocity profile. Hence, the flow rate is hence found as the EO velocity times the area of the cross section

$$Q_{\text{eo}} = \alpha_{\text{eo}}\phi_a \frac{A}{L}, \tag{3.35}$$

$$= \alpha_{\text{eo}}\phi_a \big(R_{\text{elec}}\lambda_{\text{elec}}\big)^{-1}, \tag{3.36}$$

where R_{elec} and λ_{elec} is the electrical resistance and conductivity respectively. L is the length of the EO section, and ϕ_a is the applied voltage across the EO section. Q_{eo} is the free run flow rate in an EO pump. Combining Eqs. (3.34) and (3.36) $Q_{\text{hyd}} = Q_{\text{eo}}$, we obtain the following expression for the electroosmotic pressure Δp_{eo}

$$\Delta p_{\text{eo}} = \alpha_{\text{eo}}\phi_a \frac{R_{\text{hyd,eo}}}{R_{\text{elec}}\lambda_{\text{elec}}}. \tag{3.37}$$

The EO pressure is the pressure where the EOF balances the hydrodynamic flow $Q = 0$. Therefore it is the maximum pressure an EO pump can deliver, the so-called backpressure. The corresponding pump characteristic Q-p is

$$Q = Q_{\max}\Big(1 - \frac{\Delta p}{\Delta p_{\text{eo}}}\Big), \tag{3.38}$$

where $Q_{\max}$ is the flow rate in case of zero counter pressure. For a combined hydraulic and electroosmotic flow, the flow rate is governed by the electroosmotic pressure Δp_{eo}, the dynamic counter pressure Δp_{hyd} and overall hydraulic resistance $R_{\text{hyd,total}}$.

$$Q = \frac{\Delta p_{\text{eo}} + \Delta p_{\text{hyd}}}{R_{\text{hyd,total}}} \tag{3.39}$$

$$\Delta p_{\text{hyd}} = \Delta p - \Delta\Big(\frac{\rho Q^2}{2A}\Big) \tag{3.40}$$

The last term in Eq. (3.40) is the velocity head. At a velocity of $u \approx 1$ mm/s the pressure head is $p_{\text{vel}} = \frac{1}{2}\rho u^2 \approx 5 \times 10^{-4}$ Pa. So in most microfluidic applications this term may be neglected. With this simplification, the combined effects of electroosmosis and pressure driven flow can be written as

$$Q = \frac{\Delta p_{\text{eo}} - \Delta p}{R_{\text{hyd,total}}} \tag{3.41}$$

	Hydraulic resistance R_{hyd}	Ohmic resistance $R_{\text{elec}}\lambda_{\text{elec}}$
Circular	$\frac{8\mu L}{\pi a^4}$	$\frac{L}{\pi a^2}$
Rectangular	$\frac{12\mu L}{H^3(W-0.6H)}$ for $W \gg H$	$\frac{L}{HW}$

Table 3.1: Values for the hydraulic and electrical resistances for rectangular and circular cross sections, Morf, 2001.

In Table 3.1 an approximative expression for the hydraulic resistance of the rectangular cross section is given. The expression is only a good approximation for large aspect ratios. The analytically obtained hydraulic resistance is

$$R_{\text{hyd}} = 12\mu L \left\{ H^3 W - \frac{192}{\pi^5} H^4 \sum_{m=0}^{\infty} (2m+1)^{-5} \tanh\left[\frac{(2m+1)\pi W}{2H}\right] \right\}^{-1} . \quad (3.42)$$

Eq. (3.42) is consistent with the derived expression in Eq. (3.26). The other one is stated here, because it is simpler. Only a few terms need to be included because the convergence of Eq. (3.42) is very fast.

Note that the flow rate is independent of the electrical resistivity, since $R_{\text{elec}}\lambda_{\text{elec}}$ only depends on the geometry of the channel.

The fluidic network is transformed to an equivalent electrical network. The ohmic and hydraulic resistance are calculated by the standard electronic approach. The flow rate is described as a current for which Kirchoff's law applies is equivalent to the flow incompressibility condition ($\boldsymbol{\nabla} \cdot \mathbf{u} = 0$). The voltage has the role of pressure in this context. The best way to illustrate the application, is by an example.

Consider the fluidic network and the corresponding electrical circuit shown in Fig. 3.10. We wish to find the pump characteristic Q-p.

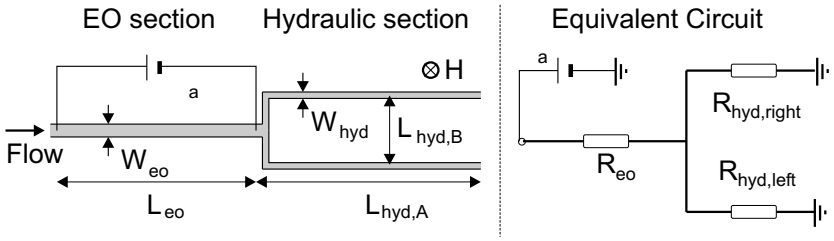

Figure 3.10: Fluidic network and the equivalent circuit. Dimensions: $L_{\text{eo}} = 20$ mm, $L_{\text{hyd,A}} = 20$ mm, $L_{\text{hyd,B}} = 5$ mm, $W_{\text{hyd}} = 100$ μm, $W_{\text{eo}} = 200$ μm, etch depth $H = 10$ μm, $\phi_a = 1000$ V, $\alpha_{\text{eo}} = 0.06$ mm^2(V s)$^{-1}$, $\mu = 1.0 \times 10^{-3}$ kg (m s)$^{-1}$.

Example: *Microfluidic system*
The procedure is to start by finding the hydraulic resistances. The aspect ratios W/H in the channels are high, they are 10 and 20 respectively, so we can use the approximation given in Table 3.1

$$R_{\text{hyd}} = \frac{12\mu L}{H^3(W - 0.6H)}. \tag{3.43}$$

Inserting the values from Fig. 3.10 we obtain

$$R_{\text{hyd,eo}} = 1.24 \times 10^{15} \text{ kg (m}^4 \text{ s)}^{-1}, \tag{3.44}$$
$$R_{\text{hyd,right}} = R_{\text{hyd,left}} = 2.87 \times 10^{15} \text{ kg (m}^4 \text{ s)}^{-1}. \tag{3.45}$$

Note that the effective length of the right and left branch is (20 + 2.5) mm = 22.5 mm. The total hydraulic resistance is

$$R_{\text{total}} = R_{\text{hyd,eo}} + \frac{1}{2}R_{\text{hyd,left}}, \tag{3.46}$$
$$= 2.68 \times 10^{15} \text{ kg (m}^4 \text{ s)}^{-1}. \tag{3.47}$$

Once the hydraulic resistances are known the EO pressure or backpressure can be found using Eq. (3.37)

$$\Delta p_{\text{eo}} = \alpha_{\text{eo}}\phi_a \frac{R_{\text{hyd,eo}}}{R_{\text{elec}}\lambda_{\text{elec}}} \tag{3.48}$$
$$= 7.43 \times 10^3 \text{ Pa}. \tag{3.49}$$

Finally Eq. (3.41) gives the Q-p characteristic of the fluidic system

$$Q = \frac{\Delta p_{\text{eo}} - \Delta p}{R_{\text{hyd,total}}} \tag{3.50}$$
$$= 2.77 \times 10^{-12} \frac{\text{m}^3}{\text{s}} \Big(1 - \frac{\Delta p}{7.43 \times 10^3 \text{ Pa}}\Big). \tag{3.51}$$

Setting $\Delta p = 0$ gives the max flow rate.

Calculations of this type may be done in a worksheet such as Excel, refer to Appendix B for more examples.

3.5 Summary

The elementary flow analysis chapter is very important in relation to modelling of microfluidic systems. Firstly, flows in two different cross section geometries were analyzed. (1) In the case of circular geometry, the EOF with finite Debye layer thickness was investigated. It was found that the EO flow rate for thin Debye layers $Q_{\text{eo}} \propto a^2$ whereas for pressure driven flow $Q_{\text{hyd}} \propto a^4$. In the case of Debye layer overlap $Q_{\text{eo}} \propto a^4$. (2) For rectangular cross sections, the velocity distributions and flow rate relations for different aspect ratios were found. It was also shown how the solutions could be superposed.

The findings were then transformed to be used in the so-called equivalent

circuit theory. This theory uses a system design approach Q-p rather than a detailed analysis $u(x, y)$. The essential concepts: Max flow rate, backpressure and hydraulic resistance were introduced.

An example of how the theory can be applied was given. The theory is highly useful and is used throughout the report.

Chapter 4

Computational Fluid Dynamics

Computational fluid dynamics (CFD) allows the user to simulate local values of velocity, pressure, electric field, mass fraction, etc. In theory, this is the ultimate design tool, but in practice there are certain factors that limit its accuracy and usefulness. Some of the disadvantages are that it is very time consuming, and that often many simplifications have to be made. However, there are also many advantages associated with CFD. It gives a visual understanding of the fluid dynamics and it can assist in the understanding of the physics. In a complex geometry, it is often the only way of analyzing the flow.

Throughout this thesis I have worked with a combination of equivalent circuit models and CFD. I found that this combination gave the optimal results. Comparing the circuit models with CFD calculations is a good way of verifying the calculations when no physical experiments are available. It cannot be stressed enough, that all CFD calculations at some point should be compared favorably with some model before they can be trusted. In other words one should always be critical towards the results.

In this chapter a brief introduction to CFD will be given followed by more specific information about the CFD-package Coventor. The possibilities and limitations of this package will be discussed. Two simple test cases are presented.

4.1 Modelling with CFD

Using a CFD program requires physical and mathematical insight. The old saying: "Garbage in, garbage out", is as true as ever before. Even the program itself may contain a considerable amount of errors. Furthermore, special care should be taken when traditional techniques are applied to new physical areas such as microfluidics.

A CFD package typically consists of a pre-processor, a solver, and a post-processor. These different elements will now be introduced.

4.1.1 The Pre-processor

The Pre-processor is the interface between the user and the solver. Several factors must be considered before the solver can be started.

- **Geometry**
  The definition of the computational domain. The minimum area that needs to be simulated. Simplification of the geometry using symmetry, periodicity, etc. can save a lot of computational time.
- **Meshing**
  It is very important to generate an efficient grid. It requires a considerable amount of insight of the problem at hand to identify the critical regions, etc. A solution should be independent of the mesh.
- **Model**
  Selection of physical, electrical and chemical processes that need to be modelled. Here the simplification process plays an important part in making good CFD. Unnecessary complexity tends to make the analysis more inaccurate and difficult.
- **Fluid parameters**
  Parameters such as EO mobility, diffusion constant, viscosity, etc. need to be specified.
- **Boundary conditions (BCs)**
  The boundary conditions are specified on the surfaces that encapsulate the computational domain. Typical boundary conditions are velocity, pressure, wall effects (EOF), voltage, etc. A more detailed overview of the BCs is given in the following sections.
- **Initial conditions (ICs)**
  Examples of IC's could be specification of a sample plug (concentration), a velocity field, an electric field, etc.

4.1.2 Solver, Finite Element Method (FEM)

The governing equations can be solved by using the FEM method. The FEM method makes use of simple piecewise functions, e.g., linear or quadratic, valid on elements to describe the local variations of unknown flow variables ϕ. The governing equation is precisely satisfied by the exact solution ϕ. If the piecewise approximating solution for ϕ is substituted into the equation, it will not hold exactly, and a residual is defined to measure the error. These residuals are then minimized by multiplying them with a set of weighting functions and integrating the so-called Galerkins method, Versteeg and Malalasekera.

The actual numerical solver is a sparse matrix solver. Gaussian elimination is far too time consuming for large matrices. The calculation time is proportional to N^3 where N is the dimension of the matrix. One simple type of sparse matrix solver is the Tri-diagonal matrix algorithm (TDMA), which is a very efficient method for solving tri-diagonal matrices. However, practical matrices are not tri-diagonal. In this case, the TDMA is applied iteratively after rewriting the equations, or a more implicit method is used.

4.1.3 Solver, Finite Volume Method (FVM)

The Finite Volume Method is the most widely used CFD technique. It is based on the concept of transport equations. The fluid domain is divided into finite volumes, and the governing equations are integrated over these volumes. The integrated equation is approximated with various finite difference methods such as central difference, upwind scheme, etc. The numerical schemes convert the integral equations into a system of algebraic equations. These equations are then solved by an iterative method.

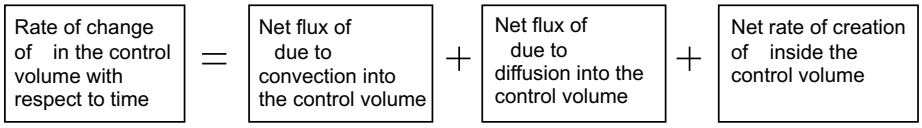

Figure 4.1: Description of the transport equation used in the (FVM).

COVENTOR 2001.3 can use both FEM and FVM. However FVM is much faster for meshes with many cells (> 1000). The specifics are discussed later.

4.1.4 Post-processing

The simulation itself is worthless, unless we can extract the data in a meaningful way. Some commonly used visualization techniques are,

- **Vector field**
  Plots the velocity field with vectors in different colors and lengths depending on the velocity.
- **Streamlines**
  A streamline is a tangent to the velocity field at a fixed time.
- **Streaklines**
  A streakline is also a tangent to the velocity field, but not at a fixed time. The streaklines follow the particles, e.g., injection of dye into a flow. In a steady state flow, the stream- and streaklines are identical.
- **Volume visualization**
  Scalar variables such as pressure and electric potential may be visualized using colors.

4.2 The COVENTOR Package

The COVENTOR package is specifically designed for microsystems. It was initially developed for MicroElectroMechanicalSystem (MEMS) applications. The program uses microns as its base length. Hence, special care should be taken when specifying and extracting values in non SI-units. COVENTOR has no turbulence module, which is unnecessary in microfluidics. Another characteristic feature is that the mesh generation emulates the manufacturing process.

The COVENTOR package contains many different types of modules. For the problem at hand the microfluidic solvers are used. Two solvers are particularly

interesting from the pumping point of view: MemCFD and NetFlow[1]. The MemCFD is a quite simple module that covers the most general CFD tasks: steady, transient, compressible and incompressible laminar flows. Standard boundary conditions such as pressure, velocity and symmetry can be applied. This solver is used for micromechanical devices such as pumps and valves. Hence the name MemCFD.

The NetFlow module covers pressure, diffusion, electrophoresis and electroosmosis. Chemical transport of up to four different species can be modelled. These are exactly the processes expected to be involved in an electroosmotic pump. The pre-processor in NetFlow consists of a Layout builder, a Foundry and a Solid Model. The total structure of the NetFlow module is given below

- **Layout**
  2D layouts of masks can be made. The masks are used for defining an area in which a foundry process will take place.

- **Foundry**
  Fabrication processes are specified to the different masks. For example, a mask may be deposited giving the substrate, and then etched with another mask giving the channel system. See Fig. 4.2 for an example.

Step	Action	Material	LayerName	Type	Thickness	Mask	EtchDepth
0	Base	SILICON	Substrate		50.0	GND	
1	Etch					default	10.0
2	Deposit	WATER	Layer	Planar	0.0		

Figure 4.2: Screen shot from the foundry menu in COVENTOR. Three processes/steps are defined. Step 0 deposits (stacked) the substrate made in silicon with the GND mask and 50 μm thick. Step 1 etches a channel system 10 μm deep with the default mask. The GND and default mask were made in the layout builder. Finally, the etched channel system is planar filled with water. It is this layer that forms the computational domain.

- **Solid Model**
  The Solid model module generates a 3D model based on the layout and the processes defined in the foundry.

- **Meshing**
  The meshing can be done semi-automatically in COVENTOR. The method is very fast, but at the expense of less control over the mesh generation. The program can handle meshes with up to 3×10^5 cells on a PC with 512 Mb ram, but in principle there should be no upper limit.

- **Analysis**
  Labelling of patches can be very slow in the analysis tool. On a Pentium III windows NT 4.0 system, the handling of the structures becomes intolerable slow for mesh sizes above 2×10^5 elements.

- **Solver setup**
  It is possible to choose between the FVM and the FEM solver. The FVM

[1] The solver SwitchSim can be used to simulate cyclic voltage BCs.

solver is much faster for large problems. The requirements for convergence (tolerance) and boundary conditions are also specified here.

The idea behind the layout and foundry steps is that the user will by guided to making realistic microfluidic designs. The possible designs have a two-dimensional character, i.e., the bending pipe shown in Fig. 1 is not a possible design. The mesh can then be generated in a external program such as I-DEAS and subsequently imported.

4.2.1 Boundary Conditions

In COVENTOR the surface boundary conditions are applied to patches. A patch is a surface section on the model, e.g., a cube has six patches. Before undertaking a large simulation project it is crucial to have a simulation logbook. The most logical settings can be forgotten after a week or a month. The logbook should contain information about the mesh generation, boundary conditions, etc., see Appendix C. The boundary conditions are very important and largely govern the solutions. Here I have described the boundary conditions used in the simulations.

- **Pressure**
  Specifies the pressure on a patch.
- **Voltage**
  Specifies the voltage on a patch.
- **Inlet/outlet (default)**
  Specifies zero velocity gradients in the normal direction of the patch. Hence one must be careful not to place the inlet/outlet in a nonuniform, region which would give spurious results. Furthermore, if the outlet condition is combined with the pressure condition the problem is under-specified[2].
- **Symmetry**
  Symmetry is invoked in order to save computational time, e.g., two symmetry planes can reduce the number of cells by a factor 4. The symmetry BC assumes that the gradients perpendicular to the symmetry plane or line are zero.
- **Wall**
  The wall BC simply sets the velocity at the patch to zero.
- **Velocity**
  Specification of a velocity on a patch.
- **EO mobility**
  In all the simulations the Debye layer is assumed infinitely thin. This is valid because a typical Debye length is 10 nm, and the considered dimensions is of the order 10 μm, a factor 10^3 larger. However, if the Debye length had been comparable with pump dimensions some corrected velocity boundary conditions could have been applied, Dutta and Beskok.

[2]If no boundary condition is specified, COVENTOR sets the patch as an inlet/outlet with zero pressure. This prevents under-specification of the numerical problem.

COVENTOR solves the Laplace equation using the voltage BCs and hence finds the potential distribution. The electric field is found as minus the gradient of the potential. Once the electric field is known at the boundaries, the flow velocity is set by multiplying with the value for the electroosmotic mobility. The approach is correct for a dielectric medium with conducting walls, or a conducting medium with nonconducting walls.

4.3 Test Cases

The COVENTOR package is only a few years old. The program is very comprehensive with more than 1600 pages in the manual, which is not enough. In many cases COVENTOR is like a black box. The NetFlow module uses a solver from another CFD program called Fluent, which is well tested. However, adding new types of boundary conditions, etc. to the code is very complex process, and errors are bound to be made. For example, I spent two weeks finding out why the EO boundary condition did not work consistently. It turned out that for simple geometries, the program solved the Laplace equation so fast that it could not initiate the FVM solver before it was finished. Hence, the program returned the zero values for everything. After contacting the support the problem was solved with a software patch. Questions to and answers from the COVENTOR support is given in Appendix E. The COVENTOR support has been very helpful and it is my belief that the upcoming version of COVENTOR will be much better than the previous one, 2001.3.

4.3.1 Steady Laminar Flow in a Circular Capillary

The solution to the steady laminar flow in circular capillary can be compared to the analytical solution. The circular geometry of the problem suggests two dimensional axi-symmetric coordinates are being utilized. The work flow in COVENTOR is described below.

- **Layout**
  A ground mask is generated in which the channel (a rectangle) is to be etched in. The etch mask 400×50 μm^2 is also generated. The x-axis is the symmetry axis. COVENTOR requires that the lower part of the etch mask must be aligned with the x-axis ($y = 0$).

- **Foundry**
  The ground mask is stack deposited in an arbitrary thickness. The layer is called the substrate. Then the substrate is etched using the etch mask. Finally, the water is planar deposited to a depth of 0 μm. This procedure generates a water layer, which is the computational domain, refer to Fig. 4.2.

- **Solid Model**
  Builds the 3D model. Only the water layer is important.

- **Meshing**
  The model is 3D, but we are only considering the xy-plane. Hence the z-direction should only contain 1 cell. In this example, the rectangular cross section suggest a brick meshing. The size of the grid cells are $50 \times$

$2.5 \times \mu m^2$. The mesh features a high spatial resolution in the y-direction (perpendicular to the flow direction), where large velocity gradients are expected.

- **Analysis**
  The three patches: inlet, outlet and wall are marked and named. Settings for water properties, patches, cell number 160, etc., are checked.

- **Solver setup**
  The inlet pressure is set to 2×10^{-6} MPa in COVENTOR units or 2 Pa. No boundary condition is specified for the symmetry axis (x-axis). The analysis tool is set to FVMtool (Finite Volume Method tool).

- **Results**
  The analytical result is

$$v(r) = -\frac{r^2 - a^2}{4\mu}\frac{dp}{dx}, \tag{4.1}$$

$$v(0) = 3064\ \mu\text{m/s}, \tag{4.2}$$

  where $a = 50\ \mu$m, $\Delta p = 2$ Pa, $\Delta x = 400\ \mu$m, $\mu = 1.0 \times 10^{-3}$ kg (m s)$^{-1}$. The program simulates the results in about 10 seconds. The maximum velocity is computed to be 3060 μm/s. The result deviates with only about 0.1%, which is very good, so the test case is successful.

4.3.2 Steady Laminar Flow in a Rectangular Channel

In this test case we wish to analyze the grid dependency. The flow is driven by EO at two of the four walls, as described in Fig. 3.3 and Sec. 3.2.1. Furthermore, a counter pressure is applied, giving the Q-p characteristic.

- **Layout**
  The channel dimensions are $L \times W \times D = 6000 \times 600 \times 200\ \mu\text{m}^3$.

- **Foundry**
  Standard approach, with substrate, etch mask and planar filling with water.

- **Solid Model**
  Builds the 3D model.

- **Meshing**
  Different mesh resolutions are applied with biasing. Only one cell in the longitudinal direction is needed. The biasing focuses the grid density in the area with large velocity gradients.

- **Analysis**
  Six patches have to be assigned with different names. Inlet, outlet, top wall, bottom wall, left EO wall and right EO wall.

- **Solver setup**
  Pressures and voltages are specified at the inlet and outlet. The EO mobility $\alpha_{\text{eo}} = 6.0 \times 10^4\ \mu\text{m}^2\ (\text{V s})^{-1}$ is specified on the EO walls. The

tolerance is set to 10^{-4} which means that when the solution after an iteration is changed below the tolerance, the simulation is stopped/converged. It is good practice to test the influence of the tolerance on the solution. I worked with the problem for some time, because the simulations with symmetry BC required a lower tolerance setting than those without symmetry. Empirically I found that simulations with symmetry BC require a tolerance setting of 10^{-6}. This is perhaps because the symmetry BC is a Neumann condition, and the wall condition is a Dirichlet condition. Problems with Neumann BCs are typically more difficult to solve numerically.

- **Results**
  The analytical solution is found by superposing two solutions: the electroosmotic driven flow and the pressure driven flow. The two types of flow are discussed in Sec. 3.2.1 and 3.2.2. The comparison between analytical results and CFD can be seen in Fig. 4.3. There is a high degree of agreement between the simulated and theoretical results. The fine mesh (40×40) is slightly closer to the theoretical line. Only two meshes have been analyzed for this geometry. A similar grid dependency analysis can be found in Appendix I.

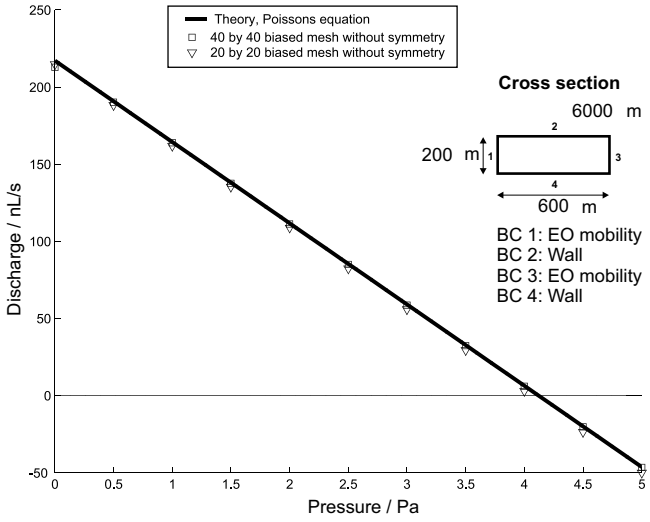

Figure 4.3: Q-p diagrams calculated by COVENTOR 2001.3 with two different meshes. The tolerance setting is 10^{-4} in both cases. The applied potential is $\phi_a = 1000$ V and the EO mobility $\alpha_{\text{eo}} = 0.06$ mm^2 (V s)$^{-1}$.

4.3.3 Diffusion

The NetFlow module can simulate a carrier liquid with up to four species. Here we will only need one additional species. Consider an infinitely long rectangular channel. Two miscible liquids each occupy half of the cross section, Fig. 4.4. From the analytical analysis we can calculate the time evolution of the concentration profile, and compare it with the solution obtained by COVENTOR, Table 4.1.

Time t/t^o	COVENTOR c/c^o	Analytical c/c^o	Deviation
0	1	1	
0.044	0.90	0.91	1%
0.072	0.80	0.81	1%
0.11	0.70	0.71	1%
0.18	0.60	0.60	0%
0.24	0.55	0.55	0%

Table 4.1: Concentration at the right boundary as a function of time. The characteristic diffusion time is $t^o = W^2/D_{\text{mass}}$. There is a high degree of agreement between the simulation and the semi-analytical results. COVENTOR slightly overshoots the values in the beginning. Perhaps because of the large gradients in the initial state.

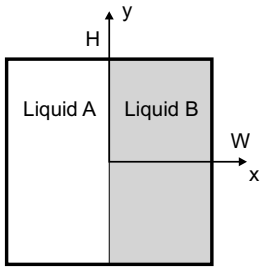

Figure 4.4: The computational domain with the species volume conditions. The time step in the simulation was $dt = 5.7 \times 10^{-4} t^o$, and the mesh was 20×20. The half-width and height is W and H respectively.

In the case of immiscible liquids a free surface module such as the volume of fluid (VOF) method, is needed. COVENTOR 2001.3 does not support this option in the NetFlow module. One can try to simulate the condition by setting the diffusion constant to zero. The effective diffusion is not zero however, because of the numerical diffusion. Furthermore, effects such as surface tension would not be included in the simulation.

Chapter 5

Micropump Overview

In this chapter we shall start by giving a brief overview of mechanical pumps. Then it will be discussed how to characterize an electroosmotic pump and finally an overview of existing EO pumps will be given.

5.1 Mechanical Pumps

This section is dedicated to giving an overview of some of the existing mechanical pumps. The overview consist of a short list of the traditional macroscopic external pumps used in laboratories, and an example of a mechanical micropump.

- **External peristaltic** pumps work in the same way as milking a cow. Tubes in the pump are periodically compressed and thereby the liquid is squeezed through the tube. This method has a tendency to generate a pulsating flow. These types of pumps offers high pressure of the order 1-5 bar and flow rates that are more than sufficient for microfluidic applications. They are therefore common in most laboratories working with microfluidics.
- **External pressurized flow**, such as a gas canister, is suitable and inexpensive, but accurate adjustment of constant flow rates might be difficult, Morf *et al.*, 2001.
- **Integrated mechanical micropumps** utilizing a membrane can be operated by different methods, such as piezoelectric, electromagnetic, pneumatic and many more. The advantage is that they can pump most liquids in the range $1-300\ \mu\text{L min}^{-1}$. However, this technique engenders a pulsating flow as well. Many of the mechanical micropumps only have a limited lifespan, due to material breakdown, Gravesen, 1993.

The external macroscopic pumps are not interesting with respect to μTAS, but are included here to demonstrate the alternative to the integrated micropumps. The mechanical micropumps and other micromechanical devices are typically developed in the research area called MicroElectroMechanicalSystems (MEMS).

Example: *An Electrostatically Actuated Micropump*
The pump consists of two electrodes, a small chamber, and two passive cantilever valves, see Fig. 5.1. Using an actuation frequency of 1kHz, a pumping rate of 300 μL min^{-1} has been achieved. At higher frequencies, the flow is reversed, and for even higher ones, it is stopped, Koch.

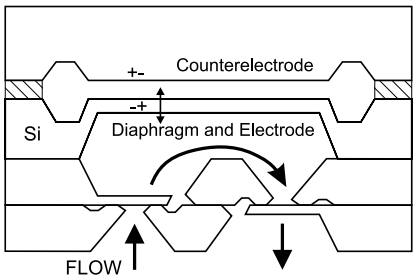

Figure 5.1: An electrostatically actuated micropump. Note the two small cantilever valves, which will open and close periodically with the actuation frequency when this is below 1 kHz, Koch.

5.2 Electroosmotic Pumps

Electroosmotic flow pumps have no moving parts. The pumping mechanism is generated by an external electric field, applied on an electric double layer (EDL), Fig. 1.2.

If the electrodes are positioned in each end of the channel, and no external tubing or pressures are applied, the flow profile will be very flat - plug flow. This type of flow is specifically suitable for capillary electrophoresis (CE), because the hydrodynamic dispersion is minimal.

The pumps considered here are intended to be used as traditional pumps, i.e., as pressure sources. In this section we will go through some of the design rules and the subsequent assessment of the pump.

Q-p characteristics

In conventional pump design, a pump is characterized by a diagram showing the flow rate Q versus the pressure p.

If the adverse pressure is high, the flow rate will be low and vice versa. The pump characteristics are important when designing a fluidic network. The pump characteristics consisting of corresponding values of flow rate and pressure can be measured in a setup as shown in Fig. 5.2.

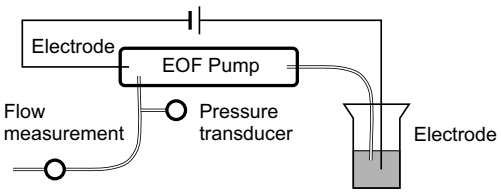

Figure 5.2: Pump setup for measuring pump characteristics. Simultaneous measurements of flow rate and backpressure is needed in order to describe the pump characteristic.

Manufacturing

A very important issue in microfluidics is the manufacturing. To a large extent, the design is governed by the various etching techniques available. This thesis does not deal with fabrication in detail, however, the manufacturing processes have been kept in mind at all times. Typical dimensions in a microchannel are $1 - 300$ μm.

Small structures $1 - 50$ μm are usually made in silicon, glass, silica or quartz by etching techniques. The etch profiles obtained with traditional wet etching techniques are either round or slightly tilted, meaning that a narrow and deep etch is not possible.

Only recently, using Inductively coupled plasma (ICP), the deep and narrow etch has been possible, working with aspect ratios up to 50, Fig. 5.3.

Figure 5.3: Scanning Electron Microscope picture showing 30×1.5 μm silicon walls (from STSystems). The system can etch 10 μm min^{-1}.

Larger channels of the order 300 μm are typically produced in polymers such as Acrylic polymer PMMA. Polymers are promising with respect to bulk production and fast prototyping. One of the fabrication methods is laser ablation, which is a technique where the laser is used to evaporate the material. The depth profile in this case is Gaussian. New types of laser ablation techniques can make channels as narrow as 1 μm.

The one thing all the fabrication techniques have in common, is that they are constantly improving. The fabrication data given here may very well be obsolete within the next 10 years.

Efficiency

Efficiency is an issue which is less in important in the laboratory. However, when the EO pumps are going to be applied to portable devices, the power consumption may be of greater interest. High voltages are also a problem. The thermodynamic efficiency is defined as the useful pressure work over total power consumption.

$$\eta = \frac{\Delta p \, Q}{U^2 / R_{\text{elec}}} \tag{5.1}$$

A high efficiency is obtained by using a liquid with low conductivity, e.g., the conductivity for deionized water (DI) is of the order $\lambda_{\text{elec}} = 10^{-3}$ S/m, Chen *et al.*, 2000.

Electrodes

Traditionally, metal electrodes, such as Pt or Au, are used in electroosmotic pumping. This means that electrolysis can take place near the electrodes generating bubbles. This may interfere with the electrical current and the flow due to clogging. Another issue is that the chemical reactions at the electrodes changes the pH-level and thereby the EO mobility. At the positive electrode (anode) the pH will tend to become low.

Anode: reduced species $\rightarrow$ oxidized species $+ne^-$
Cathode: oxidized species $+ne^- \rightarrow$ reduced species

If the bulk solution is a buffer, this will stabilize the pH until the buffer is depleted. Electrodes are therefore usually placed in an external reservoir.

Another important issue is the lifespan of the electrodes. A high electric current will quickly erode and deposit material at the electrodes. Normally it is a good idea to use a low conductivity buffer to reduce the electrical current, and thereby increase the operation time. However, some experiments with living cells require a saline solution.

Temperature

The temperature should not be too high, in order to avoid bubble formation and possible damage to biological samples. An estimate of the temperature can be done using some approximations regarding geometry and electrical and thermal conductivities. For a nonuniform section it may be difficult to estimate the temperature. Many of the governing parameters in EOF are highly temperature dependent, e.g., the viscosity and the dielectric constant. In the design process these values are often the problem, since the temperature in the capillary is unknown. Very few experiments have been done in this area. One of the first temperature measurements in microchannels was made by measuring the fluorescence intensity through a microscope with a digital video camera. As the temperature rises, so does the fluorescence intensity, Ross *et al.*, 2001.

Dispersion

For pumps in a microfluidic system, dispersion may play a role. The amount of dispersion can be estimated by making a time dependent simulation of a sample plug flowing through the pump, and comparing the width before and after the pump.

Dead volume

The peripheral volume of the pump, or dead volume such as reservoirs, can increase the response time of the pump and complicate the flushing of the device. A large system volume can also increase the sample volume requirement, so a compact design is desirable.

5.3 Electroosmotic Pump Overview

5.3.1 The Cascade EO Pump

The aim is pumps capable of high pressures and flow rates. The high flow rates can be obtained by positioning several regular electroosmotic pumps parallel to each other - in a cascade, Fig. 5.4. In this way the flow rate is increased by the number of channels, without increasing the voltage. If the pumps are positioned, in series the pressure can be accumulated, Fig. 5.5.

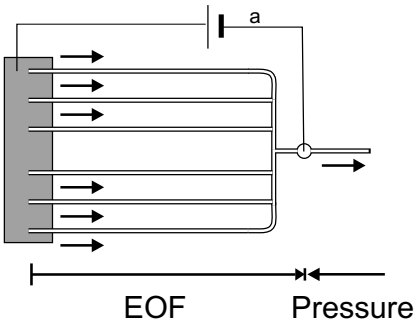

Figure 5.4: Cascade EO pump with six channels. Due to the anode position this pump is no more effective with respect to pressure and flow rate than if there had been only one channel. However the six channel pump can be operated with high voltages due to the low current in each channel and hence the low heating, Morf *et al.*, 2001.

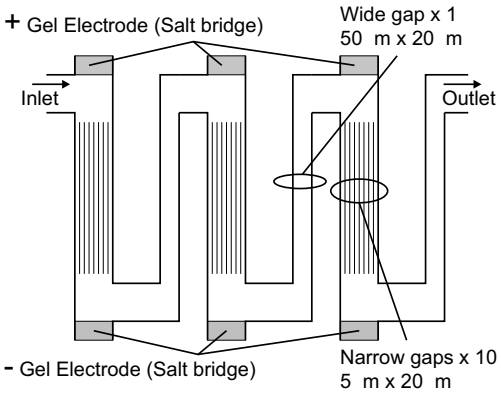

Figure 5.5: Low-Voltage Cascade EO pump with three steps. The pressure can be increased by simply increasing the number of steps. EOF generates large pressures in narrow channels, refer to Eq. (3.5b). By letting the EOF pass through many narrow channels and through one wide channel with reversed electric field a net flow is generated without accumulation of voltage, Takamura *et al.*, 2001.

One disadvantage of the cascade pump is that it often requires a lot of electrodes. The Low-Voltage Cascade pump is very interesting because it offers the possibility of high pressures at low voltages. High voltages are impractical in portable devices and can be dangerous to work with. Both of the cascade pumps are thoroughly analyzed in Chap. 6.

5.3.2 The Shallow EO Pump

The characteristic feature of this type of pump is the planar nature of its design. A design by Chen *et al.* consists of a short, wide and extremely shallow channel. The electrodes are embedded in two reservoirs. This design combines a high

pressure and with a high flow rate. Experiments have been done by Chen *et al.* at Stanford Microfluidics Lab, Fig. 5.6.

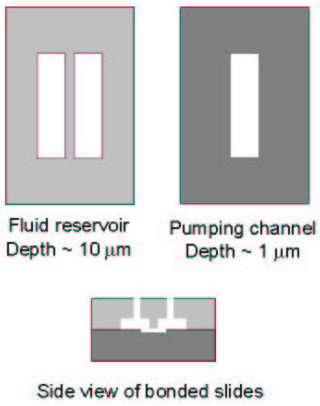

Figure 5.6: Schematic of the planar EO pump produced at Stanford Microfluidics Lab. The EO section is 4 cm wide, 1 mm long and $0.9-1$ μm deep. The potential is applied between the two reservoirs. The flow enters in one of the reservoirs perpendicular to the chip and exits through the other. The pump has a backpressure capacity of almost $p = 1.5$ bar in the range $Q = 1 - 10$ μL $(\text{min})^{-1}$.

The parallel plates were separated by some plateaus/ribs, which cannot be seen on Fig. 5.6. The plateaus should give the design structural stability, but after the bonding the plates gradually collapsed over a period of two months. Hence, the dimensions of the cross section are unknown. A picture of the actual pump setup can be seen in Fig. 5.7.

Parameters such as the EO mobility and full geometry are missing, which makes it impossible to simulate the pump characteristic accurately. However, my estimate calculations show that the flow rate should be much larger than the experimental values. This is also an indication of the plate collapse. The design cannot be directly integrated into a system. This problem will be addressed in Sec 7.2, where the the design is further developed.

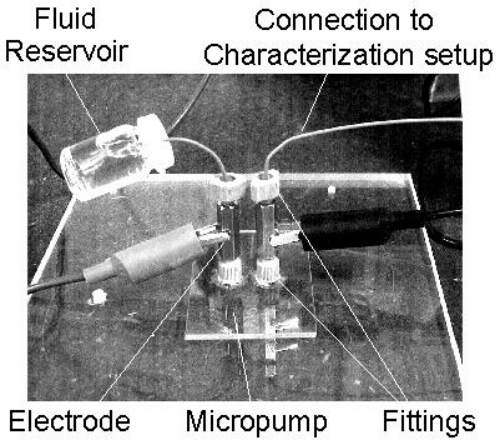

Figure 5.7: Picture of the planar EO pump setup produced at Stanford Microfluidics Lab. The electrodes, tube fittings and reservoir are clearly shown. The actual micropump lies in between the two electrodes and is difficult to see. The picture illustrates how large the lab equipment is compared to the microchannels.

5.3.3 The Porous EO Pump

The electroosmotic velocity is independent of the capillary radius, as long as the infinitely thin Debye layer approximation is valid. In pressure driven flow,

Poiseuille flow - the velocities are proportional to the radius squared $u \propto a^2$. Hence, electroosmotic pumping is much more efficient in small capillaries. One way of utilizing this effect is to pack a larger capillary with tiny nonporous particles. The particles are retained with a micro filter, a so-called frit[1], in each end, Fig. 5.8. The frit blocks the particles, but allows the liquid to pass with some hydraulic resistance. The packing effectively increases the surface-to-volume ratio within the capillary, allowing the generation of very high pressures.

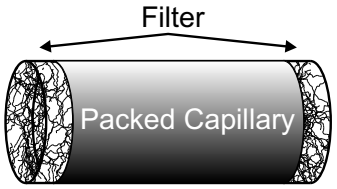

Figure 5.8: Porous pumping by use of nonporous particles and microfilters, e.g., frit. The potential is applied along the packed capillary. Pressure in excess of 20 bar have been obtained, Zeng *et al.*, 2001.

From a transport point of view, this type of pump will have a very large mixing effect due to the irregularity of the channels. Due to its physical properties, it cannot be integrated directly into a chip with the currently available fabrication techniques. With respect to pressure capacity, it is very promising. One of the challenges is to fabricate a frit with low hydraulic resistance.

Example: *Porous pump, Zeng*
Dimensions: diameter 530 μm, length 5.4 cm and packed with 3.5 μm nonporous silica particles.
Solution: Deionized water is used, but due to contact with the atmosphere an equilibrium with carbon dioxide is established, reducing pH to 5.7. The concentration of carbonic acid is estimated to $c = 7.5$ μM, giving a Debye length of $\lambda_D = 0.11$ μm, which is quite large, but still smaller than the pore radius.
Electric field: 2 kV/54 mm = 37 V/mm. This type of pump can create very large pressures (max. backpressure $p = 23.5$ bar). For zero back pressure the max flow rate is $Q = 0.08$ μL/s. The driving field is very large, so the bulk fluid must have a low conductivity in order to avoid excessive ohmic heating.

5.4 Electrodes

A very important issue in the practical realization of electroosmotic pumps is the electrodes. Some types of electrode arrangements are presented below.

5.4.1 Metal Electrodes

Rafael Taboryski from the Danish company Sophion Bioscience A/S pointed out that one of the practical problems with EO pumps is the lifespan of the electrodes. In one of their EO pumps the lifespan is as short as five minutes.

[1] The fused or partially fused materials used in making glass.

Example: *Electrode lifespan*
Using a biobuffer 150 mM NaCl allows for transportation of living cells. At lower or higher concentrations the cells are destroyed due to diffusion of salts. The reactions at the electrodes are

$$\mathrm{Ag}^+ + e^- \rightarrow \mathrm{Ag}, \tag{5.2}$$
$$\mathrm{Ag} + \mathrm{Cl}^- \rightarrow \mathrm{AgCl} + e^-. \tag{5.3}$$

The rate at which the anode disappears is

$$\left.\begin{array}{rl} I = & z\ v\ F \\ \frac{dm}{dt} = & M\ v \end{array}\right\} \frac{dm}{dt} = M\frac{I}{z\ F} \tag{5.4}$$

where v is the reaction velocity, $M_{\mathrm{Ag}} = 107.9$ g mol^{-1} the molar mass of the silver electrode, I the electric current, $z = 1$ the number of charges exchanged per reaction, and finally F is the Faraday constant. Let us consider a fictive example and assume that the electric current is $I = 1$ mA and that the electrodes weigh $m = 1$ g. Then the lifespan $t = m\left(\frac{dm}{dt}\right)^{-1} = 15$ min.

5.4.2 Gel Electrodes

Another type of electrodes is the so-called gel electrodes. The metal electrode is connected to an electrical conducting gel, which is in contact with the fluid, Takamura *et al.* 2001. Hence, the gel acts as a salt-bridge and a pressure seal and avoids bubble formation in the fluid region. In the Takamura case there were some problems with the gel electrodes, such as leaks and high resistance.

5.4.3 Indirect Electrodes

As an alternative, the electrodes ions can be introduced through side channels as shown in Fig. 5.9. The aim is to allow ions to move, while the liquid is retained, i.e., a salt-bridge.

In the process of bonding the lid to the substrate, one leaves a small gap on purpose, see Fig. 5.9. An extremely shallow channel is therefore generated, allowing ions to travel across the gap from the side channels to the main channel, Fig. 5.10. The EOF in this junction is restricted because the very small dimensions cause the Debye layers to overlap. Recalling Fig. 2.2, an overlap will occur if the channel dimension is smaller than $a < 0.1\ \lambda_D$. Hence, this type of pump will only work for low buffer concentrations/thick Debye layers, depending on the gap depth D.

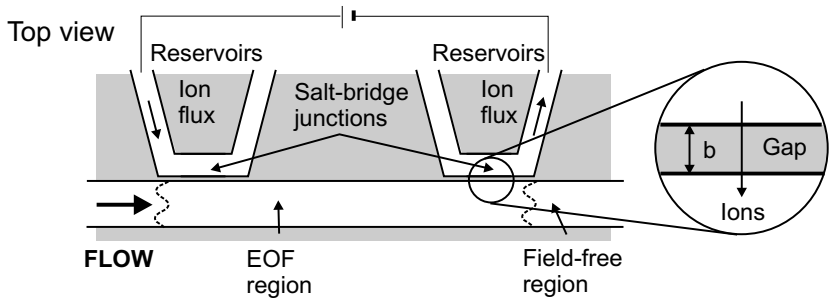

Figure 5.9: Indirect electroosmotic pumping. The potential is applied in two external reservoirs. In this way the electrodes are kept away from the channel. The gap width, $b \approx 3 - 9$ μm. More details of the gap is shown in Fig. 5.10.

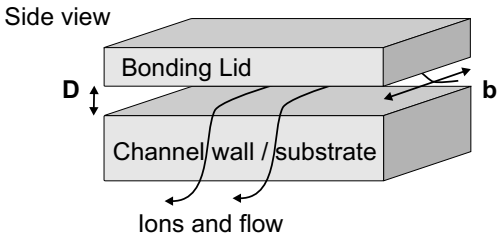

Figure 5.10: Illustration of the shallow slit between the substrate and the lid. The ions move over the wall and through the slit between the substrate and the lid. The gap depth is $D \approx 100$ nm. The setup only works if the Debye layers overlap.

In this manner, it is possible to transfer ions with only a small portion of bulk fluid. However, if the gap is too deep, there may be considerable liquid flow across the junction. In the worst case all the flow goes through the junction, and the pump is useless.

The indirect electrode arrangement is a very promising technique, because it has the same advantages as gel electrodes, but is much simpler to fabricate once the technique is available. Experiments with indirect EOF have been done in silicon by Guijt *et al.*, 2001 and Alarie *et al.* 2001.

Chapter 6

Models and Simulations

At this point in the thesis, we should possess the basic tools to analyze an EO pump. In the micropump overview chapter, different types of pumps were introduced. The idea is to select two existing EO pumps and apply the concepts from the previous chapters.

In the following sections we shall therefore model and simulate two different types of pumps - cascade pumps - using CFD. Both pumps have been introduced in the overview chapter.

The first pump is a set of pumps connected parallel to each other - The Parallel Cascade Pump. Design from Morf *et al.*, 2001.

The second pump consists of a set of pumps connected in series - The Low-Voltage Cascade Pump. Design from Takamura *et al.*, 2001.

6.1 Parallel Cascade Pump, Morf *et al.*

Based on the experimental and theoretical work by Morf *et al.*, we shall investigate a pump with six separate channels of different lengths, Fig. 6.1(a). The geometry of the pump is very simple, and a analytical approach is feasible.

The first step is to find the equivalent electrical circuit, Fig. 6.1(b). The geometrical data are inserted in a worksheet, and the hydraulic and electrical resistance of the segments are found using Table. 3.1. The total resistances are then calculated analytically by use of circuit theory. If the system had been more complex, an electronic analysis program such as SPICE could have been used. The pump characteristic can then be found using Eq. (3.39).

The calculations by Morf *et al.* are based on a whole system consisting of pump, tubes, mixer, etc. We are only considering the pump part.

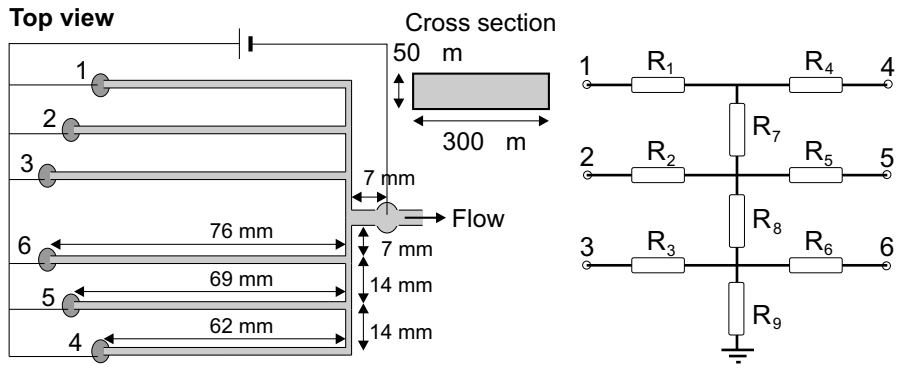

(a) Fluidic network. (b) Electrical circuit.

Figure 6.1: (a) Channels 1-6 are the inlets, and the far most right tab is the outlet. The figure has correct aspect ratios. (b) This is the electrical circuit equivalent to the fluidic network. The resistances can be calculated from the fluidic network, Morf *et al.*, 2001.

It should not be necessary to simulate the parallel cascade pump using CFD. However, we want to build confidence in using CFD, so we apply it to a problem where we know the solution in advance. This serves as a test case for the use of CFD in microfluidic devices.

In the simulations the velocities are varying from $0.4 - 2.7$ mm/s, giving a maximum pressure difference between static and dynamic pressure of $p_{\text{vel}} = \frac{1}{2}\rho u^2 = 4 \times 10^{-3}$ Pa. Pressure losses due to the bending of the channels are thus negligible[1]. The equivalent circuit theory assumes that the channels are infinitely thin - lines. This means that the regions within and near the junctions are approximated with a uniform flow. The error by making this assumption is very small in the present case, because the channels are very long compared to their width.

6.1.1 Meshing

In order to make accurate simulations a good mesh is imperative. A good mesh is more dense in regions of large spatial and/or temporal variations. Since the present simulation is time independent, we will only focus on the spatial resolution of the flow.

A 2D simulation is not possible, since the flow resistance is governed by the 3D geometry. The problem is two-fold symmetric, which gives a reduction in the number of cells by a factor 4. The length-to-width ratios of the channels are very large, 8×10^4 μm/300 μm $\simeq 300$. Insisting on cubic 3D cells, say $5 \times 5 \times 5$ μm^3 would in the symmetric case give a mesh with 1.3×10^7 cells. This quite coarse mesh would effectively be impossible to simulate on a normal computer[2]. The number of cells can be reduced by using cells with large aspect ratios. Adjacent cells must be of comparable sizes, so the mesh needs to be biased (graded) in the direction of the channel, Fig. 6.2.

[1] In hydraulic engineering the velocity head, p_{vel}, is assumed lost in a 90^o bend in turbulent flow, Pedersen.

[2] The used computer is a 933 MHz Pentium III with 512 Mb of RAM.

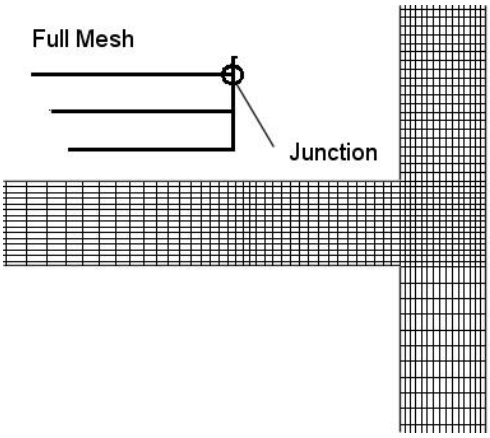

Figure 6.2: The mesh is generated in COVENTOR 2001.3 and consists of two parts. The three horizontal channels are biased towards the junctions. The mesh contains 1.56×10^5 elements, with 15×8 in the cross sections. Recalling the symmetry BC, this corresponds to 15×16.

The biasing is not straightforward in COVENTOR. Two or three separate meshes have to be created, aligned and merged into a single mesh. COVENTOR 2001.3 is not flexible with respect to biasing. Hence the horizontal and vertical channels must be generated separately. Then the horizontal channels must be biased and cut in half because it can only bias in both directions. Other more advanced programs such as I-DEAS could be used to generate the mesh. The mesh can then subsequently be imported into COVENTOR. For the present geometry, the meshing tool provided by COVENTOR is sufficient. The final mesh contains 1.56×10^5 cells and for a steady state simulation, the computing time is two hours. However, the internal handling in program such as mesh generation, assigning patches, etc., is very tedious because the graphical interface is very slow.

6.1.2 Results

Several simulations were done on this geometry. Many of the initial simulations gave poor results due to improper meshes. The meshing is difficult because of the aspect ratio of the geometry. The purpose of the simulation is to find corresponding values of flow rate and pressure (Q-p). These values are therefore the first to be evaluated in a simulation. The simulated values lie within 2% of the circuit model, Table 6.1 and Fig. 6.3.

	Flow rate Q/nL/s	Backpressure $p_{\max}$/Pa	Hydraulic resistance R_{hyd}/g $(\text{mm}^4\ \text{s})^{-1}$
Model	44.76	321.8	7190
Simulation	44.28	314.4	7099
Deviation	1%	2%	1%

Table 6.1: Comparisons between with model and simulation, Appendix B, Morf.

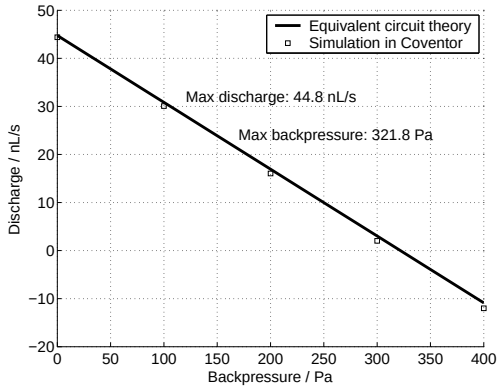

Figure 6.3: Comparison between simulated values and the analytical results from the equivalent circuit model. The simulated values are slightly below the theoretical line. Parameters: $\phi_a = 1000$ V, $\alpha_{eo} = 6 \times 10^{-8}$ m^2(V s)$^{-1}$, and $\mu = 1.00 \times 10^{-3}$ kg(m s)$^{-1}$.

The electric field is governed by the Laplace equation with the homogeneous Neumann BCs at the walls and Dirichlet BCs at the electrodes. The Neumann condition prescribes that the gradient of the potential in the normal direction is zero. This is equivalent of an insulating surface. The flux of the electric field is conserved. Hence, the fields from the side channels are added to the field in the vertical channel, Fig. 6.4.

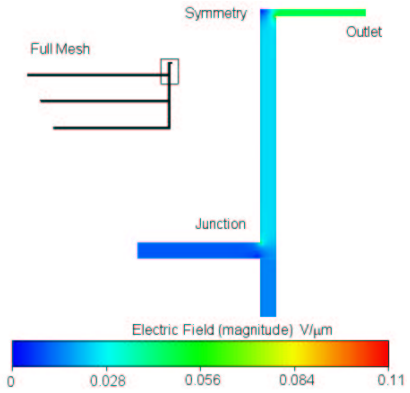

Figure 6.4: The electric field reaches its maximum after the last junction near the outlet. Due to the discontinuous nature of the BC at the corners, the field becomes distorted. A mathematical solution of the problem gives a singularity at the corner. For a mesh with a finite cell size this singularity is smeared out over a region. This effect distorts the solution near the junction. Parameters: same as Fig. 6.3.

2% for Q and p is very close to the model, but I wanted investigate how good an accuracy could be obtained with EOF and pressure in a straight channel. Using the same cross section geometry, a 1% accuracy could be obtained. The simulations converged to a slightly different value than the theoretical. A close look on the velocity field revealed that the velocities in the corners were too large. This is caused by the discontinuous BC for the electric potential. The remedy would be to make round corners or specify velocity as BC instead of EO mobility.

These effects are important for the local flow characteristics. The integrated variables Q and p are however not so sensitive. The pressure distribution is shown in Fig. 6.5.

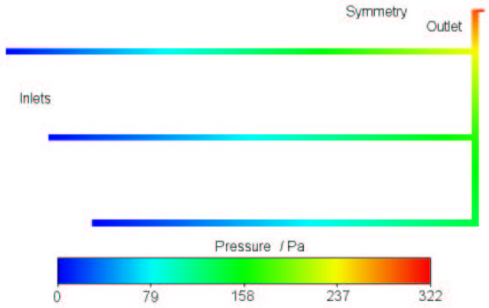

Figure 6.5: The pressure is rising continuously from the inlet to the outlet. The rate of the pressure buildup depends on the EO velocity u_{eo} and is hence proportional to the electric field. The pressure increases fast near the outlet. Parameters: same as Fig. 6.3.

6.2 Low-Voltage Cascade Pump, Takamura *et al.*

In this section we shall analyze the Low-Voltage Cascade pump described in the overview chapter, Fig. 5.5, Takamura *et al.*, 2001. It is designed to work as an effective pressure source. The main principle is to set multiple pumps in series in order to accumulate pressure. The pump design was first presented in the micro-TAS 2001 proceeding. The published article contained no calculations. From the information given in the article it is not possible to simulate the pump. So I contacted Ph. D. Yuzuru Takamura from The University of Tokyo and he agreed on giving me additional information about the geometry. So the present analysis is the first CFD analysis of this type of pump.

The analysis has two steps: an analytical model and CFD computations. Comparisons between the two approaches should ensure reliable results.

6.2.1 The Model

The flow is a combination of EOF and pressure driven flow. The calculations are based on the hydraulic resistances and the equivalent EO pressure of the narrow and wide section respectively Fig. 6.6(a).

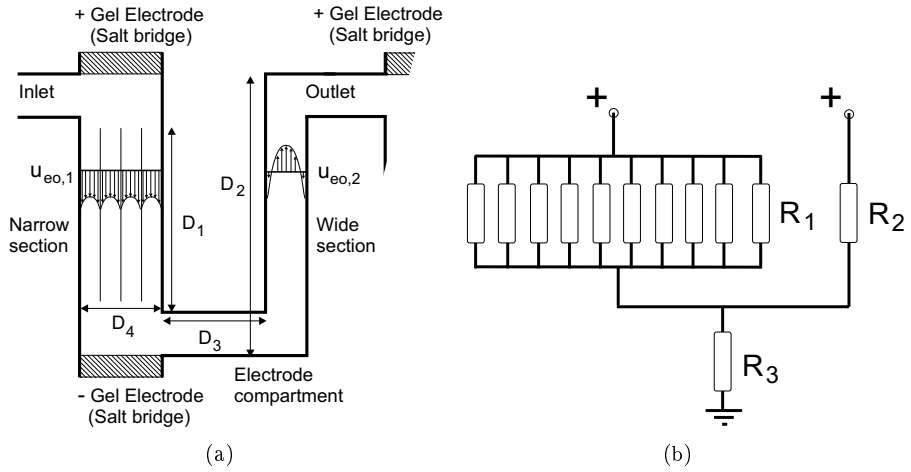

Figure 6.6: (a) Simplified schematic of the pump and the expected flow profiles, refer to Fig. 5.5 for additional geometrical information (width of channels). There are $N = 10$ channels in the narrow section (only depicted four). Even though the flow is reversed near the wall in the right channel, the netflow is still positive. Note that $u_{\mathrm{eo},1} > u_{\mathrm{eo},2}$ because the electrode spacing is different. Parameters: $D_1 = 800$ μm, $D_2 = 1230$ μm, $D_3 = 170$ μm and $D_4 = 185$ μm, (b) The electrical circuit equivalent used in calculation of potential drop across the EO section.

Combining Eqs. (3.37) and (3.42) yields Eq. (6.1). Each of the narrow channels gives the same high pressure. The wide channel gives a small counter pressure because the electric field is reversed. The pressure across the whole step is the two pressures subtracted, $\Delta p_{\mathrm{step}} = p_{\mathrm{eo,N}} - p_{\mathrm{eo,W}}$.

$$\Delta p_{\mathrm{eo}} = \frac{12\ \mu\ \alpha_{\mathrm{eo}}\ \Delta\phi_a}{H^2 - 192\pi^{-5}(H^3/W)\sum_{m=0}^{\infty}(2m+1)^{-5}\tanh[\frac{(2m+1)\pi W}{2H}]} \tag{6.1}$$

The individual hydraulic resistances $R_{\mathrm{hyd},1}$ and $R_{\mathrm{hyd},2}$ are calculated using Eq. (3.42). Only the narrow and wide section are considered in the calculations, $R_{\mathrm{hyd,total}} = N^{-1}R_{\mathrm{hyd},1} + R_{\mathrm{hyd},2}$, Fig. 6.6(b). The third hydraulic resistance is neglected because it is relatively small. Furthermore the flow is not uniform in this section so the circuit theory does not apply. The error by making this assumption is of the order a few percent. R_3 is used the calculation of the effective potential.

The potential drop across the EO section is found using the equivalent circuit shown on Fig. 6.6(b). For the potential drop only the relative resistances are relevant. The individual resistances are proportional to $R \propto L/(W \times D)$, where L, W and D are the length, width and depth of the channel respectively. The relative potential drop η across the EO section is

$$\eta = \frac{\left(\frac{N}{R_1} + \frac{1}{R_2}\right)^{-1}}{\left(\frac{N}{R_1} + \frac{1}{R_2}\right)^{-1} + R_3} = 0.885. \tag{6.2}$$

From Eq. (6.2) it can be seen that approximately $\eta = 89$ % of the applied potential ϕ_a, is used in the EO section. This potential does not equal the actual applied potential because another potential drop occurs in the gel electrodes, Fig. 6.6(a). Hence, ϕ_a is unknown but could have been estimated if the electrical current and conductivity of the liquid had been measured experimentally.

All of the above calculations are inserted in a worksheet, Appendix B, Takamura. From this worksheet the results can be extracted.

6.2.2 CFD

Identifying the minimum computational domain is important in order to save calculation time. Only one pump step needs to be analyzed. The cut should be placed where the flow is uniform. So the cut shown in Fig. 6.6(a) would not be a good choice because the flow is nonuniform near the inlet and outlet.

The computational domain may be divided because the flow is creeping, i.e., inertial effects are negligible. So it does not matter which way the flow is moving. This approximation was verified by a full geometry simulation. Furthermore a horizontal symmetry plane can be applied. A top view of the computational domain is shown on Fig. 6.7, lower corner. The flow rate is the same but the pressure buildup must be multiplied with two in order to obtain the full step pressure buildup.

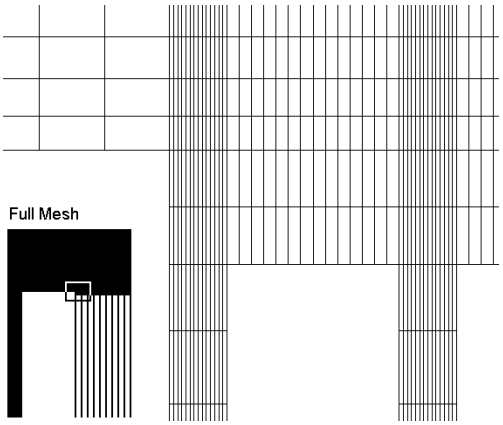

Figure 6.7: Part of the mesh used in the CFD simulations. There are 14 cells across the narrow channels and 7 cells perpendicular to the plane, corresponding to 14 without symmetry. The junction between the narrow channels and the electrode compartment is not very well resolved. Large cells are adjacent to small cells. The computations cannot be trusted near these junctions. The full mesh contains 1.02×10^5 cells.

Using the experience from other cases, a relatively simple mesh was generated. An important issue is that flow profiles in the narrow channels are resolved. In this simulation 14×7 cells are used in the cross sections. With the symmetry BC it corresponds to 14×14 which is good enough within 5% accuracy for the profiles with full EOF and superposed pressure driven flow. The mesh used could be improved in the junction areas as shown on Fig. 6.7. However, the results for flow rate and backpressure in Table 6.2 are within 3% and 2% respectively, indicating that the overall picture is good enough.

6.2.3 Results

The essential flow parameters are compared in Table 6.2. There is a good agreement between the simulation and circuit model.

	Flow rate Q/nL/s	Backpressure $p_{\max}$/Pa	Hydraulic resistance R_{hyd}/kg (m^4 s)$^{-1}$
Model	0.577	281.0	4.88×10^{14}
Simulation	0.560	274.0	4.89×10^{14}
Deviation	3%	2%	0%

Table 6.2: Comparisons between with model and simulation based on estimated values for $\phi_a = 10$V and $\alpha_{\text{eo}} = 0.06$ mm^2(V s)$^{-1}$, Appendix B, Takamura.

The flow profiles can be seen in Fig. 6.8. Remembering that the flow is symmetric, one may visualize the full flow profile. The maximum velocity in the core of the wide section is a factor 2.4 larger than the EO velocity at the walls.

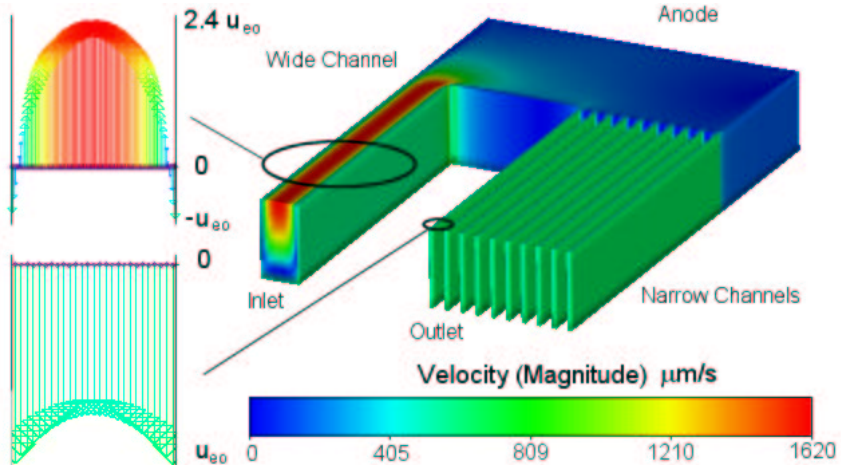

Figure 6.8: Velocity magnitude $|\mathbf{u}|$ visualized at the symmetry plane and the surface. Velocity profiles are extracted from the symmetry plane in the wide and narrow channels respectively. The computational domain has been graphically thickened for visibility. Parameters: $\alpha_{\text{eo}} = 0.06$ mm^2/(V s), $\phi_a = 5$ V (which corresponds to 10 V for a whole step) and $p_{\text{inlet}} = p_{\text{outlet}} = 0$.

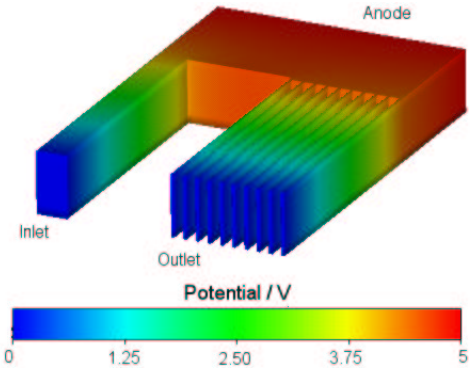

Figure 6.9: Plot of the potential. $\phi_a = 5$ V is applied to the anode and zero volts to the inlet and outlet. This is equivalent to applying $2\phi_a = 10$ V across a full pump step. Parameters: same as Fig. 6.8.

The CFD simulation gives the pressure loss $\Delta p = 23$ Pa in the area near the anode. The estimated pressure drop is a combination of pressure loss due to friction and due the reverse electroosmosis. The hydraulic pressure loss is calculated using

$$\begin{aligned} \Delta p &= R_{\text{hyd}} Q && (6.3)\\ &= 0.5 \times 3.208 \times 10^{13}\ \text{kg(m}^4\ \text{s)}^{-1}\ 0.577 \times 10^{-12}\ \text{m}^3/\text{s} && (6.4)\\ &= 9.26\ \text{Pa} && (6.5) \end{aligned}$$

We also note that the simulated values for flow rate are slightly below the model values in Table 6.2.

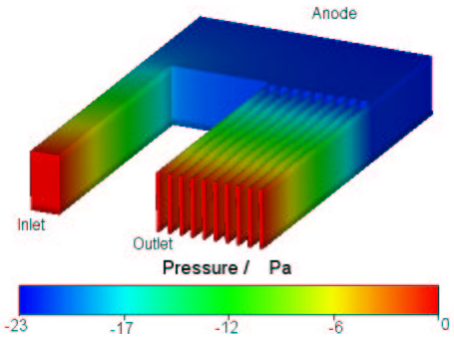

Figure 6.10: Plot of the pressure when zero backpressure is applied. Inlet and outlet are both kept at $p = 0$. A negative pressure of 23 Pa is generated in the vicinity of the anode. The flow in the anode/electrode compartment is not parallel with the EOF and is hence partially pressure driven. Hence a pressure is needed for the flow to move in this region. Parameters: same as Fig. 6.8.

In Fig 6.10 a minimum pressure of $\Delta p = 23$ Pa was simulated. In Appendix B, Takamura 1/2, it can be seen that the model calculates a electroosmotic pressure is calculated to be $\Delta p_{\text{eo,W}} = 0.521$ Pa $= 10.5$ Pa in the wide channel for a half stage.

So the overall estimated pressure loss is $\Delta p = (10.5 + 9.26)$ Pa $= 20$ Pa which should be compared with the simulated $\Delta p = 23$ Pa. The causes for this small deviation is that the hydraulic resistance of the middle section was neglected. Hence, the model overestimates the flow rate and backpressure capacity of the pump, refer Table 6.2.

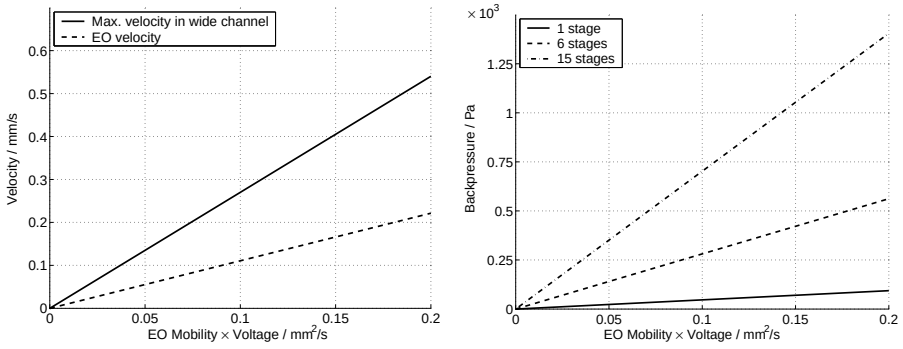

(a) (b)

Figure 6.11: (a) The calculated velocities, $u_{\rm eo}$ and $u_{\rm max}$, as a function of the EO mobility times the applied potential, $\alpha_{\rm eo} \times \phi_a$. (b) Maximum backpressure again as function of $\alpha_{\rm eo} \times \phi_a$. Parameters: $\mu = 1.00 \times 10^{-3}$ kg/(m s).

In the case of a 15 step cascade pump Takamura *et al.*, 2001, measured a static pressure of 800 Pa at an external voltage of 24 volts. From Fig. 6.11(b) this corresponds to $\alpha_{\rm eo} \times \phi_a = 0.114$ mm^2/s (calculated). In Fig. 6.11(a) the corresponding velocities are $u_{\rm eo} = 0.13$ mm/s and $u_{\rm max} = 0.31$ mm/s.

The experiments give a "Free Run EOF Velocity" of 0.50 mm/s, which is clearly more than expected. According to Takamura the measurements are conducted in the last wide section, which has no electric field. Hence, the flow is solely pressure driven. The model predicts a flow rate of 0.110 nL/s at $\alpha_{\rm eo} \times \phi_a = 0.114$ mm^2/s. The task is to convert a flow rate into a max velocity for a pressure driven flow in a given cross section. In a rectangular channel with an aspect ratio of $W/H = 2.5$, the nondimensional flow rate is $Q^* = 0.52$, refer Fig. 3.6.

$$Q = A\, u_{\rm max} Q^* \Leftrightarrow \tag{6.6}$$

$$u_{\rm max} = \frac{Q}{Q^* A} = 0.21 \text{ mm/s} \tag{6.7}$$

where $A = 50 \times 20 \mu$m^2. The velocity presented in the article is either $u_{\rm max} = 0.21$ mm/s, $u_{\rm mean} = 0.110$ mm/s or a combination. It would have been more useful to measure the flow rate. Either way, it deviates by a factor $2.4 - 4.5$ from the simulation and model value, which match within a few percent. Note that it is the ratio between backpressure and velocity that deviates. The absolute values cannot be calculated on basis of the given information.

Calculations with the EO mobility $\alpha_{\rm eo} = 0.06$ mm^2/(V s) gives considerably larger pressures than those measured. For the 15 stage pump with $\phi_a = 10$ V the backpressure is calculated to 4200 Pa. Indicating that the pressure measurements are inaccurate or the pump is leaking.

I contacted Takamura with these conclusions, and he agreed that the results from the micro-TAS 2001 proceedings were problematic. He had some possible explanations to the discrepancies:

- Dimensions of the fabricated pump is not consistent with the design. The

cross section of the fabricated narrow section was not rectangle but trapezoid.

- The pressure does not increase linearly with the number of stages. Leaks was observed at the gel electrodes.
- Accuracy of the velocity and pressure measurements.

If the dimensions are inaccurate it is difficult to estimate the backpressure capacity, recalling that $\Delta p_{\text{eo}} \propto a^{-2}$ where a is a characteristic length. The consequence is, that if the narrow channels are 2 μm wide instead of 1 μm, the backpressure would be a factor 4 smaller. The geometry of the cross section is a secondary effect compared to the effect of the dimensions.

The accumulation of pressure was not a linear function of the number of stages. This is a clear indication of a pressure leak. The first stages will hold tight, but as the pressure increases an eventual leakage will be more pronounced. The result is a lower pressure and flow rate than expected.

The above explanations can account for the large deviations and Takamura has explained that improvements have been made in the next version of the Low-Voltage Cascade Pump.

6.3 Summary

In the Morf case it has been shown that the equivalent circuit theory and CFD simulations with COVENTOR give consistent results within $1-2\%$ for the flow rate and the backpressure. Problems with the electric field have been identified and remedies are suggested. This problem is however not that important with respect to the backpressure and the flow rate. It is also concluded that CFD is not efficient for this simple geometry.

In the Takamura case an analytical model was obtained using the circuit theory. Simulations agree with the model within 3%. The larger discrepancy arises because the analytical model is a simplification of the real problem. The model was used to analyze the experimental results obtained by Takamura *et al.*, 2001, and a considerable deviation was found, i.e., by a factor $2-5$. Collaboration with Takamura illustrated the clear advantage of a theoretical/simulation approach. The combination of the circuit model and CFD calculations proved its strength.

In both cases the equivalent circuit theory is very well suited to calculate the pump characteristic. In the Parallel Cascade Pump case application of CFD was not necessary, but primarily used as a test case. In the Low-Voltage Cascade Pump, CFD provided a better understanding and a higher degree of accuracy.

Chapter 7

Novel Designs

Based on physics of liquids, elementary flow analysis, and existing designs, we can make our own innovations. In this chapter two novel concepts will be introduced. (1) The Two-liquid Viscous Pump. This pump uses an internal pumping liquid, which makes the pump independent of the working liquid (buffer). (2) The Shallow Reservoir Pump. The existing planar/shallow EO pump by Chen *et al.*, 2000, Fig. 5.6, cannot be integrated on a device without external tubing. Using two reservoirs with the appropriate dimensions, the integration may be accomplished.

7.1 The Two-liquid Viscous Pump

Electroosmosis is governed by the formation of an electric double layer. If the working liquid does not contain any ions, no electric double layer is formed. A measure for the amount of ions is the electrical conductivity. The range for the working fluids is $\lambda_{\text{elec}} > 10^{-6}$ S/m, Chen *et al.* Hence, nonpolar liquids such as oils with very low conductivity cannot be pumped with EO. The remedy is to introduce a pumping liquid that drags the working liquid by viscous forces thus the name, Two-liquid Viscous Pump. Its performance is similar to EOF in a single narrow channel.

7.1.1 Design history

The Idea

In this section the design process will be described. In the beginning of the project I was presented with the design shown in Fig. 7.1. The device had been used for focusing pressure driven flows. Oliver Geschke got the idea to use the device as a two-liquid EO pump. Some preliminary experiments were unsuccessful. There are several reasons for this which we will clarify in the following sections.

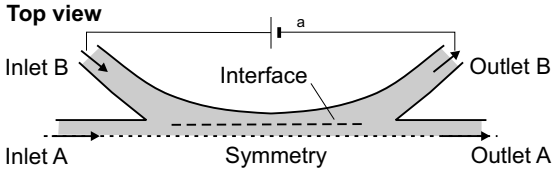

Figure 7.1: The first idea of a Two-Liquid Viscous Pump. The pumping liquid enters through inlet B, and the buffer liquid at inlet A. Inlet/outlet B are connected to external reservoirs.

The pumping liquid enters through inlet B, and the buffer liquid at inlet A. A thin layer of the pumping liquid is supposed to move along the wall from inlet B to outlet B. It is this movement that drags the buffer liquid. The thickness of this so-called pumping liquid layer is denoted D_{layer}. In the case of two equally conducting liquids, the following would happen: There would be EOF between Inlet and outlet B as expected, but the interface would be coinciding with the symmetry line. Recall that EOF cannot be regulated by tapering or expanding the channel. Hence, the pumping liquid would occupy the entire channel leaving no room for the working liquid. The phenomena was described in Sec. 3.3.1.

The solution is to reduce the EOF in the two side branches. This can be accomplished by doing one of three things. (1) Reducing the EO mobility in the branches. (2) Lowering the electric field by introducing another set of electrodes. (3) Making the branches so narrow that the Debye layers overlap, resulting in a decreased flow rate.

Assuming that the interface existed in Fig. 7.1, the pump would still not work. Inlet/outlet B are connected to external reservoirs. These reservoirs are open, and thus subjected to atmospheric pressure. The pressure buildup in the pump will therefore drive a flow from inlet A and B to outlet B. Generally, the flow will go where the hydraulic resistance is the lowest, so a pressure valve is needed.

The design in Fig. 7.1 is also heavily influenced by macroscopic thinking. Inlet B and outlet B are guided smoothly into the channel, avoiding any sharp corners, which in turbulent flow would give rise to separation and consequently pressure loss. In microfluidics the flow is laminar, and sharp bends do not give rise to any pressure loss. The pumping liquid can therefore easily be introduced perpendicular to the channel.

Tube fittings

A pressure valve could be an EO driven device with a very high hydraulic resistance. Such a device would have a constant flow rate independent of the pressure difference across the device. A simple way of realizing this setup is to place two long thin tubes between the pump and the electrodes, Fig. 7.2. The tubes can easily have a lower EO mobility, and hence a reduced flow rate. In this way, the thickness of the pumping liquid layer may be controlled.

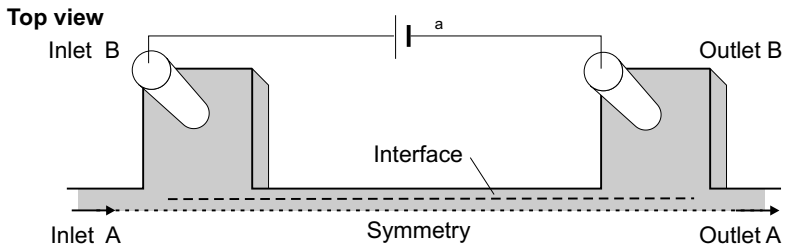

Figure 7.2: The Two-liquid Viscous Pump with two external tubes inlet/outlet B. The large hydraulic resistance of the tubes prevents any pressure driven flow from escaping through inlet/outlet B. A major problem is the large potential drop in the tubes, reducing efficiency considerably.

The problem is that the electric resistance of the thin tubes will be correspondingly large. Hence, the main potential drop will occur in the tubes and not in the EO channel. This is a problem because the pump will require high operation voltages with the associated disadvantages.

7.1.2 The final design

In the following design the previously mentioned problems are addressed. Three issues are the main concerns. (1) Design of a pressure valve. (2) Reduction of EOF in specific regions, denoted B in Fig. 7.3, in order to reduce the pumping layer thickness. (3) The main potential drop should occur in the EO section.

The optimal pump would be narrow and deep. Narrow because it gives large pressures, and deep because of a large flow rate. This type of geometry can be achieved by using the ICP etching technique discussed in Sec. 5.2.

The pump shown in Fig. 7.3 consists of two electrode compartments and a main channel. The electrode compartments are separated from the main channel by use of so-called hydraulic valves. A hydraulic valve is simply a set of narrow channels with large hydraulic resistance. The valves are needed because each electrode compartment is connected to an open reservoir, and thus subjected to atmospheric pressure. The electrodes are placed in these reservoirs.

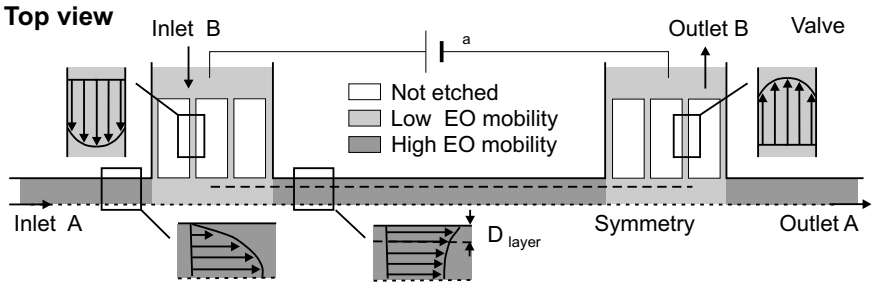

Figure 7.3: Schematic of the Two-liquid Viscous Pump. The expected velocity profiles are shown to give an idea of the overall flow. Internal friction gives rise to a counter pressure, which induces the parabolic flow profiles. The thickness of the pumping liquid layer is D_{layer}.

Hydraulic Valve

Consider a channel with a as a characteristic length and flow rate Q. For EOF the flow rate is proportional to $Q \propto a^2$, whereas in pressure driven flows it is proportional to $Q \propto a^4$. Hence, by letting the channel dimensions a become very small the pressure driven flow is suppressed compared to the EOF. This effect can be utilized to block pressure driven flows, the so-called hydraulic valve. The overall hydraulic resistance of the valve must be large compared to the resistance of the EO section, in order for the valve to be effective.

The ohmic heating is proportional to the square of the electric field strength, as shown in the energy equation Eq. (2.15). In order to reduce the ohmic heating and potential drop, the area of the cross section in the valve is increased. This is achieved by increasing the number of channels in the valve. By doubling the number of channels, the ohmic heating is reduced by a factor four. In Fig. 7.4 there are four channels connecting the electrode compartment with the buffer channel. For the given geometry approximately half of the potential drop is across the EO section.

Thickness of pumping layer

The pumping liquid that enters the main channel will generate a layer of some thickness D_{layer}. The thickness of this layer is very important with respect to the pump characteristic. If the layer is too thick, only a thin layer of buffer is pumped. The factors that govern the layer thickness are the following:

- The spatial distribution of electroosmotic mobility.
- The ratio of electric conductivities between the two liquids.
- The miscibility of the liquids

These factors make it a complex matter to determine the pumping layer thickness in general. Two cases that cover most practical situations will be considered. (1) Miscible conducting liquids with dilute salt concentrations. (2) Immiscible liquids where the buffer liquid is nonconducting.

(1) In the case of miscible liquids, the pumping layer will rapidly expand to the whole channel due to diffusion. Hence, it is not meaningful to speak of a pumping layer. The effective conductivity of the mixture will be a linear combination of the conductivities of the buffer and the pumping liquid. A further implication is that the flow leaving the pump will be a mixture of the buffer and the pumping liquid. The importance of these effects is strictly application-specific.

(2) Immiscible liquids, e.g., oil-water, will have a well defined interface, and we can use the pumping layer concept. The electric current density will essentially be zero in oil phase. This should be included in the calculation of the electric field. With the present CFD program this, however, is not possible, so the two liquids are assumed to have the same conductivity. The effects of this assumption will be discussed later. Another problem is that the two liquids are assumed to have the same viscosity. In the oil-water case this is certainly not the case. Some analytical calculation are shown in Appendix G. Since the

liquids are immiscible, the contamination should be negligible. However, water droplets may pass the valves at outlet B and then continue downstream. So it is a different type of contamination.

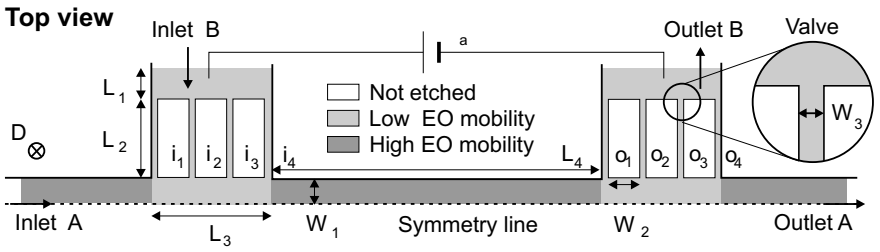

Figure 7.4: Layout of a Two-liquid Viscous Pump. The buffer flow, A, is driven by the pumping flow, B. The pumping liquid enters at inlet B, goes through the narrow valves, moves along the wall, and exits through the valve and finally through outlet B. The two electrode compartments each have four narrow channels of width W_3. The channels/valves ensure that the buffer flow does not enter inlet or outlet B. Two regions with different EO mobilities are identified. The ratio between the mobilities roughly governs the layer thickness of the pumping liquid. The high EO mobility area between the valves is the EO section. The valve regions should be given a coating with low EO mobility. Dimensions used in calculations: $W_1 = 5$ μm, $W_2 = 20$ μm, $W_3 = 1$ μm, $L_1 = 8$ μm, $L_2 = 42$ μm, $L_3 = 64$ μm, $L_4 = 150$ μm and $D = 20$ μm deep, (full geometry, 40 μm).

7.1.3 Equivalent Circuit Model

The aim is to establish a model that can predict the Q-p characteristic. In this respect, the pumping layer thickness, D_{layer}, is important. The EOF depends on the electric field, which depends on the flow in the case of different conductivities. A rigorous model of the two-liquid pump is therefore a complex matter.

We shall only consider miscible and immiscible liquids with the same conductivity. The latter case is unlikely to be of practical interest, because the conductivities will normally be different when dealing with immiscible liquids. The results, however, are of general interest. Furthermore, we assume that the hydraulic valves are so effective that the pressure driven flow through inlet/outlet B is negligible. If the hydraulic resistances of the valves are much larger than those of the EO section, this is a good assumption. R_{hyd} is calculated using Eq. (3.42), remembering that there are four channels in the valves. For the present geometry, the overall hydraulic resistance of the valves is 26 times larger than the EO section, implying that the error is small.

The first step is to find the effective potential $\phi_{\text{eff}} = \eta\ \phi_a$ drop across the EO section. The procedure is to analyze the equivalent electric circuit shown in Fig. 7.5. The calculations are done in Appendix B, Two-Liquid Viscous Pump.

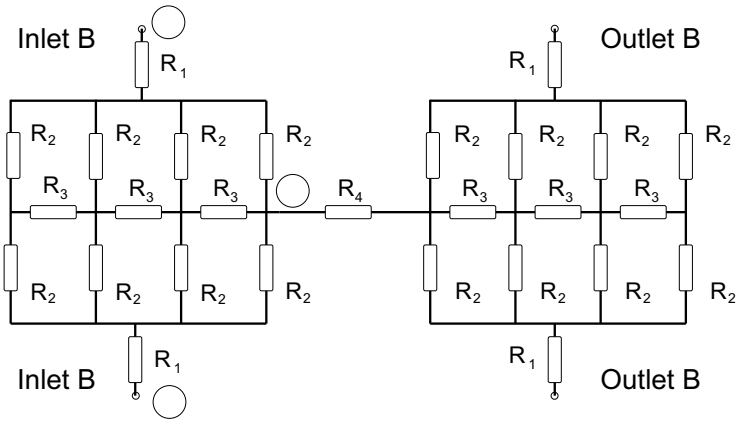

Figure 7.5: The equivalent electric circuit of the Two-Liquid Viscous Pump. Note that the whole pump/circuit is depicted. The overall resistance is calculated as $R_{\text{total}} = 2R_{\alpha\beta} + R_4$, where R_4 is the resistance of the EO section. $R_1 \propto L_1/(L_3 \times D)$, $R_2 \propto L_2/(W_3 \times D)$, $R_3 \propto W_2/(2W_1 \times D)$ and $R_4 \propto L_4/(2W_1 \times D)$. The proportionality factor is in all cases $1/\lambda_{\text{elec}}$.

The second step is to find the electric field in all EO driven sections. We need to find the electric field in the valves. The flux of the electric field is constant. The electric field in the EO section is known because the effective potential drop and the channel length is known. Multiplying the electric field with the area of the cross-section gives us the electric flux. From this we can calculate the average electric field in the valves.

Example: *Electric field*
The relative effective potential η and spacing L are known. $\eta = 0.523$, $\phi_a = 10$ V, and $L = 150$ μm. Hence, the electric field becomes $E = (\eta\phi_a)/L = 0.0349$ V/μm. The ratio between the areas of the cross-sections is 4/5. So the average electric field in the narrow sections becomes $E = (4/5)^{-1}0.0349$ V/μm $= 0.0436$ V/μm.

The third step is to find the effective EO mobility. Simulating with COVENTOR requires that the EO mobility is specified on the walls. In reality, the EO mobility is governed by the interplay between liquid and surface. This makes it difficult to set up the right boundary conditions for a two-liquid simulation, because it requires that the position of the liquids is known beforehand.

In the main channel, it is approximated that the vertical walls have a high mobility, and the bed and lid have low mobilities. The pumping liquid is in contact with the wall, and therefore has a high mobility. The working liquid has a low/no EO mobility, and is in contact with the bed and the lid.

EOF with two different EO mobilities is analyzed in an example in Sec. 3.2.1. The effective mobility is used in the calculations.

Example: *Effective Mobility*
Consider a rectangular channel with two sets of opposing walls. The one set having EO mobilities of $\alpha_{\text{eo,low}} = 5000\ \mu\text{m}^2\ (\text{V s})^{-1}$ and $\alpha_{\text{eo,high}} = 50000\ \mu\text{m}^2\ (\text{V s})^{-1}$ respectively. The aspect ratio of the channel is 2.5. From Fig. 3.4 the nondimensional flow rate is read to be $Q^* = 0.85$. The effective EO mobility, $\alpha_{\text{eo,eff}} = Q^*\big(\alpha_{\text{eo,high}} - \alpha_{\text{eo,low}}\big) + \alpha_{\text{eo,low}} = 43250\ \mu\text{m}^2\ (\text{V s})^{-1}$.

The final step is to couple the different flow rates. The flow rate through the valves (inlet/outlet B) can be found using the electric field and EO mobility, and recalling that the pressure driven flow is negligible.

$$Q_{\text{valve}} = \alpha_{\text{eo}}\ E\ A, \tag{7.1}$$

where A is the area of the cross section. We are not interested in the internal flow rate Q_{int}, but rather in the in/outgoing flow rate, Q_{pump}. For the complete model worksheet, refer to Appendix B, Two-Liquid Viscous Pump.

$$\left.\begin{aligned} Q_{\text{pump}} &= Q_{\text{int}} - 2\ Q_{\text{valve}} \\ Q_{\text{int}} &= Q_{\text{eo}} - Q_{\text{p}} \\ Q_{\text{p}} &\approx Q_{\text{pump}} \end{aligned}\right\} \quad Q_{\text{pump}} = \frac{1}{2}Q_{\text{eo}} - Q_{\text{valve}} \tag{7.2}$$

where Q_{eo} is the flow rate of the EO section in case of zero counter pressure. Q_{p} is the reduction in flow rate due to the counter pressure. In Eq. (7.2) we have set $Q_{\text{p}} \approx Q_{\text{pump}}$, this is not correct in general, but is only true when the hydraulic resistance of the EO section is similar to that of the pressure driven section.

CFD Simulations

Calculations with different EO mobilities are considered for comparisons with the model. In the immiscible case, the thickness of the pumping liquid layer is investigated. In the miscible case, the terminal concentration is investigated.

Meshing of the two-liquid pump requires different cell sizes. The valve channels are an order of magnitude more narrow than the EO section. Optimally, the mesh should have been biased towards the junctions, Fig. 7.6. However, the experience has shown that it makes little difference when considering pressures and flow rates.

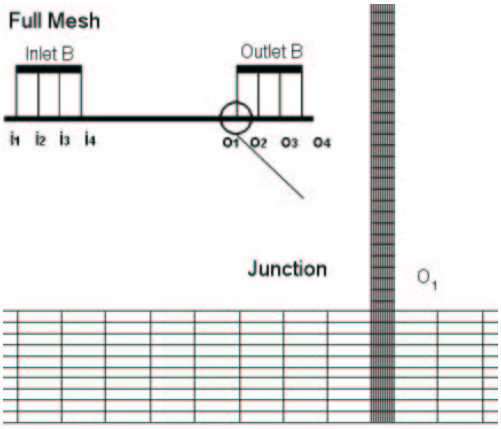

Figure 7.6: The mesh in a junction. The number of cells in the cross-sections is important. The wide (W) and narrow (N) section has 10×10 and 10×10 respectively. Due to symmetry it corresponds to 20×20 (W) and 10×20 (N) respectively. The cells in the wide and narrow section measure $2.5 \times 2 \times 0.5$ μm^3 and $0.1 \times 2 \times 0.5$ μm^3 respectively. The worst cell aspect ratio is therefore 5 (W) and 20 (N). The full mesh contains 112.000 cells.

The transitions between EOF and pressure driven flow can be seen in Fig. 7.7. The aspect ratio of the EO section is $W_1/D = 0.25$, so the profiles in the symmetry plane are expected to resemble parabolas, as those in a Couette flow with and without EOF.

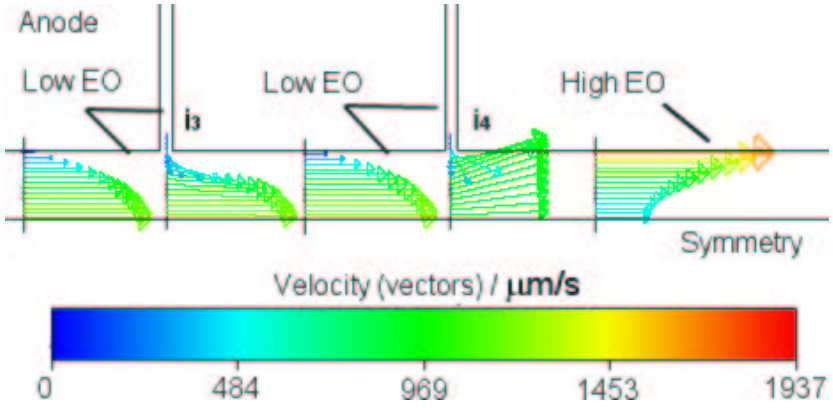

Figure 7.7: Velocity vectors in the symmetry plane. The transition from pressure driven flow to EOF is clear. In the regions with low EO mobility, the flow profile is positive parabolic. After the last junction, the EOF drags the liquid, generating a negative parabolic profile. Compare with Fig. 7.3. Parameters: as Fig. 7.9.

The laminar nature of the flow can be visualized using streaklines, Fig. 7.8. Note that streaklines are coincident with streamlines in the steady state case.

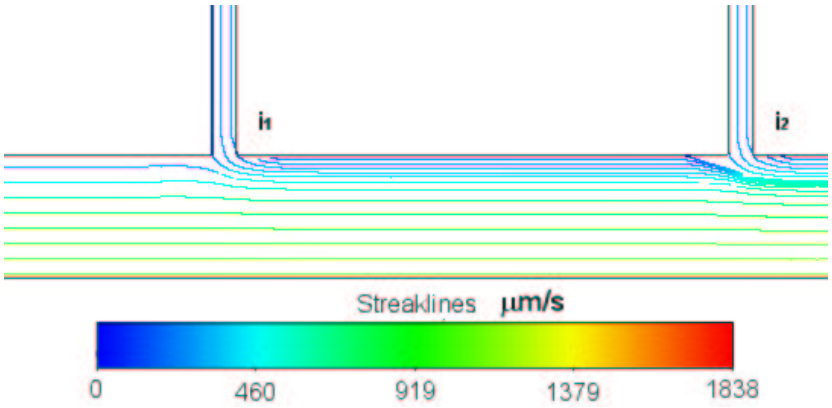

Figure 7.8: Streaklines at the anode junctions. Even though the channels are orthogonal, the lamination is clear. The Reynolds number is of the order $Re = 0.01 < 5$, i.e., creeping flow. In the case of immiscible two-liquid flow, the expected pumping layer thickness would be about 20% of the half-width. Please note that the figure is composed of three figures, so the density of the streaklines is not meaningful. Parameters: as in Fig. 7.9.

7.1.4 Comparison between Model and CFD

The relative effective potential drop η is voltage drop across the EO section, divided by the applied potential. The CFD program solves the Laplace equation, and hence obtains the potential and electric field. In the model, we assumed that the electric field was constant in each section. This is not entirely true, so there is a small deviation between the model and CFD, see Table 7.1.

	Effective potential η
Model	52.3%
Simulation	51.5%
Deviation	2%

Table 7.1: Comparisons between model and simulation. The relative effective potential η is the fraction of the applied potential that is across the EO section, Appendix B, Two-Liquid Viscous Pump

Three simulations with different EO mobilities in the low EO region, Fig. 7.4, have been made. Comparisons between model and simulation can be seen in Table 7.2. The model slightly exaggerates the flow rate and backpressure. One of the reasons for this is that a small fraction of pressure driven liquid escapes through the valves.

	EO mobility $\alpha_{eo}/\mu m^2(V\ s)^{-1}$	Max flow rate Q / nL/s	Backpressure Pa
Model	0	0.296	31.6
Simulation	0	0.290	30.6
Deviation		2%	3%
Model	5000	0.267	28.5
Simulation	5000	0.260	27.4
Deviation		3%	4%
Model	10000	0.237	25.3
Simulation	10000	0.230	24.3
Deviation		3%	4%

Table 7.2: Comparisons between model and simulation. The EO mobility in the low mobility regions is changed. Agreement in max flow rate and backpressure is within 4%. Parameters: dimensions as in Fig. 7.4, $\phi_a = 10$ V, $p_{in} = p_{out} = 0$, Appendix B, Two-Liquid Viscous Pump.

The pump is only partially driven by EOF. The sections with low EO mobility or no electric field are driven by pressure. The pressure distribution within the pump can be seen in Fig. 7.9. This figure has helped in the construction of the model. The two approaches supplement each other.

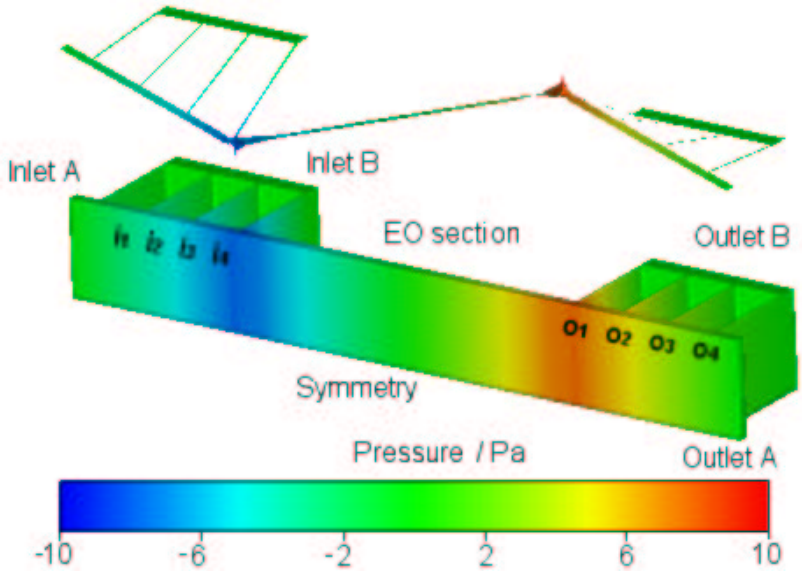

Figure 7.9: Visualization of the pressure distribution. The floating figure above the pump also displays the pressure. The float shows that the pressure varies linearly from junction to junction, implying uniform flow. Small peaks appear in both ends of the EO section. The cause os this is the divergence of the electric field. Parameters: dimension as in Fig. 7.4, $\alpha_{eo,low} = 5000\ \mu m^2\ (V\ s)^{-1}$, $\alpha_{eo,high} = 50000\ \mu m^2\ (V\ s)^{-1}$, $p_{in} = p_{out} = 0$, $\phi_a = 10$ V.

One of the unsolved problems in the circuit model is the pressure. In the

equivalent circuit theory, the pressure is related to the flow rate through the hydraulic resistance. The situation becomes rather complicated when multiple channels with different EO mobilities merge. An analytic approach should be feasible, but a more strategic approach is required. The upcoming version of COVENTOR will have a system design module, but the complex nature of this pump will require simulations.

Immiscible Liquids

The thickness of the pumping layer in a uniform flow can be found from the ratio between the valve and total flow rate.

$$D_{\text{layer}} = 2W_1 \frac{Q_{\text{valve}}}{Q_{\text{int}}}, \tag{7.3}$$

$$= 2W_1 \frac{Q_{\text{valve}}}{Q_{\text{pump}} + 2Q_{\text{valve}}} \tag{7.4}$$

where $2W_1$ is the width of the EO channel, Fig. 7.4. This equation, however, is only valid for an EOF without pressure. As we shall see later, there will always be a pressure gradient in the EO section. A counter pressure reduces the velocities in the middle of the channel. The pumping layer will be thinner because it moves faster, i.e., it is stretched compared to the inner flow. Eq. (7.4) should be regarded as a rough estimate on the pumping layer thickness, D_{layer}. The thicker the pumping layer is the less working liquid is pumped. The optimal pumping layer thickness is therefore only a few Debye lengths ensuring the full development of the EOF.

From a simulation point of view, it should be possible to find the pumping layer thickness. COVENTOR 2001.3, however, does not support the free surface BC in the Netflow module. As an approximation, the diffusion constant was set to zero. In laminar flow, this approximation is not that bad. However, the numerical diffusion will play an important role, so the mass fraction results are not that reliable.

Eq. (7.4) estimates the pumping layer thickness. Mass fraction profiles are extracted from the simulations. The measurement line is shown in Fig. 7.10. This line is placed at the bed or at the center. The simulation results are shown in Fig. 7.11.

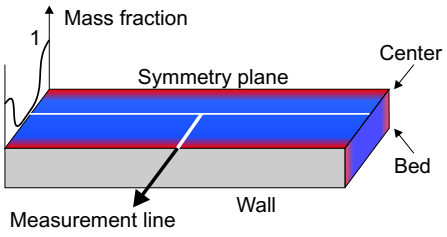

Figure 7.10: Schematic figure of how the plots in Fig. 7.11 are made. The measurement line is placed in the middle of the EO section either near the center or the bed.

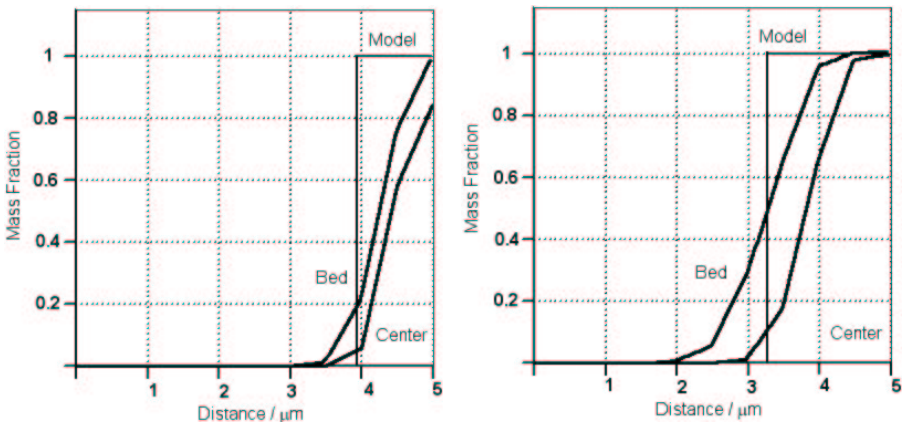

(a) (b)

Figure 7.11: Line plots of the mass fraction. Two line plots for each simulation are shown. They are extracted in the middle of the EO section at the two indicated depths (bed and center). (a) $\alpha_{\text{eo,low}}/\alpha_{\text{eo,high}} = 1/10$. The model estimates $D_{\text{layer}} = 1.04$ μm. The discrepancy is quite large due to the nonuniform velocity profile. (b) $\alpha_{\text{eo,low}}/\alpha_{\text{eo,high}} = 1/5$. The model estimates $D_{\text{layer}} = 1.85$ μm, so it still overestimates the thickness. In the limit $\alpha_{\text{eo,low}}/\alpha_{\text{eo,high}} \to 1$, the model should give the right result. Parameters: dimension as in Fig. 7.4, $p_{\text{in}} = p_{\text{out}} = 0$, $\phi_a = 10$ V

The model overestimates the thickness of the pumping layer, because the flow in the inner section is reduced due to the adverse pressure, refer to Fig. 7.9. In the lower part of the wall, the flow is slower due to the low EO mobility specified at the bed. Compare with the analytical solution to the double moving wall problem, Fig. 3.5. Hence, the pumping layer should be thicker near the bed, as also the simulations show.

Fig. 7.12 shows the overall distribution of the mass fraction. Note how the pumping layer grows until the last junction, where the flow profile changes and stretches the pumping layer, recall Fig. 7.7.

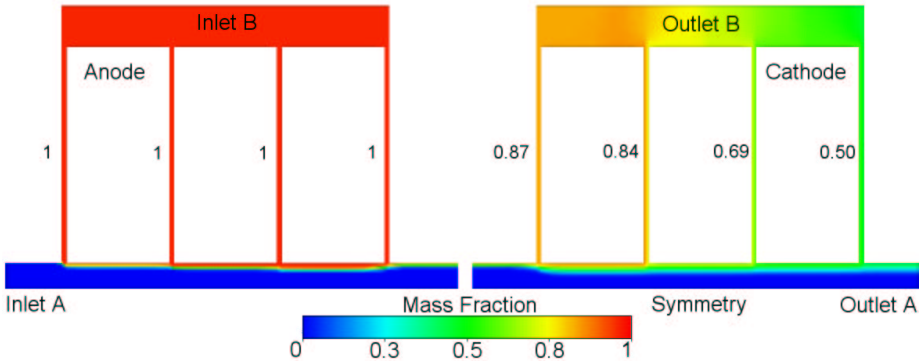

Figure 7.12: Immiscible case: Top view of the mass fraction in the symmetry plane. The diffusion is set to zero, trying to simulate immiscible two-phase flow. The pumping liquid, mass fraction 1, is introduced through inlet B. Anode: From left to right we see an increasingly thick pumping layer. After the last junction the thickness is constant. Cathode: A mixture of pumping liquid and buffer is extracted through outlet B. Since the flow rate is the same in inlet and outlet, there is a net flow of pumping liquid. Indeed, there is a layer of residual pumping liquid continuing downstream. Parameters: as in Fig. 7.9.

Miscible Liquids

The miscible case is shown in Fig. 7.13. The self-diffusion constant of water is used. The differences between the miscible and immiscible cases are large, as was expected. The two liquids rapidly mix, and a terminal concentration c_{ter} is obtained. The characteristic diffusion time is $t^o = W^2/D_{\text{mass}} = 0.044\ s$. Velocities are of the order 1 mm/s so the liquids completely mix within approximately 40 microns. Hence, it will be impossible to see any spatial variation of the concentration after this length. The terminal concentration c_{ter} can be calculated using Eq. (7.6).

$$c_{\text{ter}} = \frac{2Q_{\text{valve}}}{Q_{\text{int}}}, \tag{7.5}$$

$$= \frac{2Q_{\text{valve}}}{Q_{\text{pump}} + 2Q_{\text{valve}}} \tag{7.6}$$

The model is based on the conservation of mass. So if the flow rates are correct, the concentration is correct. The results can be seen in Table 7.3.

	Mass fraction c_{ter}
Model	20.7%
Simulation	20.9%
Deviation	1%

Table 7.3: Terminal concentration in the miscible case. The EO mobilities are: $\alpha_{\text{eo,low}} = 5000\ \mu\text{m}^2\ (\text{V s})^{-1}$, $\alpha_{\text{eo,high}} = 50000\ \mu\text{m}^2\ (\text{V s})^{-1}$, Appendix B, Two-Liquid Viscous Pump, 2/2.

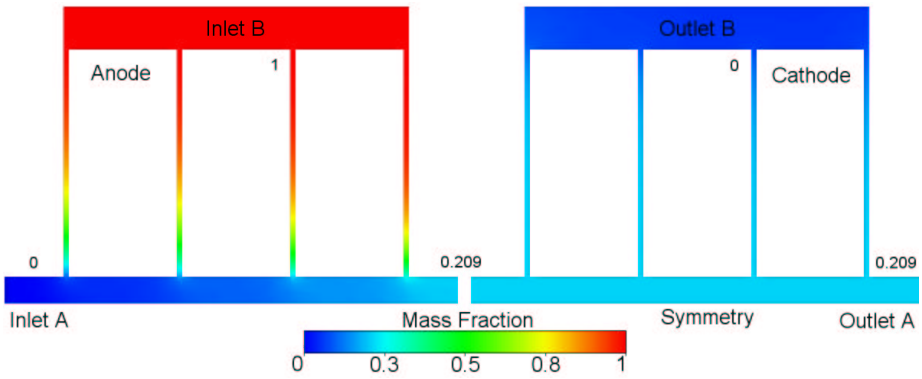

Figure 7.13: Miscible case: Top view of the mass fraction in the symmetry plane. The diffusion is set to self-diffusion of water, $D_{\text{mass}} = 2260\ \mu\text{m}^2/\text{s}$ giving a Peclet number of $Pe_{\text{mass}} \approx 20$ based on $L_2 = 42\ \mu$m in Fig. 7.4 and $u \approx 1000\ \mu$m/s. The pumping liquid with mass fraction 1 is introduced through inlet B. Anode: From left to right we see that the buffer liquid diffuses upstream towards inlet B, but only reaches about halfway in. The mixing is so fast that we cannot see the pumping liquid layer. If the velocities had been faster, this would have been possible. The terminal concentration is $c_{\text{ter}} = 0.209$, which is what the model predicts. Parameters: as in Fig. 7.9, except the diffusion constant.

7.1.5 Summary, Two-Liquid Viscous Pump

A novel Two-Liquid Viscous Pump has been presented. The idea and development is described in detail. Finally, a model was compared with CFD simulations. Agreement within 4% for the flow rate and backpressure was obtained. However, it was also stated that a more strategic modelling approach would be beneficial for this and more complex designs. With the currently available software, it was only possible to simulate the immiscible two-phase flow under restrictive assumptions on the conductivity, viscosity, etc. Calculation of the pumping layer thickness was more complex than expected. The model only gave a rough estimate. The optimal the pumping layer thickness is no more than a few Debye lengths. A realistic simulation of this problem will be very difficult if the pumping layer is very thin. Effects such as surface roughness, surface tension and other surface effects may play an important role. Experiments are essential for further progress.

In the miscible case, the two-phase flow mixed very rapidly, as expected. Accurate prediction and simulation of the terminal concentration was achieved.

One of its obvious applications for the Two-Liquid Viscous Pump, would be to pump oil. From a hydraulic engineering point of view, this may be problematic because oil is highly viscous. With the currently available etching techniques the pump cannot generate very large pressures. Transporting oil droplets suspended in water may be another possible application. In the miscible case the design could be used as a mixer.

A novel EO pump design that works with all types of liquids has been devel-

oped. The pump characteristic Q-p is largely governed by the possible channel dimensions. Practical dimensions and problems are the topics of further work.

7.2 The Shallow Reservoir Pump

The Shallow Reservoir pump is similar to the planar pump presented in Sec. 5.3.2. The horizontal orientation enables the use of standard etching techniques and extremely small plate spacing. Initially, we will investigate the effects of changing different parameters in the layout. From the parametric study we will conclude that a very wide and extremely shallow cross section is optimal, Fig. 7.14.

The aim is to integrate this type of pump into the device. Preliminary simulations showed that a direct integration gave a very poor efficiency. A detailed investigation revealed the problem.

I discovered that by placing a reservoir at each end of the EO section, the integration can be accomplished. The problems and remedies are discussed in relation to this.

7.2.1 Optimizing the Geometry

We start by making some preliminary investigations regarding the geometry. Consider an EO pump (EO section) with a rectangular cross section, Fig. 7.14. Three essential parameters are identified. The length L, the width W and the depth D. These parameters effectively govern the pump characteristic Q-p.

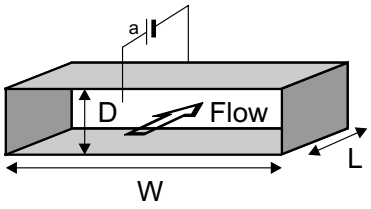

Figure 7.14: Channel with a rectangular cross section. The depth D, width W and length L are shown on the figure. Across the length of the channel, a potential is applied, ϕ_a. The EO mobility is α_{eo}.

The following assumptions are made in the analysis: Across the length L, there is a fixed voltage drop ϕ_a and zero pressure difference Δp. The problem is most conveniently analyzed using a worksheet such as Excel. CFD is not efficient for this geometrical simple type of analysis. The important elements in the analysis are given here.

- Geometrical data: width W, depth D and length L.
- Dynamic viscosity μ, EO mobility α_{eo} and electrical conductivity λ_{elec}.
- Hydraulic resistance R_{hyd}, Eq. (3.42).
- Backpressure Δp_{eo}, Eq. (3.37), and flow rate Q, Eq. (3.39).
- Applied voltage ϕ_a, and corresponding electric field $E = \phi_a/L$.
- The electric resistance, $R_{\text{elec}} = \frac{L}{WD\lambda_{\text{elec}}}$.
- Electric current, $I = \phi_a/R_{\text{elec}}$.

Once the model has been made, one can easily change the parameters and see what the effect is. A geometrical study is shown in Table 7.4. From Table 7.4 it is concluded that the optimal design has a wide ($W >$) and shallow ($D <$)

cross section, or a narrow ($W <$) and high ($D >$) one. It is the same geometry, simply rotated by 90°. However, it is much easier to fabricate a wide and shallow etch than a narrow and deep etch, such as that used in the Two-Liquid Viscous Pump. The geometry should be shallow in order to generate large pressures, and wide in order to obtain large flow rates. This is possible because the backpressure is asymptotically independent of the width W, and the flow rate is proportional to the width W.

		Electric field	Current	Backpressure	Flow rate
Length	$\downarrow$	$\uparrow$	$\uparrow$	$-$	$\uparrow$
	$\uparrow$	$\downarrow$	$\downarrow$	$-$	$\downarrow$
Width	$\downarrow$	$-$	$\downarrow$	$\uparrow$	$\downarrow$
	$\uparrow$	$-$	$\uparrow$	$\downarrow, \asymp$	$\uparrow$
Depth	$\downarrow$	$-$	$\downarrow$	$\uparrow$	$\downarrow$
	$\uparrow$	$-$	$\uparrow$	$\downarrow, \asymp$	$\uparrow$

Table 7.4: The equations used are Ohm's law and Eq. (3.37) for the backpressure. The relations are simplified by an arrow (up $\uparrow$, down $\downarrow$, converges asymptotically $\asymp$, or equal $-$), and do not say anything about the rate of change. By changing one parameter at the time, the dependence could be determined, assuming that the temperature remains the same, Appendix B, Layout.

According to Table. 7.4, the layout should be short in order to generate large flow rates. This is because of the increase in the electric field. The ohmic heating is proportional to the electric field squared. The electric field is therefore often the limiting factor, due to the allowed temperature in the liquid. In order to minimize ohmic heating, it is preferable to use a liquid with low conductivity.

If the electric field becomes very high, it could result in uncontrolled electric currents due to electric breakdown.

Temperature Dependence

Temperature is an important, but widely unexplored, issue in microfluidics. The model proposed here is able to estimate the pump characteristic as a function of temperature, Fig. 7.15. This is very useful, but it requires that the temperature is known. The temperature could be estimated using a heat conduction model, or by measurements on the actual device. A temperature model combined with the hydraulic model would give the backpressure and max flow rate as a function of the applied potential. This is an advantage, since the applied potential is externally controlled.

In this section we assume that the temperature is known, and we expand the hydraulic model to incorporate the temperature effects. This is achieved by modelling the dynamic viscosity, electrical conductivity, and EO mobility empirically. The following parameters are added to the hydraulic model.

- Temperature, T
- Dynamic viscosity μ, which is temperature dependent. Using tabulated data, Andersen *et al.*, a continuous curve is approximated with a 4th order polynomial.

- EO mobility, α_{eo}, which is temperature dependent. Using the data from Fig. 2.8, a continuous curve is approximated, using a 2nd order polynomial.
- Reference values for μ, α_{eo} and λ_{elec} at $T = 25^oC$.

Curves showing the temperature dependence of the backpressure and the max flow rate are is shown on Fig. 7.15. It should be pointed out that the temperature dependence for the EO mobility is derived with several approximations, refer to Sec. 2.12.

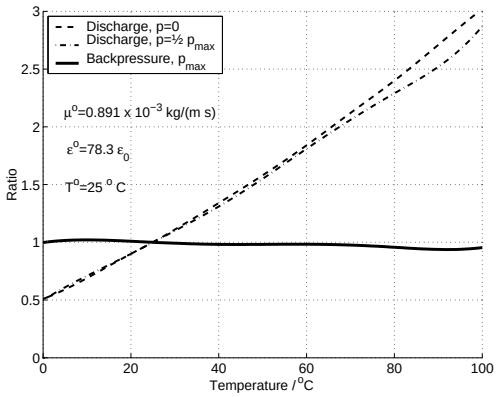

Figure 7.15: Flow rate and backpressure as a function of temperature, made nondimensional by values at $T = 25\ ^oC$. The flow rate exhibits linear dependence because the EO mobility grows almost linearly, Fig. 2.8. When a counter pressure is applied, $0.5p_{\max}$ at $T = 25\ ^oC$, the increased mobility is balanced by a small decrease in backpressure. The backpressure decreases slightly, because the viscosity decreases faster than the EO mobility increases.

The main conclusions from Fig. 7.15 are that the flow rate increases linearly with temperature, and that the backpressure is independent of temperature.

7.2.2 Design History

The initial idea was simply to combine a wide and a shallow EO section with a channel, as shown in Fig. 7.16.

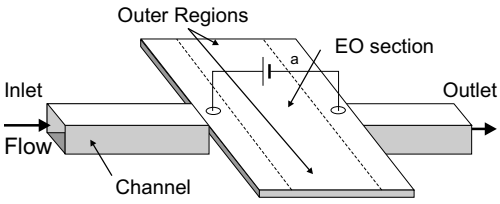

Figure 7.16: The first idea of the integrated planar/shallow pump. As shown, the electrodes are introduced from above.

One of the problems with the electrode arrangement shown in Fig. 7.16 is that the electric field will not be uniform in the EO section. Only the middle part of the EO section will have EOF, while the outer regions will have very low EOF.

Imagine then, that many electrodes were distributed in such a way that the electric field was uniform across the EO section. This does not solve the problem either, because the flow in the outer regions at some point will have to move towards the center, where the inlet and the outlet are. This movement is not

parallel to the imaginary electric field lines, and gives rise to pressure loss. A more detailed description is given in the following sections, refer Fig. 7.23.

7.2.3 The final Design

The geometry of the shallow pump requires a fitting between the channel and the pressure building EO section. A very wide and shallow channel has to merge with a narrow and relatively deep channel. The remedy is to introduce a reservoir between the EO section and the channel, as shown in Fig. 7.17.

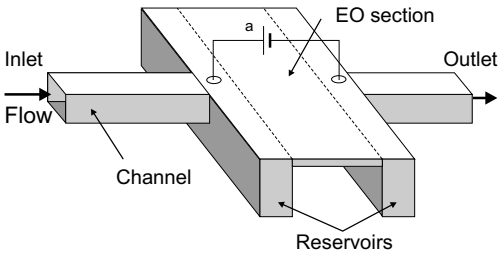

Figure 7.17: The shallow/planar pump combines high pressure and a high flow rate. It can be made using standard etching techniques. The reservoir concept is new, and it enables the pump to be integrated into a fluidic network.

The reservoirs do two things. (1) The electric resistance of the reservoirs is small compared to the EO section. Consequently, the potential will be almost constant in the reservoirs. The electric field will therefore be approximately uniform in the EO section. (2) The flow in the outer regions can move towards the center with only a small pressure loss, because the hydraulic resistance of the reservoirs is small compared to the EO section.

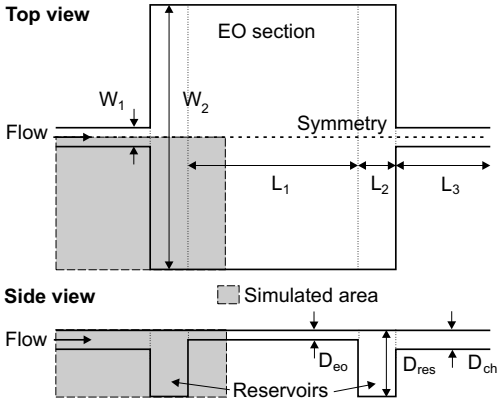

Figure 7.18: Schematic view of the Shallow Reservoir Pump. The area used in simulating the reservoirs is marked. Dimensions: $W_1 = 200\ \mu$m, $W_2 = 1200\ \mu$m, $D_1 = 5\ \mu$m, D_2 is variable, $D_3 = 50\ \mu$m, L_1 is not used, $L_2 = 100\ \mu$m, $L_3 = 200\ \mu$m, $u_{eo} = 2000\ \mu$m/s.

The reservoir serves as a coupling device between the two sections. The design factors are:

- Minimum pressure loss
- Minimum dead volume
- Minimum dispersion

Minimum pressure loss can be obtained by making the reservoirs large, but this counteracts the second and third requirement, the small dead volume and the small dispersion. Hence, the dimensions of the reservoirs should be as small as possible, without creating too large a flow resistance. The governing factors are the hydraulic resistances of the individual components. The hydraulic resistance ratio does not scale linearly with the depth ratio.

7.2.4 Equivalent Circuit Model

The aim is to establish a model that can predict the Q-p characteristic.

The system consists of three hydraulic elements. The channel, the reservoir and the EO section. The three elements are not coupled in series. The flow rate through the reservoir depends on the cross section chosen.

$$Q_{\mathrm{ch}} = Q_{\mathrm{eo}} = Q_{\mathrm{total}} \tag{7.7}$$

$$0 < Q_{\mathrm{res}} < Q_{\mathrm{total}} \tag{7.8}$$

Eq. 7.8 is important when estimating the hydraulic resistances. In the case where the reservoir has a small hydraulic resistance, the overall hydraulic resistance is estimated using the following arguments, Fig. 7.19.

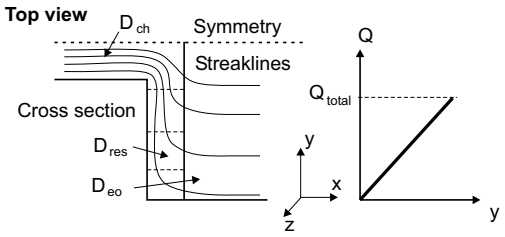

Figure 7.19: The flow rate through a cross section in the reservoir is expected to increase linearly from zero to Q_{total}. This is because there is a constant inflow from the EO section.

The pressure loss is dependent on the flow rate, which on average is $Q_{\mathrm{total}}/2$. Hence, the effective hydraulic resistance of the reservoir may be approximated to half of the geometrically based value.

$$R_{\mathrm{hyd,total}} = R_{\mathrm{hyd,ch}} + \tfrac{1}{2}R_{\mathrm{hyd,res}} + R_{\mathrm{hyd,eo}} \tag{7.9}$$

Using Eq. 7.9 and the standard equivalent circuit approach, the Q-p relation is obtained.

7.2.5 CFD Simulations

The computational domain is selected to be as small as possible. Using symmetry, we can reduce the problem by a factor two. The flow in the large shallow EO section is completely uniform, so instead of simulating the whole shallow pump, we only select the section near the reservoir. The selected computational domain is shown in Fig. 7.18. Five simulations with various reservoir depths were done, Appendix B, Reservoir Design.

It is the same type of geometry used in a grid dependency test. The grid used is therefore well tested, and should give flow rate results within 3% of the best

possible, Appendix I. A section of a Shallow Reservoir Pump mesh is shown in Fig. 7.20.

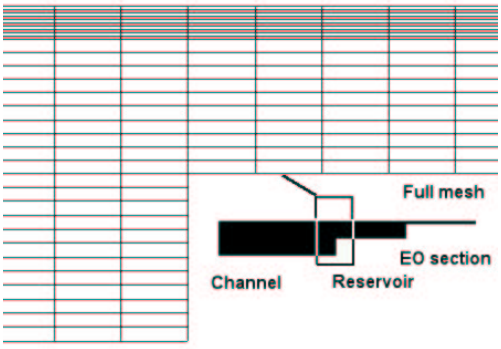

Figure 7.20: Side view of the mesh. The reservoir in this particular case is only half as deep as the channel. There are two cell sizes. The very flat cells in the EO section and the flat cells everywhere else. There are 10 cells across the shallow EO section. The full mesh contains 46.660 cells, and is only a fraction of the whole geometry.

We are only interested in how the reservoir depth influences the flow. The electric field also depends on the depth, so instead of specifying an electric potential and an EO mobility, a velocity u_{eo} was specified in the EO section. Consequently, the electric field is decoupled from the problem, because a constant velocity is the same as a uniform electric field and an EO mobility.

The Reynolds number is important when estimating the type of flow that we may encounter. In the EO section the Reynolds number is of the order

$$Re = \frac{u_{\text{eo}} D_{\text{eo}}}{\nu} = 0.01, \tag{7.10}$$

with $u_{\text{eo}} = 2000$ μm/s, $D_{\text{eo}} = 5$ μm and $\nu = 1.0 \times 10^6$ μm^2/s. The Reynolds number ranges from $Re = 0.01 - 0.2$, depending on the depth ratio in the given simulation. Inertial effects should therefore be negligible in all cases, and it does not matter at which end of the pump we are simulating.

The depth ratio $D_{\text{res}}/D_{\text{eo}}$ is varied, while D_{eo} is fixed, and the corresponding flow rates are measured. The results are shown in Table 7.5.

depth ratio $D_{\text{res}}/D_{\text{eo}}$	hydraulic resistance ratio $R_{\text{hyd,res}}/R_{\text{hyd,eo}}$	Simulation flow rate Q/Q^o	Circuit Model flow rate Q/Q^o	Deviation
20	0.010	1.00	1.04	4%
10	0.052	0.99	1.02	3%
5	0.34	0.92	0.90	2%
2	4.8	0.49	0.31	37%
1	37	0.16	0.05	65%

Table 7.5: Values for the flow rate trough the outlet, as a function of depth ratios. Both simulated and estimated values are presented. Flow rates are made nondimensional with the first simulated value. The governing factor is the hydraulic resistance ratio, Appendix B, Reservoir Design.

Table 7.5 shows, that in the first three simulations, the circuit model and simulation agree well. A closer inspection of the second simulation with $D_{\text{res}}/D_{\text{eo}} = 10$

reveals that the streaklines shown in Fig. 7.21 are positioned as expected.

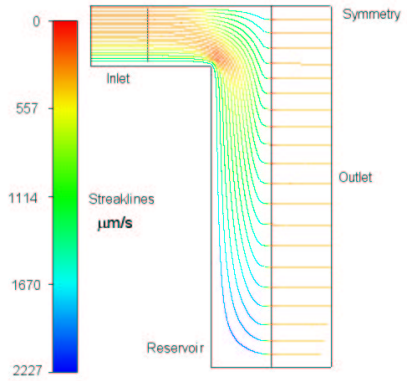

Figure 7.21: Top view of the streaklines. The simulation is done for a depth ratio $D_{\text{res}}/D_{\text{eo}} = 10$. The flow is nicely distributed across the whole width of the pump, indicating that the flow in the EO section is not affected by the hydraulic resistance of the reservoir. We also notice that the density of the streaklines increase towards the horizontal symmetry line. Parameters: as Fig. 7.18, $p_{\text{in}} = p_{\text{out}} = 0$.

In the circuit model, it was assumed that the flow rate in the reservoir increased linearly due to the inflow from the EO section. The y-velocity in the reservoir is approximately proportional to the flow rate, see Fig. 7.22(a). Hence, by plotting the Y-velocity along a line going from the outer region to the symmetry line, we can measure the linearity of the flow rate, see Fig. 7.22(b). The first three simulations are linear, whereas the last are nonlinear.

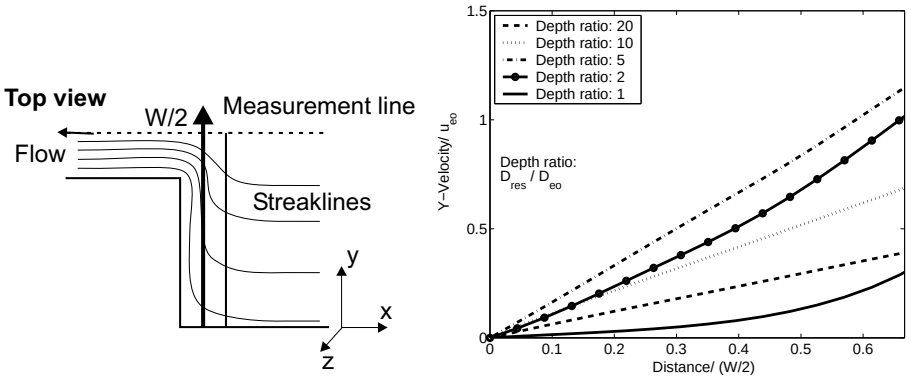

(a) (b)

Figure 7.22: (a) The flow is visualized by use of streaklines. The number of the streaklines crossing a cross section is proportional to the flow rate. (b) Simulated results of the Y-velocities along a centered measurement line for different depth ratios. The results are made nondimensional with the half width and the EO velocity.

If the hydraulic resistance of the reservoir becomes larger than that of the EO section, the flow characteristic changes. The streaklines change. Streaklines from the fourth simulation with $D_{\text{res}}/D_{\text{eo}} = 2$ can be seen in Fig. 7.23.

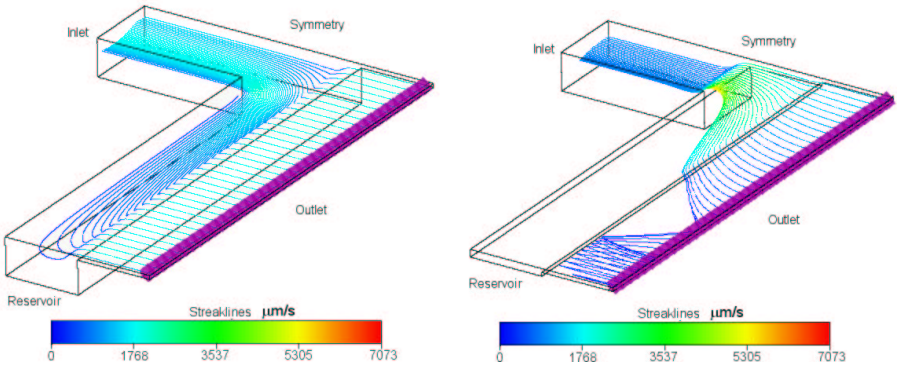

Figure 7.23: (a) $D_2/D_1 = 10$ and $R_{\mathrm{hyd},1}/R_{\mathrm{hyd},2} = 0.052$. The hydraulic resistance of the reservoir is so small that is does not affect the flow in the shallow section. (b) $D_2/D_1 = 2$ and $R_{\mathrm{hyd},1}/R_{\mathrm{hyd},2} = 4.8$. The flow in the shallow section is highly influenced by the reservoir. In the outer part of the shallow section, the flow reverses and does not enter the reservoir. In this situation, the pump efficiency is significantly decreased.

The last two simulations deviate significantly from the model due to the altered flow characteristic, Table. 7.5. Recalling the design factors it is concluded that the optimum hydraulic resistance ratio is approximately between $5\%-30\%$. If it is below 5%, there is unnecessary dead volume, and if it is above 30%, there is a large pressure loss associated with the design.

The importance of dispersion is application specific, and will not be addressed here. Furthermore, a finer mesh should be used for solving the advection/diffusion problem.

Certain unaddressed practical issues exist. One of them is the electrodes. Different types of electrodes may be fitted to the pump, but gel electrodes are preferable, in order to reduce bubble formation, while still maintaining pressure. Other electrode arrangements, such as nanochannels with Debye layer overlap, connected to an open reservoir, might also be possible solutions.

Another issue is the shallow plate spacing. The bonding process may collapse the plates. This problem was encountered by Chen *et al.* The remedy is to make a considerable amount of ribs across the channel width.

7.3 Summary, Shallow Reservoir Pump

The Shallow Reservoir pump, which is a new and promising design, has been developed. It makes efficient use of the advantages of EOF. The design can be fabricated using standard etching techniques, and it can be completely integrated into a microfluidic system, i.e., Lab-on-a-Chip.

For a simple rectangular channel it was concluded that a short, wide and shallow channel gives the largest values of flow rate and backpressure. Furthermore the temperature dependence of the flow rate and backpressure was investigated. The backpressure was found to be independent on temperature whereas the flow rate increased linearly. The model is based on physical constants and the previously described temperature model for the EO mobility.

An equivalent circuit model has been developed and compared to CFD simulations. Agreement within 4% was achieved for the flow rate in the linear region. The limitations of the model were also investigated. Large discrepancies between model and simulation were found when the hydraulic resistances of the reservoir and the EO section were comparable.

The geometry of the reservoirs have been investigated, and the main conclusion is that the hydraulic resistance of the reservoir should be about in the range $5\% - 30\%$ of the hydraulic resistance of the EO section.

Chapter 8

Conclusion

At this point it should be clear that microfluidics is a very multi-disciplinary field. The structure of the report should have helped the reader to a smooth introduction to the topic.

An understanding of the underlying physics is essential for any progress. The basic physical properties of liquids such as viscosity and diffusion are described. During my literature study I found different spurious versions of the energy equation, e.g., Chen. So a rigorous treatment of the energy equation was needed. Furthermore, the classic momentum and continuity equation are introduced.

A temperature model for the EO mobility is proposed. The model predicts an almost linear increasing EO mobility as a function of temperature. The model has not been compared to any experiments, possibly because there are none. So the model stands alone, but the nonlinear pump characteristics give a clear indication of an EO mobility, increasing with temperature.

In the elementary flow analysis, the fluid dynamics are coupled with the electrokinetic effects, showing that the flow rate for pressure driven flows scales as $Q \propto a^4$, whereas for EOF $Q \propto a^2$. This effect is the essence of EOF, and can be utilized particularly well in microfluidic pumping.

Flows in different geometries were analyzed using theory for partial differential equations. The geometries considered were inspired by the novel designs. In practice, the ideas for the novel designs appeared first and the theory was then subsequently developed. The results were then generalized to be of use in the equivalent circuit theory and in other designs. Plots of nondimensional flow rates versus aspect ratio and flow profiles are indeed very useful in the design process.

The equivalent circuit theory is a well-known theory, and it is used by many hydraulic engineers throughout the world. The theory is also very applicable to microfluidics. All the devices presented in this thesis are successfully modelled with the equivalent circuit model.

Computational fluid dynamics was used in conjunction with the circuit model. The dynamic interaction between the circuit model and CFD proved to be very efficient. Errors of different kinds were quickly discovered and corrected. COVENTOR 2001.3 is a relatively new CFD-package and it contains a fair amount of bugs. Fortunately, the support group was very helpful. The di-

rect focus on microfluidics is unparallel in any other CFD software available. Typically, the agreement between circuit model and CFD was within $3-4\%$ for the flow rate and backpressure. This high degree of accuracy was achieved with structurally simple meshes. The governing factor was the number of cells in the cross sections.

Theory and simulation are the keywords of this thesis. The lack of experiments is evident. Hence, I searched the literature for well described experiments with EO pumps and found two cascade pumps. From this survey a description of the different types of EO pumps arose.

Two different types of cascade pumps were chosen from the micropump overview. The Parallel Cascade Pump is well suited for the equivalent circuit theory. Agreement within $1-2\%$ between model and simulation was achieved. Morf *et al.*, 2001, also used the circuit theory for comparison with the experiments. There was excellent agreement for low voltages.

The Low-Voltage Cascade pump by Takamura *et al.*, 2001, is very interesting because it can be operated with low voltages and is relatively simple to manufacture. There was not enough information in the published article to commence a flow analysis. Takamura agreed to provide the details. The investigation led to the conclusion that there was something wrong with either the measurements or the pump. Upon contact it became clear, that there were several problems that had not been published. The case illustrated the need for a better simulation effort in microfluidics. It is my belief that an equal distribution between experiments and simulation is the most efficient way to progress.

Two novel designs were presented: (1) Introducing the first EO pump that should be able to pump nonconducting liquids. The pump was denoted the Two-liquid Viscous Pump. The expected performance with respect to flow rate and backpressure is similar to that of a single EO channel. Further investigations of microscale two-phase flows are needed. (2) Modification of the planar/shallow pump by Chen *et al.*, 2000, allowing for integration into a chip system. The pump is denoted the Shallow Reservoir Pump. A detailed analysis of a simple rectangular channel was made. Flow rates and backpressures were found as functions of geometry and temperature. This type of pump may in fact prove to be the leading type of EO pumps for some time. The potentially most effective EO pump is the porous pumps. New fabrication techniques may enable them to be integrated into a chip in the future.

Bibliography

[1] A. W. Adamson, A. P. Gast *Physical Chemistry of Surfaces, 6th. Edition*

[2] J. P. Alarie, S. C. Jacobson, B. S. Broyles, T. E. McKnight and C. T. Culbertson. *Electroosmotically induced hydraulic pumping on microchips.* Micro Total Analysis Systems 2001, J. M. Ramsey and A. van den Berg (eds.) Kluwer Academic Publishers, p. 131-132, 2001.

[3] B. J. Alder, J. H. Hildebrand *Activation Energy: Not Involved in Transport Processes in Liquids* Industrial Engineering Chemistry, Fundamentals, University of California, 1973.

[4] E. S. Andersen, P. Jespergaard, O. G. Østergaard *Databog i fysik og kemi.* F og K forlaget, 10. udgave.

[5] N. Asmar, p. 145. *Partial differential equations and boundary value problems* Prentice Hall, 2000.

[6] P. W. Atkins *The Elements of Physical Chemistry* Oxford University Press, Oxford, 1995.

[7] P. W. Atkins *Physical Chemistry, 5th. Edition* Oxford University Press, Oxford, 1995.

[8] R. B. Bird, W. E. Stewart, E. N. Lightfoot *Transport Phenomena.* Wiley International Edition, p. 54f, 1980.

[9] E. Both, G. Christiansen *Termodynamik* Den private ingeniørfond, Danmarks Teknisk Universitet, 1995.

[10] C.H. Chen, S. Zeng, J. C. Mikkelsen, J. G. Santiago *Development of planar electrokinetic micropump.* Presented at ASME International Mechanical Engineering Congress and Exposition, Orlando, FL, Nov. 7, 2000.

[11] E.B. Cummings, S. K. Griffiths, R. H. Nilson, P. H. Paul *Conditions for Similitude between the Fluid Velocity and Electric Field in Electroosmotic Flow.* Analytical Chemistry, Vol. 72 No. 11, June 1, 2000.

[12] P. Dutta, A. Beskok *Analytical Solution of Combined Electroosmotic/ Pressure Driven Flows in Two-Dimension Straight Channels: Finite Debye Layer Effects.* Analytical Chemistry, vol. 73 p. 1979-1986, 2001.

[13] R. M. Guijt, J. Lichtenberg, E. Baltussen, E. Verpoorte, N. F. de Rooij and W. K. Gijs. *Indirect electroosmotic pumping for direct sampling from bioreactors.* Micro Total Analysis Systems 2001, J. M. Ramsey and A. van den Berg (eds.) Kluwer Academic Publishers, p. 399-400, 2001.

[14] P. Gravesen, J. Branebjerg and O. S. Jensen *Microfluidcs - a review* J. Micromech. Microeng. 3, 1993.

[15] R. J. Hunter., B. R. Midmore and H. Zhang *Zeta Potential of Highly Charged Thin Double-Layer Systems* Journal of Colloid and Interface Science 237, p. 147-149, 2001.

[16] D. B. Keith, M. G. Cikalo and M. M. Robson *An Introduction to Capillary Electrochromatography.*

[17] M. Koch, A. Evans and A. Brunnsweiler *Microfluidic Technology and Application* Research Studies Press.

[18] L. D. Landau and E. M. Lifshitz *Fluid Mechanics*
Course in Theoretical Physics, Volume 6 Institue of Physical Problems, USSR Academy of Sciences, Moscow, 2000.

[19] B. Lautrup *Continuum Physics*
Exotic and everyday phenomena
in the macroscopic world. The Niels Bohr Institute, Denmark, 1999 .

[20] R. Mills *Self-diffusion in normal and heavy water in the range 1-45 ^oC* J. Phys. Chem, 77, 685-688, 1973.

[21] W.E. Morf, O.T. Guenat, N.F. de Rooij *Partial electroosmotic pumping in complex capillary systems*
Part 1: Principles and general theoretical approach. Sensors and Actuators B72, p. 266-272, 2001

[22] F. B. Pedersen *Hydraulik for bygningsingeniører* Den private ingeniørfond, Lyngby 1988.

[23] R. F. Probstein *Physicochemical Hydrodynamics, An Introduction 2nd. Edition.* John Wiley and Sons, Massachusetts Institute of Technology, 1994.

[24] L. Rice and R. Whitehead *Electrokinetic Flow in a Narrow Cylindrical Capillary.* The Journal of Physical Chemistry, Vol. 69, 11 p. 4017-4024, 1965.

[25] D. Ross, M. Gaitan and L. E. Locascio *Temperature measurement and control in microfluidic systems. Micro Total Analysis Systems 2001.* Kluwer Academic Publishers, p. 239-241, 2001.

[26] G. A. Shaposhnikova *Electrical Phenomena at Interfaces* International Conference on Dielectric Liquids (ICDL' 99), 1999.

[27] D. J. Shaw *Electrophoresis* Academic Press London and New York, 1969.

[28] W. A. Strauss *Partial Differential Equations, An Introduction* J. Wiley and Sons, Inc., Brown University, 1992.

[29] Y. Takamura, H. Onoda, H. Inokuchi, S. Adachi, A. Oki and Y. Horiike. Micro Total Analysis Systems 2001, J. M. Ramsey and A. van den Berg (eds.) Kluwer Academic Publishers, p. 230-232, 2001.

[30] H. K. Versteeg and W. Malalasekera (My teachers in the spring year 2000 at Loughborough University.) *An introduction to Computational Fluid Dynamics, The Finite Volume Method.* Longman, Loughborough University, 1995.

[31] R. -J. Yang, L.-M. Fu, Y. -C. Lin *Electroosmotic Flow in Microchannels.* Journal of Colloid and Interface Science 239, p. 98-105, 2001.

[32] S. Zeng, C. -H. Chen, J. C. Mikkelsen Jr., J. G. Santiago *Fabrication and characterization of electroosmotic micropumps.* Sensors and Actuators B79, p. 107-114, 2001

Appendix A

Flow in a Rectangular Channel with moving Lid

Consider a steady uniform laminar flow in a rectangular channel with a moving lid. In mathematical terms this is the Laplace equation with inhomogeneous Dirichlet BCs. The BVP is represented in Fig A.1. One must start with an initial guess at the flow profile. The obvious choice is Couette flow profile. The solution will converge to this profile for large aspect ratios, $\kappa = 2\ W/H$.

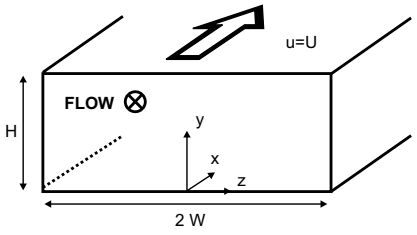

Figure A.1: Rectangular channel flow driven by moving lid. Width: $2W$, height: H.

$$u(y,W) = u(y,-W) = 0 \tag{A.1}$$

$$u(0,z) = 0 \tag{A.2}$$

$$u(H,z) = U \tag{A.3}$$

$$\text{Initial guess} \quad : \quad u(y,z) = U\frac{y}{H} + f(y,z) \tag{A.4}$$

$$\text{Navier-Stokes} \quad : \quad 0 = \nu\left(\frac{\partial^2 u}{\partial y^2} + \frac{\partial^2 u}{\partial z^2}\right) \tag{A.5}$$

Inserting the initial guess into Navier-Stokes equation

$$0 = u_{yy} + u_{zz} \tag{A.6}$$

$$0 = f_{yy} + f_{zz} \tag{A.7}$$

$$\text{BC1} \quad : \quad f(0,z) = f(H,z) = 0 \tag{A.8}$$

$$\text{BC2} \quad : \quad f(y,-W) = f(y,W) = -U\frac{y}{H} \tag{A.9}$$

The governing equation is recognized as the Laplace equation with Dirichlet boundary conditions. Such a boundary value problem can be solved by the method of separation.

$$f(y,z) = F(y)G(z) \tag{A.10}$$
$$-\frac{F''(y)}{F(y)} = \frac{G''(z)}{G(z)} = \lambda_n \tag{A.11}$$
$$F''(y) = -\lambda_n F(y) \tag{A.12}$$

λ_n are constants and are referred to as the eigenvalues for the problem. There exist now four cases depending on the nature of the eigenvalues which may be zero, negative, positive or complex. Each solution to $F(y)$ is investigated by inserting the appropriate boundary conditions. It turns out that eigenvalues has to be positive.

$$f(y,z) = \sum f_n \tag{A.13}$$
$$f_n = (A_n \cosh(\lambda_n z) + B_n \sinh(\lambda_n z)) \times \tag{A.14}$$
$$(C_n \cos(\lambda_n y) + D_n \sin(\lambda_n y)) \tag{A.15}$$

Due to symmetry of the solution ($B_n = D_n = 0$). The boundary condition (BC1) gives the eigenvalues ($\lambda_n = n\pi/H$). From this set of eigenfunctions (f_n) the solution may be found by determining the Fourier coefficients. Inserting the reduced guess into the (BC2) boundary condition gives

$$-U\frac{y}{H} = \sum_{n=1}^{\infty} A_n \cosh(\lambda_n W)\sin(\lambda_n y) \tag{A.16}$$
$$-U\frac{y}{H} = \sum_{n=1}^{\infty} A_n^* \sin(\lambda_n y) \tag{A.17}$$
$$A_n^* = \frac{2}{H}\int_0^H -U\frac{y}{H}\sin(\lambda_n y)dy \tag{A.18}$$
Integration by parts (A.19)
$$A_n^* = \frac{2U}{n\pi}(-1)^n \tag{A.20}$$

Finally the overall velocity field may be written as

$$\frac{u(y,z)}{U} = \frac{y}{H} + 2\sum_{n=1}^{\infty}\frac{(-1)^n}{n\pi}\frac{\cosh(n\pi\frac{z}{H})}{\cosh(n\pi\frac{W}{H})}\sin(n\pi\frac{y}{H}) \tag{A.21}$$

Evaluating this expression on a computer using a finite number of digits may be a problem. The fraction with the hyperbolic cosines will cause a problem when n becomes large. The remedy is to write $\cosh(x) = (e^x + e^{-x})/2$ and divide by e^x in both nominator and denominator. The MATLAB source code can be seen in Appendix D, Moving Lid. One solution is shown in Fig. A.2.

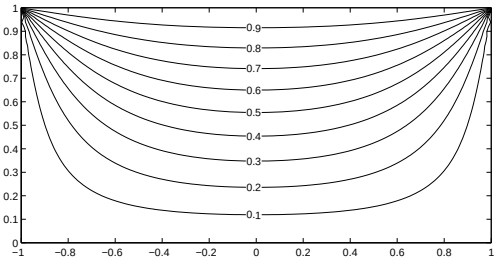

Figure A.2: Contour lines of the solution $u(x, y)$ made nondimensional by U and H. The aspect ratio is 2 $W/H = 2$.

The flow rate may be found by integrating the solution, Fig. A.3.

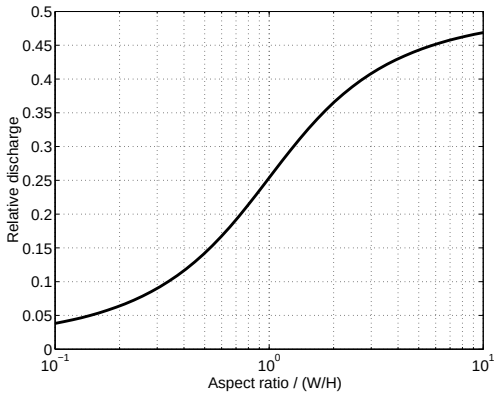

Figure A.3: Relative flow rate of a single wall EO pump as function of aspect ratio. Note that the graph is symmetric. $Q = WHQ^*$ where W and H is the full width and full height respectively. The flow rate approaches $Q^* \to 0.5$ asymptotically corresponding to Couette flow, $u(y) = Uy/H$.

Appendix B

Pump Calculations

The following worksheets are made in Microsoft Excel 2000. The equations used are not displayed and reader is left to the respective sections. The equations can be found almost exclusively in Chap. 3. I have used different colors and typesetting for readability.

- Bold face: numbers, are used to display a calculated value.
- Bold face: titles, are used to emphasize the title.
- Plain face: constants and units.
- Gray font: workings.

The following worksheets are included.

- Morf, 1 page.
- Takamura, 2 pages.
- Two-Liquid Viscous Pump, 2 pages.
- Reservoir Design, 1 page.
- Shallow Reservoir Pump, 3 pages.
- Layout, 1 page.

Morf et al.

Calculated values are bold face

by Anders Brask

Model

Dyn. Visc g/(mm s)	Voltage V	EO Mobility mm^2/(V s)	Hyd. Res. g/(mm^4 s)	Discharge p=0 nL/s	Backpressure Pa
0,001	1000	0,06	**7190**	**44,76**	**321,8**

Length mm	Width mm	Depth mm		Hyd. Res. g/(s mm^4)	Elec. Res. 1/mm
62	0,30	0,050		22169	4,13E+03
69	0,30	0,050		24672	4,60E+03
76	0,30	0,050		27174	5,07E+03
62	0,30	0,050		22169	4,13E+03
69	0,30	0,050		24672	4,60E+03
76	0,30	0,050		27174	5,07E+03
14	0,30	0,050		5006	9,33E+02
14	0,30	0,050		5006	9,33E+02
5	0,30	0,050		1788	3,33E+02
			R_c	12932	2,41E+03
			R_b	17938	3,34E+03
			R_a	10805	2,01E+03
			Total	**7190**	1,3406E+03

Model and simulation comparisons

EOF with counter pressure

	Pressure Pa	Discharge nL/s	Hyd. Res. g/(mm^4 s)	Max Discharge nL/s	Backpressure Pa
Sm_1	0	44,40	**7099**	**44,28**	**314,4**
	100	30,08			
	200	16,04			
	300	2,02	-0,14086	44,28	
	400	-12,00			
Model			7190	44,76	321,8
Simulation			7099	44,28	314,4
Deviation			**1%**	**1%**	**2%**

Pressure driven flow

	Pressure Pa	Discharge µm^3/s	Discharge nl/s	Hyd. Res. g/(mm^4 s)
Sm_2	50	1,75	7,00	**7123**
	100	3,51	14,04	
	150	5,26	21,04	
	200	7,02	28,08	
	250	8,77	35,08	
	300	10,5	42,00	
	350	12,3	49,20	
Model				7190
Simulation				7123
Deviation				**1%**

Figure B.1: Page 1/1

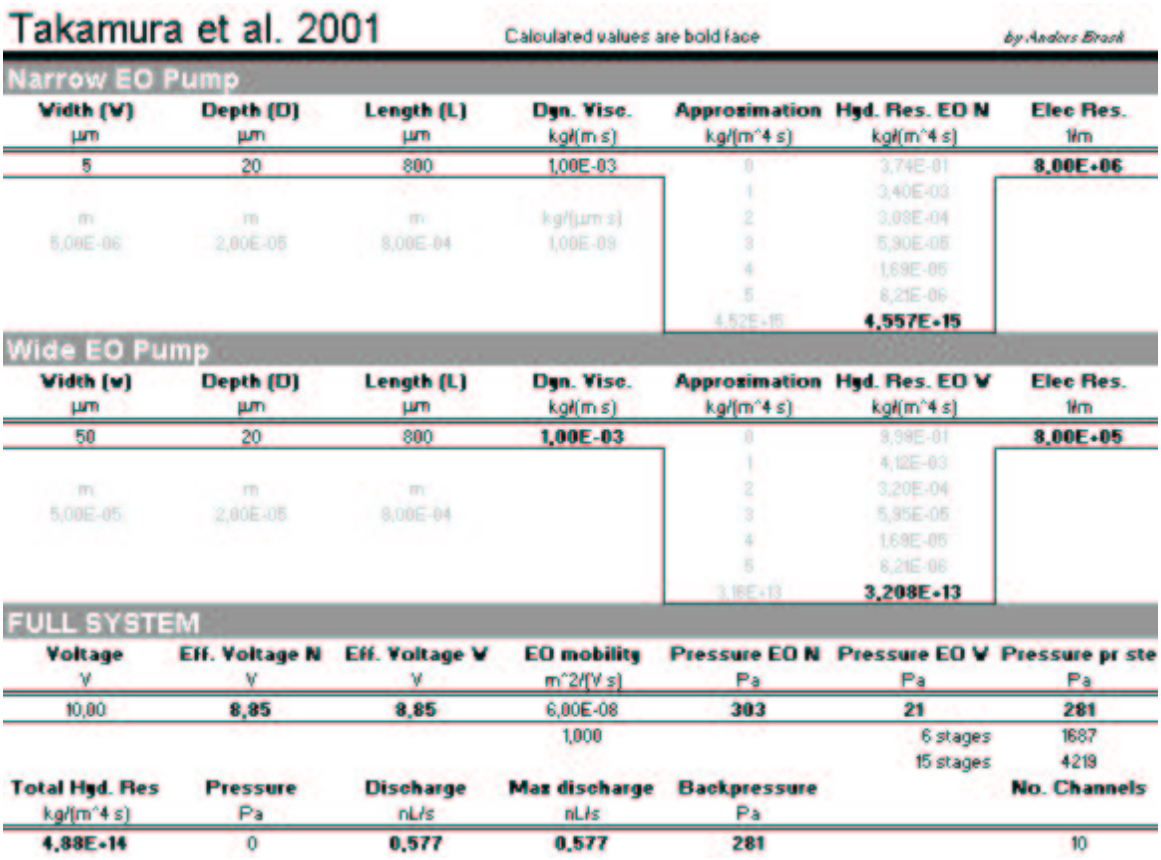

Takamura et al. 2001 — Calculated values are bold face — by Anders Brask

Narrow EO Pump

Width (W) µm	Depth (D) µm	Length (L) µm	Dyn. Visc. kg/(m s)	Approximation kg/(m^4 s)	Hyd. Res. EO N kg/(m^4 s)	Elec Res. 1/m
5	20	800	1,00E-03	0	3,74E-01	**8,00E+06**
				1	3,40E-03	
m	m	m	kg/(µm s)	2	3,09E-04	
5,00E-06	2,00E-05	8,00E-04	1,00E-09	3	5,90E-05	
				4	1,69E-05	
				5	6,21E-06	
				4,52E+15	**4,557E+15**	

Wide EO Pump

Width (w) µm	Depth (D) µm	Length (L) µm	Dyn. Visc. kg/(m s)	Approximation kg/(m^4 s)	Hyd. Res. EO W kg/(m^4 s)	Elec Res. 1/m
50	20	800	**1,00E-03**	0	9,39E-01	**8,00E+05**
				1	4,12E-03	
m	m	m		2	3,20E-04	
5,00E-05	2,00E-05	8,00E-04		3	5,95E-05	
				4	1,69E-05	
				5	6,21E-06	
				3,16E+13	**3,208E+13**	

FULL SYSTEM

Voltage V	Eff. Voltage N V	Eff. Voltage W V	EO mobility m^2/[V s]	Pressure EO N Pa	Pressure EO W Pa	Pressure pr ste Pa
10,00	**8,85**	**8,85**	6,00E-08	**303**	**21**	**281**
			1,000		6 stages	1687
					15 stages	4219

Total Hyd. Res kg/(m^4 s)	Pressure Pa	Discharge nL/s	Max discharge nL/s	Backpressure Pa	No. Channels
4,88E+14	0	**0,577**	**0,577**	**281**	10

Figure B.2: Page 1/2

Effective potential drop in EO section

	Resistance 1/µm	Voltage Drop across EO section
R_1	4,0000	
R_2	0,4000	**88,52%**
R_3	0,0259	
R_total	0,2259	

Model and simulation comparisons

nf_6, nf_7 Half geometry and full anode

Pressure Pa	**Discharge** nL/s		**Max Discharge** nL/s	**Backpressure** Pa
0	5,58E-01	-0,004087082	**0,558**	**273,1**
141	-1,83E-02			
Model			0,577	281,0
Simulation			0,558	273,1
Deviation			**-3%**	**-3%**

nf_8, sm_2 Half geometry and full anode

Pressure Pa	**Discharge** nL/s		**Max Discharge** nL/s	**Backpressure** Pa
0	0,56	-0,004083143	**0,560**	**274,0**
25	0,458			
50	0,356			
75	0,254			
100	0,1512			
125	0,049			
150	-0,0532			
Model			0,577	281,0
Simulation			0,560	274,0
Deviation from model			**-3%**	**-2%**

Figure B.3: Page 2/2

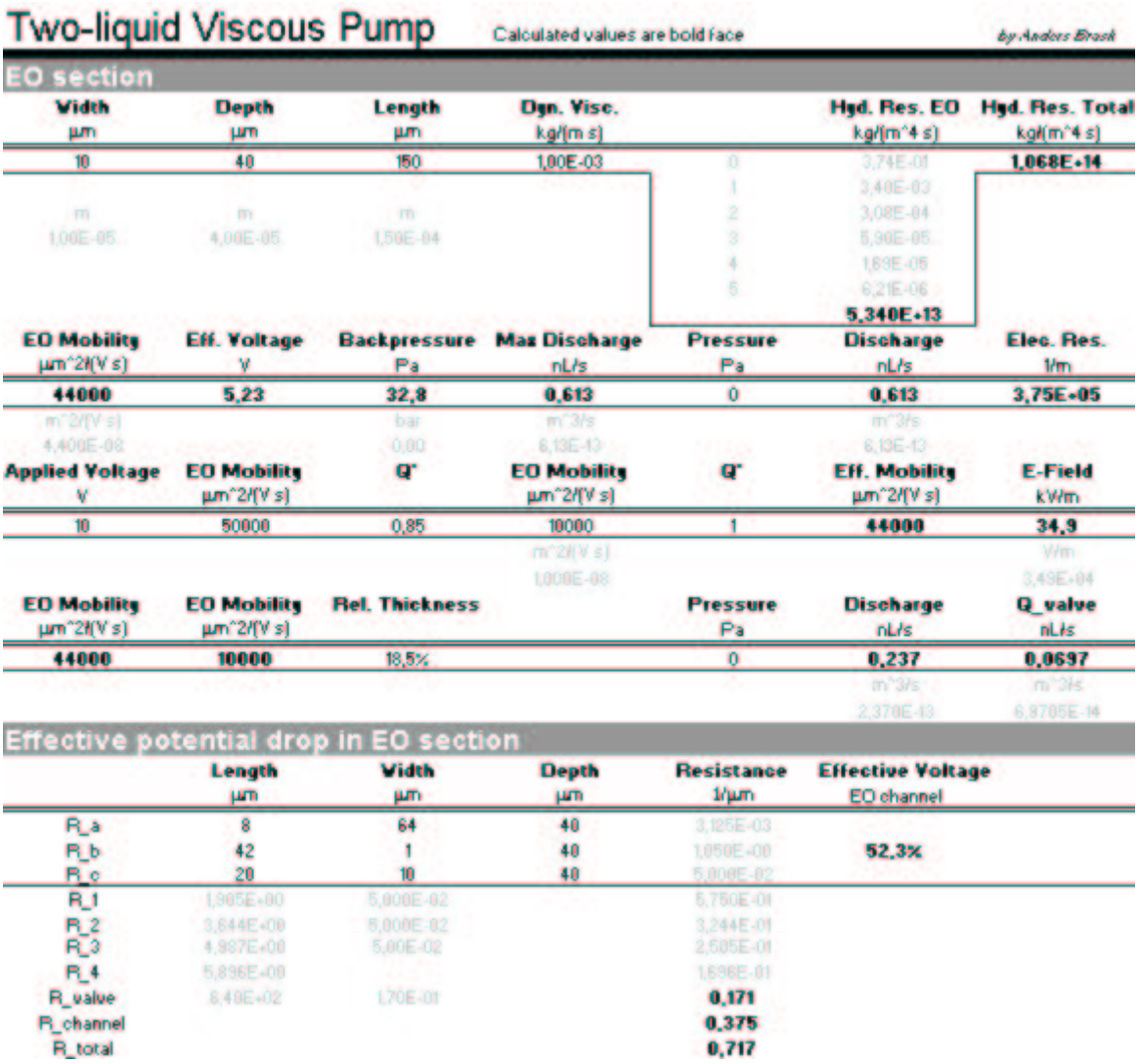

Two-liquid Viscous Pump

Calculated values are bold face

by Anders Brask

EO section

Width	Depth	Length	Dyn. Visc.		Hyd. Res. EO	Hyd. Res. Total
µm	µm	µm	kg/(m s)		kg/(m^4 s)	kg/(m^4 s)
10	40	150	1,00E-03	0	3,74E-01	**1,068E+14**
				1	3,40E-03	
m	m	m		2	3,08E-04	
1,00E-05	4,00E-05	1,50E-04		3	5,90E-05	
				4	1,89E-05	
				5	6,21E-06	
					5,340E+13	

EO Mobility	Eff. Voltage	Backpressure	Max Discharge	Pressure	Discharge	Elec. Res.
µm^2/(V s)	V	Pa	nL/s	Pa	nL/s	1/m
44000	**5,23**	**32,8**	**0,613**	0	**0,613**	**3,75E+05**
m^2/(V s)		bar	m^3/s		m^3/s	
4,40E-08		0,00	6,13E-13		6,13E-13	

Applied Voltage	EO Mobility	Q*	EO Mobility	Q*	Eff. Mobility	E-Field
V	µm^2/(V s)		µm^2/(V s)		µm^2/(V s)	kV/m
10	50000	0,85	10000	1	**44000**	**34,9**
			m^2/(V s)			V/m
			1,00E-08			3,49E+04

EO Mobility	EO Mobility	Rel. Thickness	Pressure	Discharge	Q_valve
µm^2/(V s)	µm^2/(V s)		Pa	nL/s	nL/s
44000	**10000**	18,5%	0	**0,237**	**0,0697**
				m^3/s	m^3/s
				2,37E-13	6,97E-14

Effective potential drop in EO section

	Length	Width	Depth	Resistance	Effective Voltage
	µm	µm	µm	1/µm	EO channel
R_a	8	64	40	3,12E-03	
R_b	42	1	40	1,05E+00	**52,3%**
R_c	20	10	40	5,00E-02	
R_1	1,96E+00	5,00E-02		5,75E-01	
R_2	3,84E+00	5,00E-02		3,24E-01	
R_3	4,98E+00	5,00E-02		2,50E-01	
R_4	5,89E+00			1,69E-01	
R_valve	6,49E+02	1,70E-01		**0,171**	
R_channel				**0,375**	
R_total				**0,717**	

Figure B.4: Page 1/2

Model and simulation comparisons

All simulations	Potential drop	E-field
	V	kV/m
Model	5,23	34,9
Simulation	5,10	33,9
Deviation	**3%**	**3%**

Sm_2. EO 0 (no diffusion)	Backpressure	Max Discharge	Pressure EO section
	Pa	nL/s	Pa
Model	31,6	0,296	
Simulation	30,6	0,290	15,2
Deviation	**3%**	**2%**	

Sm_1. EO 5000 (no diffusion)	Backpressure	Max Discharge	Pressure EO section
	Pa	nL/s	Pa
Model	28,5	0,267	
Simulation	27,4	0,260	13,6
Deviation	**4%**	**3%**	

Sm_3. EO 10000 (no diffusion)	Backpressure	Max Discharge	Pressure EO section
	Pa	nL/s	Pa
Model	25,3	0,237	
Simulation	24,3	0,230	12,0
Deviation	**4%**	**3%**	

nf_6. EO 5000 (no diffusion)	Pumping lager thickness	
	µm	
Model	1,04	
Simulation	0,8	Average of top, middle and bed.
Deviation	**30%**	

nf_8. EO 10000 (no diffusion)	Pumping lager thickness	
	µm	
Model	1,85	
Simulation	1,62	Average of top, middle and bed.
Deviation	**14%**	

nf_7. EO 5000 (self-diffusion of water)	Terminal Mass Fraction
Model	20,7%
Simulation	20,9%
Deviation	**-1%**

Figure B.5: Page 2/2

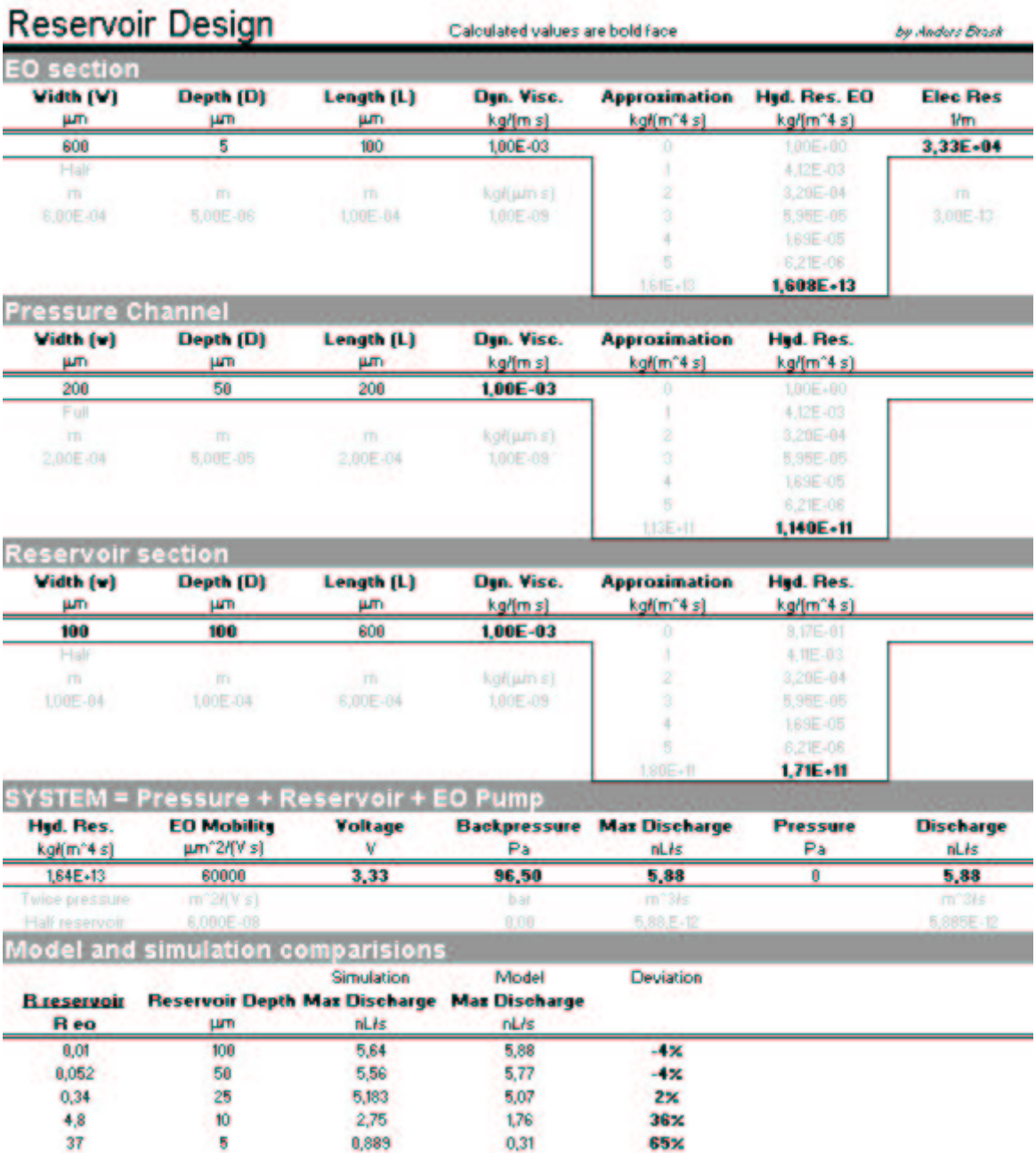

Reservoir Design

Calculated values are bold face

by Anders Brask

EO section

Width (W)	Depth (D)	Length (L)	Dyn. Visc.	Approximation	Hyd. Res. EO	Elec Res
µm	µm	µm	kg/(m s)	kg/(m^4 s)	kg/(m^4 s)	1/m
600	5	100	1,00E-03	0	1,00E+00	**3,33E+04**
Half				1	4,12E-03	
m	m	m	kg/(µm s)	2	3,20E-04	m
6,00E-04	5,00E-06	1,00E-04	1,00E-09	3	5,95E-05	3,00E-12
				4	1,69E-05	
				5	6,21E-06	
				1,61E+13	**1,608E+13**	

Pressure Channel

Width (w)	Depth (D)	Length (L)	Dyn. Visc.	Approximation	Hyd. Res.
µm	µm	µm	kg/(m s)	kg/(m^4 s)	kg/(m^4 s)
200	50	200	**1,00E-03**	0	1,00E+00
Full				1	4,12E-03
m	m	m	kg/(µm s)	2	3,20E-04
2,00E-04	5,00E-05	2,00E-04	1,00E-09	3	5,95E-05
				4	1,69E-05
				5	6,21E-06
				1,13E+11	**1,140E+11**

Reservoir section

Width (w)	Depth (D)	Length (L)	Dyn. Visc.	Approximation	Hyd. Res.
µm	µm	µm	kg/(m s)	kg/(m^4 s)	kg/(m^4 s)
100	**100**	600	**1,00E-03**	0	9,17E-01
Half				1	4,11E-03
m	m	m	kg/(µm s)	2	3,20E-04
1,00E-04	1,00E-04	6,00E-04	1,00E-09	3	5,95E-05
				4	1,69E-05
				5	6,21E-06
				1,69E+11	**1,71E+11**

SYSTEM = Pressure + Reservoir + EO Pump

Hyd. Res.	EO Mobility	Voltage	Backpressure	Max Discharge	Pressure	Discharge
kg/(m^4 s)	µm^2/(V s)	V	Pa	nL/s	Pa	nL/s
1,64E+13	60000	**3,33**	**96,50**	**5,88**	0	**5,88**
Twice pressure	m^2/(V s)		bar	m^3/s		m^3/s
Half reservoir	6,00E-08		0,00	5,88,E-12		5,885E-12

Model and simulation comparisions

R reservoir / R eo	Reservoir Depth µm	Simulation Max Discharge nL/s	Model Max Discharge nL/s	Deviation
0,01	100	5,64	5,88	**-4%**
0,052	50	5,56	5,77	**-4%**
0,34	25	5,183	5,07	**2%**
4,8	10	2,75	1,76	**36%**
37	5	0,889	0,31	**65%**

Figure B.6: Page 1/1

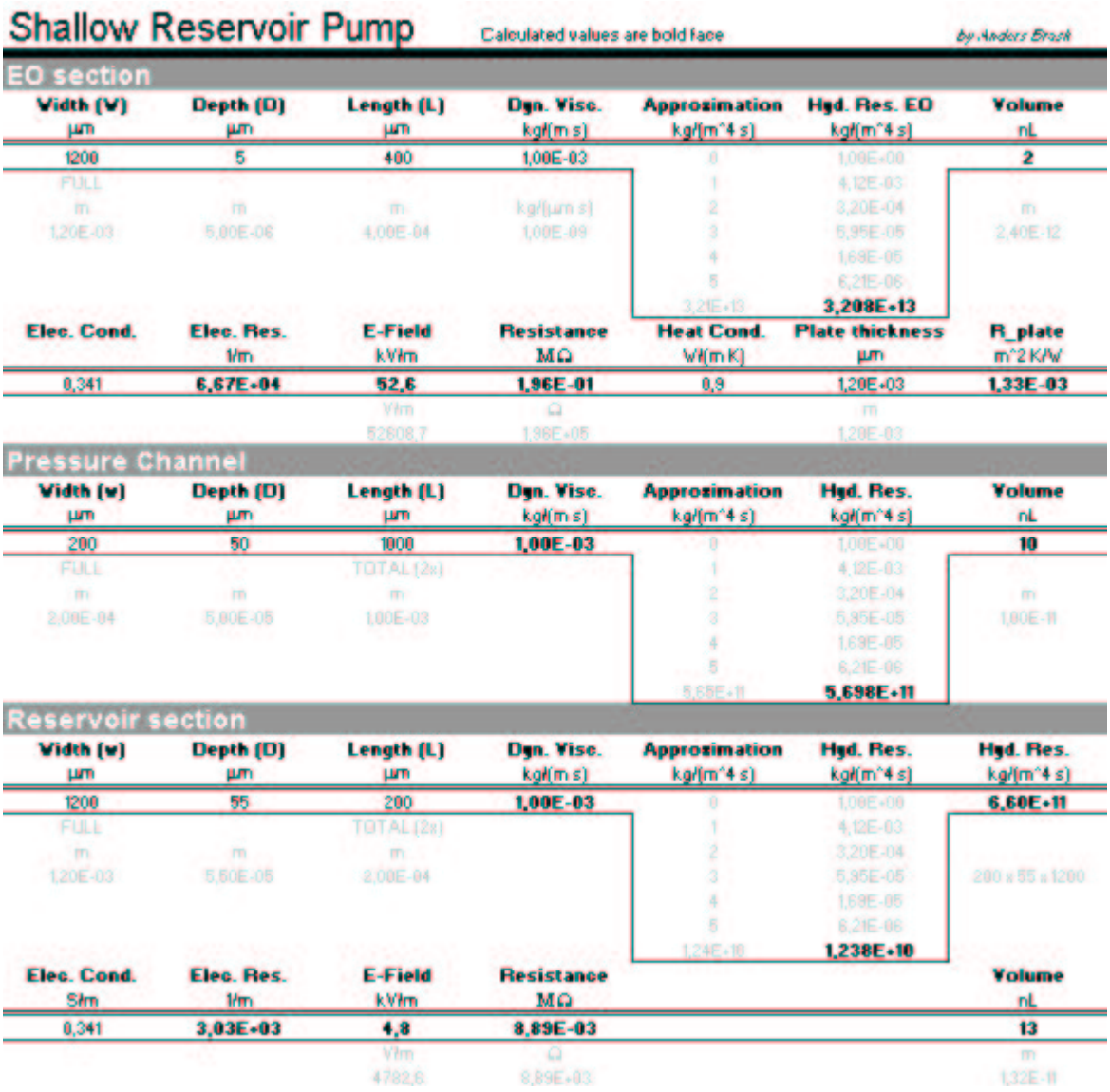

Shallow Reservoir Pump

Calculated values are bold face

by Anders Brask

EO section

Width (W)	Depth (D)	Length (L)	Dyn. Visc.	Approximation	Hyd. Res. EO	Volume
µm	µm	µm	kg/(m s)	kg/(m^4 s)	kg/(m^4 s)	nL
1200	5	400	1,00E-03	0	1,09E+00	**2**
FULL				1	4,12E-03	
m	m	m	kg/(µm s)	2	3,20E-04	m
1,20E-03	5,00E-06	4,00E-04	1,00E-09	3	5,95E-05	2,40E-12
				4	1,69E-05	
				5	6,21E-06	
				3,21E+13	**3,208E+13**	

Elec. Cond.	Elec. Res.	E-Field	Resistance	Heat Cond.	Plate thickness	R_plate
	1/m	kV/m	MΩ	W/(m K)	µm	m^2 K/W
0,341	**6,67E+04**	**52,6**	**1,96E-01**	0,9	1,20E+03	**1,33E-03**
		V/m	Ω		m	
		52608,7	1,96E+05		1,20E-03	

Pressure Channel

Width (w)	Depth (D)	Length (L)	Dyn. Visc.	Approximation	Hyd. Res.	Volume
µm	µm	µm	kg/(m s)	kg/(m^4 s)	kg/(m^4 s)	nL
200	50	1000	**1,00E-03**	0	1,09E+00	**10**
FULL		TOTAL (2x)		1	4,12E-03	
m	m	m		2	3,20E-04	m
2,00E-04	5,00E-05	1,00E-03		3	5,95E-05	1,00E-11
				4	1,69E-05	
				5	6,21E-06	
				5,65E+11	**5,698E+11**	

Reservoir section

Width (w)	Depth (D)	Length (L)	Dyn. Visc.	Approximation	Hyd. Res.	Hyd. Res.
µm	µm	µm	kg/(m s)	kg/(m^4 s)	kg/(m^4 s)	kg/(m^4 s)
1200	55	200	**1,00E-03**	0	1,09E+00	**6,60E+11**
FULL		TOTAL (2x)		1	4,12E-03	
m	m	m		2	3,20E-04	
1,20E-03	5,50E-05	2,00E-04		3	5,95E-05	200 x 55 x 1200
				4	1,69E-05	
				5	6,21E-06	
				1,24E+10	**1,238E+10**	

Elec. Cond.	Elec. Res.	E-Field	Resistance			Volume
S/m	1/m	kV/m	MΩ			nL
0,341	**3,03E+03**	**4,8**	**8,89E-03**			**13**
		V/m	Ω			m
		4782,6	8,89E+03			1,32E-11

Figure B.7: Page 1/3

SYSTEM = Pressure + Reservoir + EO Pump

Applied Voltage			Hgd. Res.	Current	Resistance	System Volume
V			kg/(m^4 s)	µA	MΩ	nL
22			3,33E+13	**107,6**	**0,20**	**16**
				A		
				1,08E-04	204389,94	
EO Mobility	**Eff. Voltage**	**Backpressure**	**Max Discharge**	**Pressure**	**Discharge**	
µm^2/(V s)	V	Pa	nL/s	Pa	nL/s	
60000	**21,0**	**607,6**	**18,24**	0,00	**18,24**	
m^2/(V s)		bar	m^3/s		m^3/s	
6,000E-08		0,01	1,82E-11		1,824E-11	

Model and simulation comparisons

Shallow 3

	Cells/Tolerance	Pressure	Discharge	Max Discharge	Backpressure	Hgd. Res.
		Pa	nL/s	nL/s	Pa	kg/(m^4 s)
nf 1	14500/1e-4	0	17,11			
nf 2	14500/1e-6	0	17,11			
sm 1	91000/1e-6	0	17,58	-0,03027619	17,57266667	3,028E-14
		100	14,54	**17,57**	**580,4**	**3,303E+13**
		200	11,52			
		300	8,48			
		400	5,46			
		500	2,44			
		600	-0,59			
		700	-3,62			
Model				18,24	607,6	3,331E+13
Simulation				17,57	580,4	3,303E+13
Deviation				**4%**	**5%**	**1%**

Figure B.8: Page 2/3

Shallow 2

Geometry A

Sim./Mesh	Cells	Tolerance	Discharge x10 nL/s	Max velocity µm/s	z-cells	Max aspect ratio
nf 1/5	66000	1,00E-04	4,96	4981	15	3
nf 2/1	11000	1,00E-04	4,84	3610	10	4
nf 3/2	15000	1,00E-04	4,84	3639	10	4
nf 4/3	60000	1,00E-04	4,92	4451	10	2
nf 5/4	120000	1,00E-04	4,97	5024	20	4
nf 8/1	11000	1,00E-06	4,84	3610	10	3
nf 9/5	66000	1,00E-06	4,97	4981	15	2
nf 10/2	15000	1,00E-06	4,85	3638	10	4
nf 11/4	120000	1,00E-06	4,99	5024	20	2

Geometry B

Sim./Mesh	Cells	Pressure Pa	Discharge nL/s	Max Discharge nL/s	Backpressure Pa	Hyd. Res. kg/(m^4 s)
nf 12/6	33000/1e-6	0	8,86	-0,815164835	8,86	
nf 13/6	33000/1e-6	637	-0,800	**8,86**	**584**	**6,59E+13**
sm 1/7	43000/1e-6	0	9,07	-0,815131513	9,069551833	1,51315E-14
		100	7,56	**9,07**	**593**	**6,61E+13**
		200	6,04			
		300	4,53			
		400	3,01			
		500	1,50			
		600	0,02			
		700	-1,54			
Model				9,321	606,6	6,50786E+13
Simulation				9,07	593	6,61E+13
Deviation				**3%**	**1%**	**-2%**

Figure B.9: Page 3/3

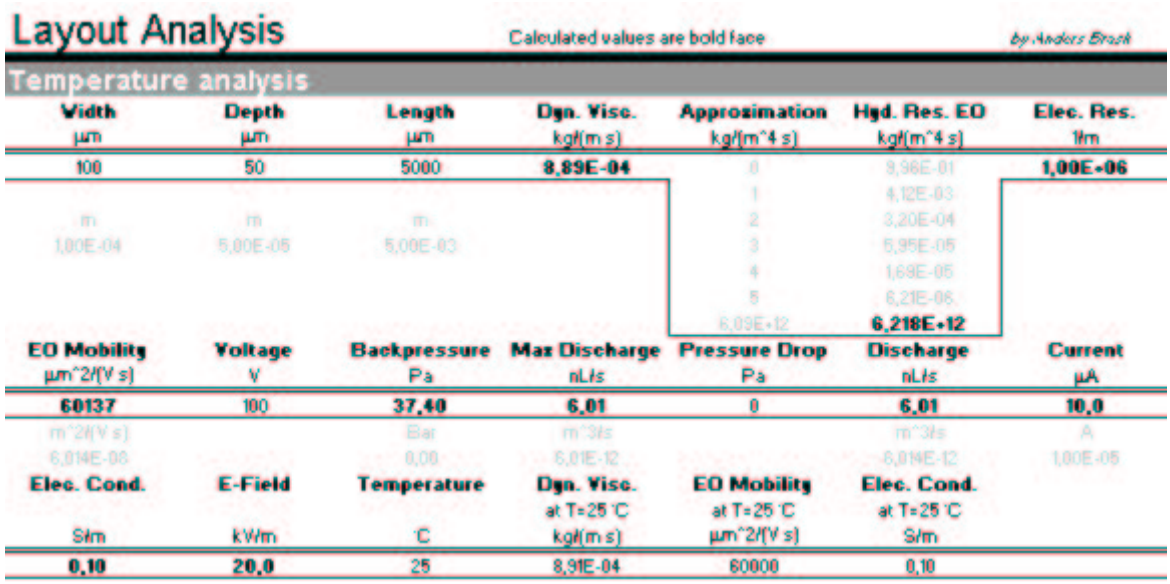

Layout Analysis — Calculated values are bold face — by Anders Brask

Temperature analysis

Width	Depth	Length	Dyn. Visc.	Approximation	Hyd. Res. EO	Elec. Res.
µm	µm	µm	kg/(m s)	kg/(m^4 s)	kg/(m^4 s)	1/m
100	50	5000	**8,89E-04**	0	3,96E-01	**1,00E+06**
				1	4,12E-03	
m	m	m		2	3,20E-04	
1,00E-04	5,00E-05	5,00E-03		3	5,95E-05	
				4	1,69E-05	
				5	6,21E-06	
				6,03E+12	**6,218E+12**	

EO Mobility	Voltage	Backpressure	Max Discharge	Pressure Drop	Discharge	Current
µm^2/(V s)	V	Pa	nL/s	Pa	nL/s	µA
60137	100	**37,40**	**6,01**	0	**6,01**	**10,0**
m^2/(V s)		Bar	m^3/s		m^3/s	A
6,014E-06		0,00	6,01E-12		6,014E-12	1,00E-05

Elec. Cond.	E-Field	Temperature	Dyn. Visc. at T=25 °C	EO Mobility at T=25 °C	Elec. Cond. at T=25 °C
S/m	kV/m	°C	kg/(m s)	µm^2/(V s)	S/m
0,10	**20,0**	25	8,91E-04	60000	0,10

Figure B.10: Page 1/1

Appendix C

Simulation Logbook

Before undertaking a large simulation effort it is crucial to have a simulation logbook. The most logical settings can be forgotten after a week or a month. I have not included the actual simulation sheets because they are handwritten in my native language (Danish). Furthermore all of the important results are transferred to Appendix B.

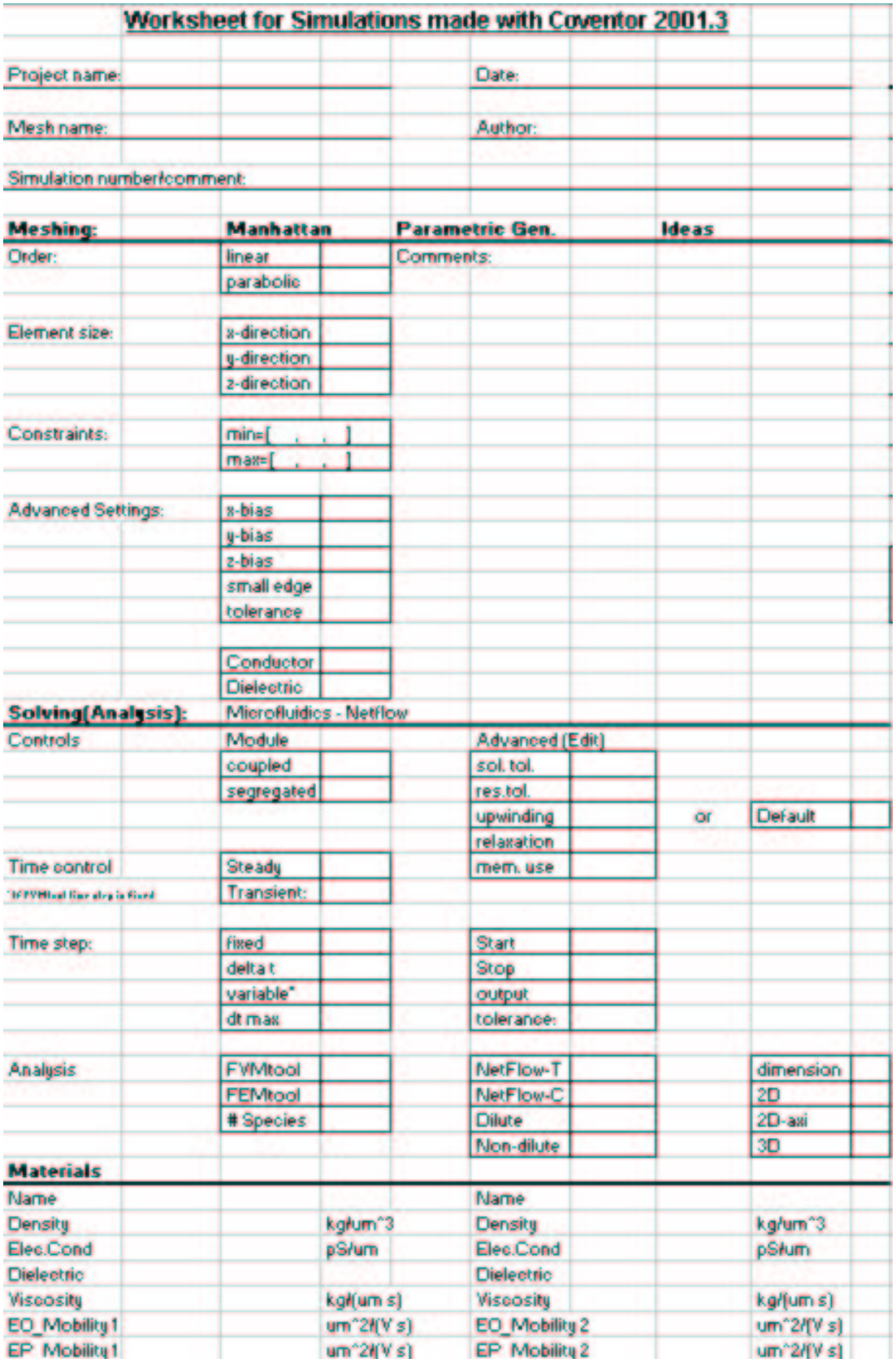

Worksheet for Simulations made with Coventor 2001.3

Project name:				Date:			
Mesh name:				Author:			
Simulation number/comment:							
Meshing:	**Manhattan**		**Parametric Gen.**		**Ideas**		
Order:	linear		Comments:				
	parabolic						
Element size:	x-direction						
	y-direction						
	z-direction						
Constraints:	min=[, ,]						
	max=[, ,]						
Advanced Settings:	x-bias						
	y-bias						
	z-bias						
	small edge						
	tolerance						
	Conductor						
	Dielectric						
Solving(Analysis):	Microfluidics - Netflow						
Controls	Module		Advanced (Edit)				
	coupled		sol. tol.				
	segregated		res.tol.				
			upwinding		or	Default	
			relaxation				
Time control	Steady		mem. use				
	Transient:						
Time step:	fixed		Start				
	delta t		Stop				
	variable*		output				
	dt max		tolerance:				
Analysis	FVMtool		NetFlow-T			dimension	
	FEMtool		NetFlow-C			2D	
	# Species		Dilute			2D-axi	
			Non-dilute			3D	
Materials							
Name			Name				
Density		kg/um^3	Density			kg/um^3	
Elec.Cond		pS/um	Elec.Cond			pS/um	
Dielectric			Dielectric				
Viscosity		kg/(um s)	Viscosity			kg/(um s)	
EO_Mobility 1		um^2/(V s)	EO_Mobility 2			um^2/(V s)	
EP_Mobility 1		um^2/(V s)	EP_Mobility 2			um^2/(V s)	

Figure C.1: Page 1/2

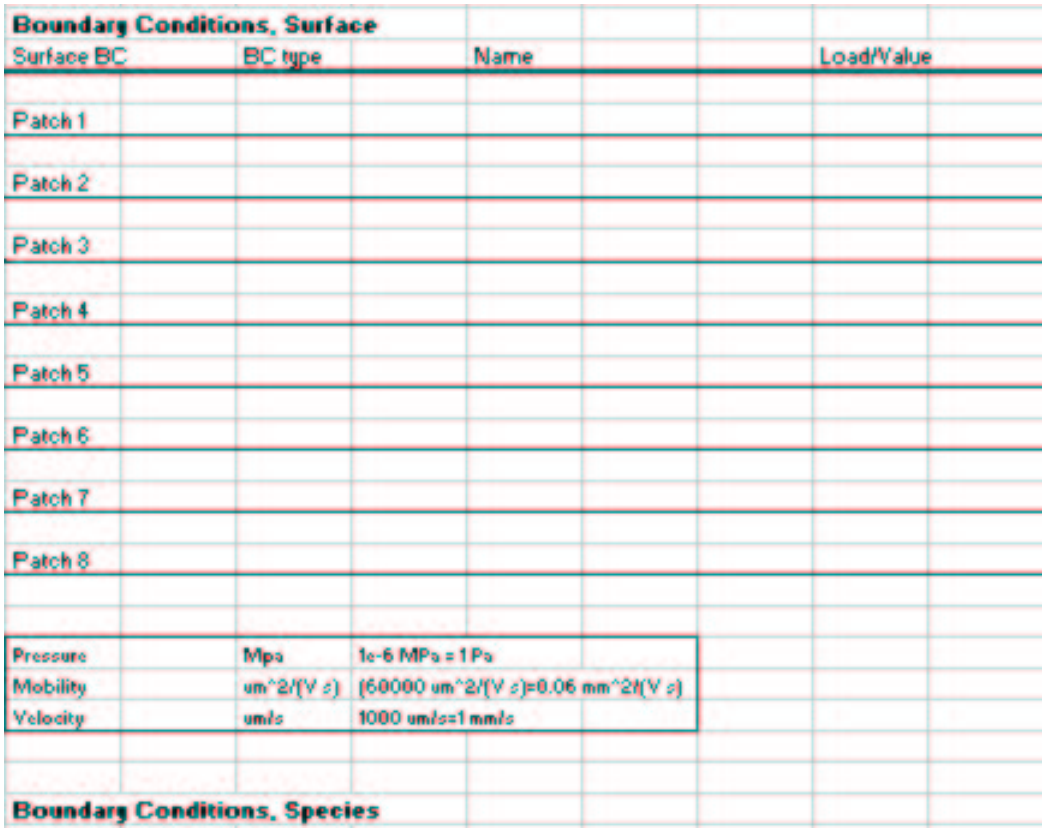

Boundary Conditions, Surface

Surface BC	BC type	Name	Load/Value
Patch 1			
Patch 2			
Patch 3			
Patch 4			
Patch 5			
Patch 6			
Patch 7			
Patch 8			

Pressure	Mpa	1e-6 MPa = 1 Pa
Mobility	um^2/(V s)	(60000 um^2/(V s)=0.06 mm^2/(V s)
Velocity	um/s	1000 um/s=1 mm/s

Boundary Conditions, Species

Figure C.2: Page 2/2

Appendix D

MATLAB Source Code

Many small MATLAB programs have been used in the report. In total I have written 28 small programs. Either used for calculations or for plotting data. Here three of the most important are included.

- **Potential Solver**
  Solves the potential/velocity distribution in a circular capillary, Fig. 2.2(a). The BVP is a nonlinear so a shoot and correct method was implemented.
- **Moving Lid**
  Flow in a rectangular channel with a moving lid, Fig A.2 and Fig. A.3.
- **Two Moving Walls**
  Flow in a rectangular channel with two moving walls, Fig 3.5 and Fig. 3.4.
- **Diffusion**
  Diffusion problem in one dimension. Again the problem is solved analytically and evaluated numerically using MATLAB, Fig. 2.7.

D.1 Potential Solver

```
%Program to solve the potential/velocity distribution
%in circular capillary with finite sized Debye layers.
%Nonlinear BVP is solved by internal ODE-solver
%and a implemented shoot and correct method.
%Verified by calculations in Probstein, chap. 6
%by Anders Brask, MIC 2001
%Note:    SIGN OF THE ZETA POTENTIAL
%         FORMULA FOR CIRCULAR CAPILLARIES USED!!!
clear all close all global lambda

f=input('Plot velocity profile(1, default) or potential (2)?'); if
isempty(f) f=1; end

lambdavec=[2 1 0.4 0.2 0.1 0.01]; %Dimensionless Debye layer thickness

figure(1) hold on for j=1:1:size(lambdavec,2) zero=1e-6;
guess=0.0; delta=1e-10; error=1; maxerror=1e-4; zeta=2.79; p=0;
lambda=lambdavec(j);

if lambda==0.01 %Special case for small lambda
    zero=0.9;
end

while error>maxerror p=p+1; for i=1:2
   %[r,psi] = ode45(@vdp1,[zero 1],[guess+(i-1)*delta; 0]);
[r,psi] = ode45('vdp1',[zero 1],[guess+(i-1)*delta; 0]);
rightbc(i)=psi(length(psi(:,1)),1); end
slope=(rightbc(2)-rightbc(1))/delta;
guess=guess-(rightbc(1)-zeta)/slope;
error=abs(rightbc(2)-zeta)/zeta;
end %while

%Plotting either velocity of potential
if f==1 plot(r,-(psi(:,1)/zeta-1),'k','linewidth',2) hold on end

if f==2 plot(r,psi(:,1),'k','linewidth',2) hold on end

end %Lambda loop

%Labelling of graphs
%-------------------------------------------------------
if f==1 plot([0 0.9],[1 1],'k-','linewidth',2) axis([0 1 0 1])
xlabel('r/a','fontsize',12); ylabel('u/u_{\infty}','fontsize',12);
text(0.40,0.05,'\lambda*=2','fontsize',12);
text(0.45,0.20,'\lambda*=1','fontsize',12);
text(0.50,0.50,'\lambda*=0.4','fontsize',12);
text(0.60,0.70,'\lambda*=0.2','fontsize',12);
text(0.7,0.83,'\lambda*=0.1','fontsize',12);
text(0.81,0.93,'\lambda*=0.01','fontsize',12); end

if f==2 plot([0 1],[zeta zeta],'k--','linewidth',2)
xlabel('r/a','fontsize',12); ylabel('\psi'','fontsize',12);
text(0.6,2.9,'\zeta=2.79','fontsize',12);
text(0.1,2.55,'\lambda*=2','fontsize',12);
text(0.2,2.0,'\lambda*=1','fontsize',12);
text(0.35,1.2,'\lambda*=0.4','fontsize',12);
text(0.50,0.55,'\lambda*=0.2','fontsize',12);
text(0.65,0.35,'\lambda*=0.1','fontsize',12);
text(0.82,0.15,'\lambda*=0.01','fontsize',12); end
```

D.2 Moving Lid

```
%Flow in a rectangular channel with moving lid.
%PDE solved analytically and the expression is evaluated.
%Sherman - Viscous Flow, p. 154
%No pressure gradient. Velocities are made nondimensional by U.
%Two plot options
%(1) Contour plot of velocity distribution for a given aspect ratio.
%(2) Nondimensional flow rate as function of aspect ratio
%by Anders Brask
%MIC 2002
%--------------------------------------------------------------------------
clear all

disp('1: Contour Plot of velocity') disp('2: Aspect Ratio')

p=input('Plot results (default=1):'); if isempty(p) p=1; end

if p==1 aspectratio=input('What is the aspect ratio (W/H) (max
10)(default=1): '); if isempty(aspectratio) aspectratio=1; end
aspectratio=0.5*aspectratio; %W is half width but H is full height.

N=50; %Resolution of mesh
M=30; %Number of terms in sum
yvec=linspace(0,1,N); %y/H
zvec=linspace(0,aspectratio,N); %z/H
u=zeros(N); signvec=ones(1,M);
signvec(1:2:M)=-1;              %signvec=[-1 1 -1...]
nvec=pi*linspace(1,M,M);        %nvec=pi [1 2 3 ...]

for i=1:N for j=1:N y=yvec(i); z=zvec(j);
    u(i,j)=y+2*sum(signvec.*cosh(nvec*z).*sin(nvec*y)./(cosh(nvec*aspectratio).*nvec)); %i-th row
end end figure(1) cn=[0.1 0.2 0.3 0.4 0.5 0.6 0.7 0.8 0.9];
temp=[fliplr(u) u];
[cs,h]=contour(linspace(-aspectratio,aspectratio,2*N),linspace(0,1,N),temp(1:N,1:2*N),cn,'-k');
axis equal axis([-aspectratio aspectratio 0 1])

disp('Non-dimensional discharge'); disp(mean(mean(u))); end

if p==2
%--------------------------------------------------------------------
L=50; M=30; N=50;

maxa=5; mina=0.05; discharge=zeros(1,L);
aspectratio=logspace(log(mina)/log(10),log(maxa)/log(10),L);
yvec=linspace(0,1,N); %y/H
signvec=ones(1,M);
signvec(1:2:M)=-1;              %signvec=[-1 1 -1...]
nvec=pi*linspace(1,M,M);        %nvec=pi [1 2 3 ...]
for k=1:L u=zeros(N);
zvec=linspace(0,aspectratio(k),N); %z/H
for i=1:N for j=1:N y=yvec(i); z=zvec(j);
    u(i,j)=y+2*sum(signvec.*cosh(nvec*z).*sin(nvec*y)./(cosh(nvec*aspectratio(k)).*nvec)); %i-th row
end end discharge(k)=mean(mean(u)); end figure(1) close(1)
figure(1) semilogx(2*aspectratio,discharge,'-k','Linewidth',3);
axis([2*mina 2*maxa 0 0.5]) xlabel('Aspect ratio
(H/W)','Fontsize',14);5 ylabel('Relative
discharge','Fontsize',14); grid on
end %p
```

D.3 Two Moving Walls

```
%Duct Flow
%Based on equations derived
%by Anders Brask
%MIC 2002
%--------------------------------------------------------------------------

aspectratio=input('What is the aspect ratio (W/H) (default=1): ');
if isempty(aspectratio) aspectratio=1; end

N=25; %Resolution of mesh
M=100; %Number of terms in sum
yvec=linspace(0,1,N); %y/H
zvec=linspace(0,aspectratio,N); %z/H
u=zeros(N); signvec=ones(1,M);
signvec(2:2:M)=-1;                  %signvec=[-1 1 -1...]
nvec=pi*linspace(0,M-1,M)+pi/2;     %nvec=pi [1/2 3/2 5/2...]

for i=1:N for j=1:N y=yvec(i); z=zvec(j);
    u(i,j)=1-2*sum(signvec.*cos(nvec*y).*(exp(nvec.*(z-aspectratio))+exp(-nvec.*(z+aspectratio)))...
    ./nvec./(1+exp(-2*aspectratio*nvec))); %i-th row
end end figure(1) cn=[0.1 0.2 0.3 0.4 0.5 0.6 0.7 0.8 0.9];
temp=rot90([flipud(fliplr(u)) flipud(u); fliplr(u) u]);
[cs,h]=contour(linspace(-aspectratio,aspectratio,2*N),linspace(-1,1,2*N),temp(1:2*N,1:2*N)',cn,'-k');
clabel(cs,h,'manual') axis equal axis([-aspectratio aspectratio -1
1])
discharge=1-(2/aspectratio)*sum(signvec.*tanh(nvec*aspectratio).*sin(nvec)./(nvec.^3))
```

D.4 Diffusion

```
%Diffusion problem in one dimension, part 1/2
%The initial condition is placed in a function, part 2/2.
%The Fourier coefficients are found by integrating this function.
%by Anders Brask
%MIC 2002
%--------------------------------------------------------------------------
clear all

global gamma a m W

N=20; %Fourier terms
M=40; %Spatial resolution
T=6;  %Time resolution

k=2.26e-9;  %Diffusion coefficient (m^2/s)
W=1e-5;     %Width (m)
W=1; k=1/0.044; gamma=20; a=0.5*W; A(1:N+1)=0;
xvec=linspace(0,W,M); tvec=[0 0.015 0.05 0.1 0.2 1]*W^2/k;
%Fourier Coefficients
for m=0:1:N A(m+1)=2*quadl('stepfun',0,W)/W; end

figure(1) close(1)

for j=1:T for i=1:M
   phi(i)=0.5*A(1)+sum(A(2:N+1).*cos((1:N)*pi*xvec(i)/W).*exp(-k*tvec(j)*((1:N)*pi/W).^2));
end hold on plot(xvec,phi,'k-') end figure(1) axis([0 W 0 1])
xlabel('x/W','Fontsize',14) ylabel('c/c^o','Fontsize',14)
text(0.5*W,0.96,'t=0','Fontsize',14) text(0.6*W,0.94,'t=0.015
t^o','Fontsize',14) text(0.7*W,0.85,'t=0.05 t^o','Fontsize',14)
text(0.8*W,0.75,'t=0.1 t^o','Fontsize',14) text(0.85*W,0.64,'t=0.2
t^o','Fontsize',14) text(0.9*W,0.54,'t=t^o','Fontsize',14)
text(0.1*W,0.8,sprintf('Characteristic \ndiffusion time,\nt^o=%0.2g s',W^2/k),'Fontsize',14)

%Diffusion part 2/2
%Function used in evaluation of Fourier coefficients A_n.
%By Anders Brask
%MIC 2002

function stepfun = stepfun(x)

global gamma a m W

stepfun = 0.5*cos(pi*m*x/W).*(1+tanh(gamma*(x-a)/W));
```

Appendix E

COVENTOR Support Q&A

In the following appendix questions and answers from COVENTOR Support are presented. The answers have been written by Technical director, Dr. ir. Joost van Kuijk and senior application engineer Chris Welham.

Q:

```
I have worked the Wall Effects, EO mobility BC in a simple
straight channel. Why does it only return zero velocities.
```

A:

```
There is a numerical problem in the FVMTool. Briefly, for some
models the potential equation can solve so fast that there are not
valid boundary conditions for the momentum equation so that it is
not solved.

This problem has been fixed and will be included in the next
official patch release, due out next year. In the meantime I can
send you the required replacement FluentWrapper.exe. Please could
you let me know the OS you are using, so that I can send the
appropriate file. The new file must be put into
/coventorWare2001.3/bin. The as installed FluentWrapper.exe that
is present should be re-named so that it is not over-written.
```

Q:

```
What is the molecular weight used for in \textsc{Coventor} (just
briefly). Is it mandatory?
```

A:

```
The molecular weight is not used anywhere, and does not need to be
set. It will be removed in the next release.
```

Q:

```
How large aspect ratios be used with the FVM tool?
```

A:

```
Element aspect ratios should generally be less than 100 to 1.
Higher aspect ratios will cause solver divergence or unphysical
answers.  It is actually possible to run problems with 1 million
elements, using the FVMTool, but you need about 1.5 gigs of RAM
```

for this, so its typically not a good idea. I don't really know anything about your simulation, but the best approach is usually to run a shorter sample with detailed simulation, extract the behaviour, and build a system model to simulate the larger system.

Q:

I have question regarding the mass fraction. I have just simulated a simple flow in a T-junction. At the one end I introduced species with mass fraction 1 (SpeciesSurfBCs). The simulation gave mass fractions as high as 1.26. In my opinion mass fractions should not exceed 1! How does it calculate it? The carrier is water and I have not specified the density of species 1. If have searched through the microfluidic analysis and reference guide documents. The simulation was done nondilute which is perhaps why it goes wrong? However as I understand it the difference between the dilute and nondilute option is only relevant for conductivity calculations.

A:

Nondilute simulations can often result in increasing species fractions. This usually occurs when a species is being transported by electrophoresis, and has a nonzero species conductivity. This results in an effective velocity field that has a nonzero divergence, so the mass fraction can increase (this is often called stacking, and the effect is used for sample pre-concentration in Capillary Zone Electrophoresis). Remember that all nondilute simulations should be done with the FVMTool. Its also possible to get increasing mass fractions for dilute simulations if very coarse timesteps are used (this would obviously be a numerical error).

Q:

The FlowRate patch query should give the Flux through a patch. But this is not the case (unless the flow is perpendicular to the patch). Patch query on a patch that is parallel to the flow does also give considerable values.

A:

The flow rate query calculates the flow rate of fluid perpendicular to the patch (mathematically, the integral of the fluid velocity dotted with the patch normal). It typically gives very small answers for flow rate through walls, but not exactly zero, we are not sure why and are looking into this.

Appendix F

Similitude between the Velocity and Electric field

Direct numerical simulation of the Navier-Stokes equation with species transport coupled with the Poisson equation is extremely complicated. Hence it is preferable if some simplifications could be made. The flow is strictly laminar so no turbulence modelling is needed. If the Debye layer is disregarded, the Poisson equation may be replaced with the Laplace equation. The Debye layer is important from a physical point of view and determines the similitude between the fluid and the electric field. However it is not important to resolve this layer in the numerical simulations. Even if this was necessary it would be very difficult because of differences in the order of magnitude of the length scales, Cummings *et al.*, 2000.

In some situations it may be possible to determine the flow from the Laplace equation solely. The conditions for this major simplification are partly shown on Fig. F.1 and discussed thoroughly in the following.

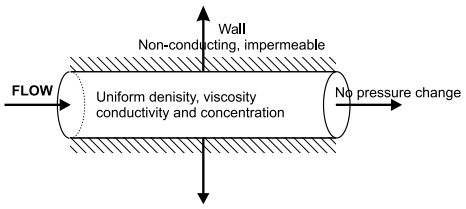

Figure F.1: Conditions for Similitude between the fluid and Electric field in EOF.

- In order for a flow to exhibit similitude the electric field must be quasi-stationary. For a given system there will be a transient time and as long as the field changes slow compared to that time it will not violate this condition.
- A laminar pressure driven flow generates a parabolic velocity profile. Hence the pressures must be the same at the inlet and outlet, i.e., no pressure gradients can be present.

- Gravity may also induce a parabolic velocity profile so the flow must be orthogonal to the gravity field.
- The Debye layer must be thin $\lambda_D \ll a$ where a is the radius of the channel. This assumption was used in the derivation of the Helmholtz-Smoluchowski relation. If indeed the double layer covered the entire channel it would have a uniform charge density and hence a parabolic velocity profile would be induced.
- Other less stringent conditions also have to fulfilled in order to meet full similitude. Uniform density, viscosity and conductance for the bulk flow. The boundaries must be impermeable, nonconducting and with constant zeta potential (constant double layer thickness).
- There cannot be any electrodes within the domain of similitude.
- The inlet and outlet velocities Fig. F.1 have to fulfill the Helmholtz-Smoluchowski relation. If all these conditions are met the flow will be a simple potential flow[1] which can be calculated from the Laplace equation by means of finite element method (FEM) or another numerical method. Orthogonal intersections of streamlines and isopotentials indicate a potential flow.

[1] Potential flow is free of vorticity.

Appendix G

Two-Phase Flow

In some types of EO pumps it may be desirable to use two different liquids. If the liquids are to be separate for a long period of time they have to be immiscible. An example of such to liquids could be water and oil. Which leads us to the next point namely that the liquids have different viscosities, Fig. G.1. One should imagine that the figure could be mirrored in the symmetry line - layer of zero stress.

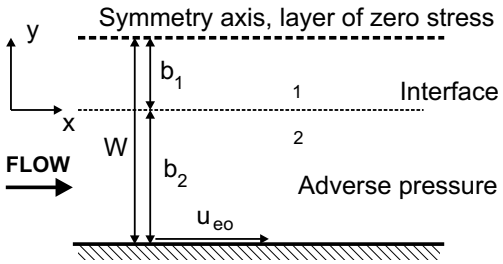

Figure G.1: Velocity profile in laminar adjacent flow of two immiscible fluids with different viscosities. The velocity and shear stress must match at the interface, $y = 0$.

Introducing nondimensional coordinates, and ratios of viscosity σ and layer thickness κ. μ_0 is a reference viscosity.

$$y^* = \frac{y}{W} \qquad \tau^*_{yx} = \frac{\tau_{yx}}{\mu_0 \frac{u_\infty}{W}} \qquad \boldsymbol{\nabla} p^* = \frac{\boldsymbol{\nabla} p}{\frac{\mu_0 u_\infty}{W^2}} \tag{G.1a}$$

$$u^*_i = \frac{u_i}{u_\infty} \qquad \mu^*_i = \frac{\mu_i}{\mu_0} \tag{G.1b}$$

$$\sigma = \frac{\mu_1}{\mu_2} \qquad \kappa = \frac{b_1}{b_2} \tag{G.1c}$$

Inserting these terms in the steady state, incompressible Navier-Stokes equation for creeping flow we obtain

$$\boldsymbol{\nabla} p^* = \mu^*_i \frac{d^2 u^*_i}{dy^{*2}}. \tag{G.2}$$

Eq. (G.2) is then integrated twice with respect to $y*$ and the appropriate bound-

ary conditions (BCs) are applied.

$$\text{BC1} \qquad \tau^*_{yx,1} = \tau^*_{yx,2} \qquad \text{at} \qquad y^* = 0 \tag{G.3a}$$

$$\text{BC2} \qquad u^*_1 = u^*_2 \qquad \text{at} \qquad y^* = 0 \tag{G.3b}$$

$$\text{BC3} \qquad u^*_2 = 1 \qquad \text{at} \qquad y^* = \frac{-b_2}{W} \tag{G.3c}$$

$$\text{BC4} \qquad \frac{du^*_1}{dy^*} = 0 \qquad \text{at} \qquad y^* = \frac{b_1}{W} \tag{G.3d}$$

After some calculations the two velocity profiles $u^*_i\left(y^*, \frac{\boldsymbol{\nabla} p^*}{\mu^*_2}, \kappa, \sigma\right)$ are obtained, Fig. G.2. Here two different cases are shown.

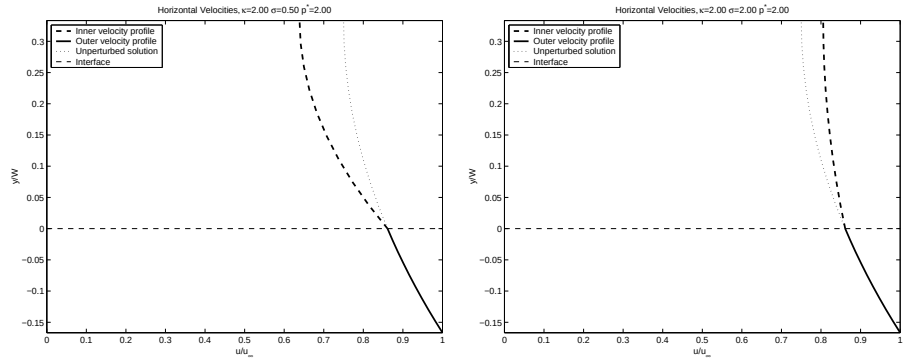

(a) (b)

Figure G.2: Velocity profile in laminar adjacent flow of two immiscible fluids. (a) The dynamic viscosity is higher in the bottom layer. (b) Here the situation is the opposite.

Appendix H

Temperature in a Capillary

Here we begin by making a rough estimate on the heat dissipated in a channel. Let us consider a capillary with an inner radius r_1 and outer radius r_2, see Fig. H.1. The outer part of the capillary is in thermal contact with a reservoir at a fixed temperature T_2. The heat dissipated within the capillary is therefore transported throughout the capillary wall. We are interested in finding the temperature within the capillary T_1 in the stationary situation.

$$P = \dot{q}_{\text{heat,trans.}}, \tag{H.1}$$

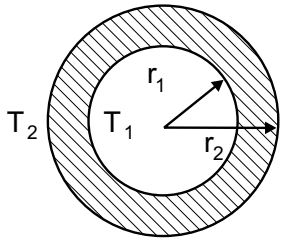

Figure H.1: Heat conduction in a radial channel.

where the ohmic heating is

$$P = E^2 c \lambda_{\text{elec}}, \tag{H.2}$$

and the heat transport rate is

$$\dot{q}_{\text{heat,trans.}} = \frac{2\lambda_{\text{heat}}}{r_1^2 \ln \frac{r_2}{r_1}} (T_1 - T_2) \tag{H.3}$$

$$\tag{H.4}$$

$\dot{q}$ is the energy per volume per time. P is the ohmic heating and $\dot{q}_{\text{heat,trans}}$ is the heat transport. If the expressions are matched one obtains

$$T_1 = T_2 + \frac{r_1^2 E^2 c \lambda_{\text{elec}} \ln \frac{r_2}{r_1}}{2\lambda_{\text{heat}}} \tag{H.5}$$

Remark that the terminal temperature is proportional to the square of radius and electric field. Recalling that the EO velocity is proportional the electric field there may be a conflict limiting the size of applicable field size.

Example: *Heating of a capillary*
A solution with a concentration of 0.01 M KCl ($c = 10^1$ mol/m^3) is considered. The capillary's inner radius is $r_1 = 50$ μm and the outer radius is $r_2 = 200$ μm. Conductivity of KCl $\lambda_{\text{elec}} = 150 \times 10^{-4}$ m^{2}S/mol, electric field $E = 2 \times 10^5$ V/m, ambient temperature $T_2 = 293$ K. Then $T_1 - T_2 = \underline{12 \text{ K}}$.

Appendix I

Grid Dependency

The following analysis is based on the Shallow Reservoir Pump. In the preliminary study of the Shallow Reservoir Pump the whole geometry as shown on Fig. I.1 was simulated. For that purpose a grid dependency analysis was made.

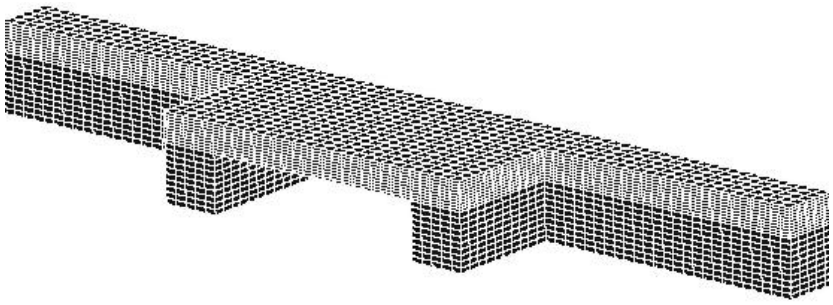

Figure I.1: The computational domain used in the grid dependency analysis.

The data in Table I.1 is taken from Appendix B, Shallow Reservoir Pump (Shallow 2, geometry A).

Simulation	Cells	Tolerance	Flow rate $\times 10$ nL/s	Max velocity μm/s	z-cells
2	11000	10^{-4}	4.84	3610	10
8	11000	10^{-6}	4.84	3610	10
3	15000	10^{-4}	4.84	3639	10
10	15000	10^{-6}	4.85	3638	10
4	60000	10^{-4}	4.92	4451	10
1	66000	10^{-4}	4.96	4981	15
9	66000	10^{-6}	4.97	4981	15
5	120000	10^{-4}	4.97	5024	20
9	120000	10^{-6}	4.99	4981	20

Table I.1: Grid and tolerance dependency for the Shallow Reservoir Pump. The z-cell column is the number of vertical cells in shallow region.

The number of cells is varied from 11000 to 120000. A series of observations is made. Regarding the tolerance it is noticed that for fine meshes it is more important than for coarse meshes. This must be due to its definition.

The flow rate changes 3% from the coarsest to the finest mesh. The computation time is however, changed from 2 minutes to 2 hours. So a Q-p simulation with 10 points takes a day for the finest mesh. Hence, in many simulation relatively coarse meshes were used since the last few percents of accuracy costs a great deal in work and computational time. In the present case I would have used the simulation 9 as a good compromise.

The max velocity changes a great deal. This because of the divergence of the electric field. The velocity is coupled to the electric field through the EO mobility. As the cell size become smaller the divergence become increasingly pronounced.

The number of z-cells is important because it determines the resolution of the velocity profile in the large shallow section.